國　立　交　通　大　學

電信工程研究所

碩士論文

奇偶模雙頻帶通濾波器

Even- and Odd-Mode Dual Band Bandpass Filters

研究生 ： 陳如屏

指導教授 ： 張志揚 博士

中華民國　九十八 年 七 月

奇偶模雙頻帶通濾波器

Even- and Odd-Mode Dual Band Bandpass Filters

研 究 生 ： 陳如屏　　Student : Lu-Pin Chen

指導教授 ： 張志揚 博士　　Advisor : Dr. Chi-Yang Chang

國立交通大學

電信工程研究所

碩士論文

A Thesis
Submitted to Department of Communication Engineering
College of Electrical and Computer Engineering
National Chiao Tung University
In Partial Fulfillment of the Requirements
for the Degree of Master of Science
In
Communication Engineering
July 2009
Hsinchu, Taiwan, Republic of China

中華民國　九十八 年 七 月

奇偶模雙頻帶通濾波器

研究生 ： 陳如屏　　指導教授 ： 張志揚 博士

國立交通大學電信工程研究所

摘要

本篇論文提出一個新的雙頻濾波器架構，此濾波器的兩個通帶分別呈現在兩種不同的輸入訊號下，一種是奇模訊號，另一種是偶模訊號。其中，主要利用耦合微帶線在針對此兩種訊號輸入時，會有不同波速與特性阻抗的特點，將分別以步階阻抗諧振器或均勻阻抗諧振器架構設計的兩個帶通濾波器加以組合。並且，適當的控制微帶線的耦合強度能有效調整兩個通帶的距離。更進一步，利用步階阻抗的諧振特性，將原本二倍頻的諧振頻率推遠。

Even- and Odd-Mode Dual Band Bandpass Filters

Student : Lu-Pin Chen Advisor : Dr. Chi-Yang Chang

Department of Communication Engineering
National Chiao Tung University

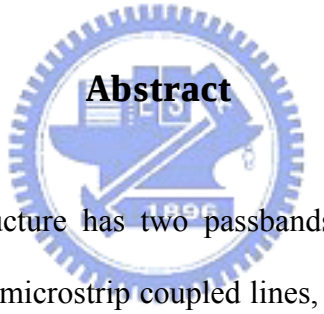

Abstract

In this thesis, a new filter structure has two passbands while exciting differential or common signals is proposed. In microstrip coupled lines, there are different characteristic impedances and phase velocities for even- and odd- mode signals. Using the characteristics, the filters can be realized with both stepped-impedance and uniform impedance resonators. By controlling the coupling strength of the coupled lines, the two passbands can be separated effectively. Based on the resonant characteristics of a stepped-impedance resonator, the first spurious harmonic can be higher than $2f_0$.

Acknowledgement

誌 謝

本篇論文的完成，最要感謝的是指導教授張志揚老師在我念研究所這兩年的指導，不管是在課業、生活與人生規劃上都給予不少有用的建議。研究上，老師總是親切又熱心的解答問題，給予很多有創意的想法，並且不乏生活上的關心，培養我能自動自發敦促自己的能力。其樂觀開朗的生活態度也深深影響著實驗室的每個成員，讓我們的研究生涯能充滿溫馨與歡笑。在此，真的非常感謝老師。同時，感謝口試委員郭仁財教授、黃瑞彬教授與邱煥凱教授提供的寶貴建議，使本篇論文更臻完善。

感謝實驗室學長們無私地指導，幫忙解決在研究上遇到的問題。金雄學長總是不厭其煩並且有耐心的接我求救電話，遇到研究上的瓶頸時，也時時鼓勵我，讓人感念在心，無厘頭的人生建言也讓研究生活充滿樂趣。此外，哲慶學長在研究上總是非常熱心地給予一針見血的指導，讓這篇論文能更加順利的完成，其對研究的熱忱與努力更是我所要學習的。感謝爽朗的正憲學長幫忙解答我不少研究上的問題，他認真而追求完美的做事態度也讓我印象深刻。有賴眾多學長姐們的幫忙，這篇論文才能順利完成。

感謝實驗室同學與學弟妹們在學業與生活上的陪伴與照顧，尤其是繼續攻讀博班的昀緯，總是很有耐心地與我一起討論問題，雖然不能完全了解，卻總是能在討論中得到一些意外的收穫。感謝忠傑、殿靖、耿宏、姵潔等等學弟妹們，有你們的存在讓我的研究生活不曾平淡。此外，感謝在求學過程上一路陪伴我的各方好友與室友們，有你們的陪伴，即使經歷挫折也能勇敢站起來，感謝你們。

最後要感謝的是默默支持的家人們，爸、媽與弟妹。有了你們的支持，讓我能放心而專注地完成學業，真的非常感謝你們。

Table of Contents

Abstract(Chinese) i

Abstract iii

Acknowledgement v

Table of Contents vii

List of Figures ix

List of Tables xv

Chapter 1 Introduction 1

Chapter 2 Basic Theory 5

2.1 Analysis and Characteristics of SIR 5

2.1.1 Resonance condition and resonator electrical length 5

2.1.2 Basic structure of the Half-wavelength Type SIR 8

2.1.3 Spurious Resonance Frequency 10

2.2 Lowpass Prototype Circuit and the transformation from lowpass prototype to bandpass filter 13

2.2.1 The Lowpass Prototype 14

2.2.2 Transformation of elements by J- or K-inverter 15

2.2.3 Lowpass to Bandpass Transformation 18

2.2.4 Slope Parameters 19

2.3 Dishal's Method 21

2.4 Coupled Line Theory 23

2.4.1 even-and odd- mode approach[17] 24

2.5 J- and K-inverters with distributed circuits 27

2.5.1 Equivalent Circuit of Parallel-Coupled Line 27

2.5.2 Equivalent Circuit of Antiparallel-Coupled Line 31

2.6 Second-Order Gap Coupling Bandpass Filter 34
Chapter 3 Second-Order Tapped Coupling Bandpass Filter 41
3.1 Input/Output Tapping 41
3.2 Second-Order Bandpass Filter with Tapped Line 47
3.3 Dual- Frequency Transformer[19] 49
Chapter 4 The Proposed Dual-Band Bandpass Filter 51
4.1 Design Procedure and Realization with Type I tapping 51
4.1.1 Second-Order Filter with Open-Ended λ/2 SIR 51
4.1.2 Second-Order Filter with Short-Ended λ/2 SIR 58
4.1.3 Third-Order Filter with Short-Ended λ/2 SIR 63
4.2 Design Procedure and Realization with Type II tapping 70
4.2.1 Third-Order Filter with Short-Ended λ/2 SIR 70
4.3 Design Procedure and Realization with Type III tapping 75
4.3.1 Third-Order Filter with Open-Ended λ/2 SIR 75
4.3.2 Second-Order Filter with Open-Ended λ/2 SIR 85
Chapter 5 Conclusion 92
References 96

List of Figures

Figure 1.1 The general scheme of a diplexer. 2

Figure 1.2 The diplexer structures in a balanced transceiver system. (a) The original Structure. (b) The modified structure with the proposed even and odd-mode bandpass filter. 3

Figure 1.3 The structures of a two channel system in a balanced receiver. (a) The general structure. (b) The modified structure with the proposed even and odd-mode bandpass filter. 4

Figure2.1 Basic structure of SIR. (a) Quarter-wavelength type. (b) Half-wavelength type. 6

Figure 2.2 Electrical parameters of fundamental building element of a SIR. 6

Figure 2.3 Resonance condition of SIR. 8

Figure 2.4 Basic structure of λ/2-type open-end SIRs. (a) $R<1$. (b) $R=1$. (c) $R>1$. 9

Figure 2.5 Basic structure of λ/2-type short-end SIRs. (a) $R<1$. (b) $R=1$. (c) $R>1$. 10

Figure 2.6 The relationship between impedance ratio and normalized spurious resonance frequencies 12

Figure 2.7 Normalized resonant frequencies of an SIR. 13

Figure 2.8 Lowpass prototype ladder networks. (a) The leading component is a shunt capacitor; (b) The dual of the network in (a). 14

Figure 2. 9 Admittance and impedance inverters 15

Figure2.10 The transformation between series and shunt components. (a) Transformation of series to shunt components. (b) Transformation of shunt

to series components. 16
Figure 2.11 Transformation of J inverter. 16
Figure 2.12 The series inductors can be transformed to shunt capacitor. 18
Figure 2.13 Lowpass to bandpass transformation. 19
Figure 2.14 Parallel resonances are represented with slope parameters. 20
Figure 2.15 Parameters Q_{ex} and coupling coefficients k 21
Figure 2.16 Analysis of coupled microstrip lines in terms of capacitances: (a) even-mode capacitance. (b) odd-mode capacitance. 25
Figure 2.17 An unsymmetrical pair of parallel-coupled lines. C_a, C_b and C_{ab} are line capacitances per unit length. 28
Figure 2.18 An unsymmetrical parallel-coupled line and its equivalent circuit. 28
Figure 2.19 A symmetrical parallel-coupled line and its equivalent circuit. 29
Figure 2.20 An unsymmetrical parallel-coupled line and its equivalent circuit. 30
Figure 2.21 A symmetrical parallel-coupled line and its equivalent circuit. 30
Figure 2.22 An unsymmetrical parallel-coupled line and its equivalent circuit. 32
Figure 2.23 A symmetrical parallel-coupled line and its equivalent circuit. 32
Figure 2.24 An unsymmetrical antiparallel-coupled line and its equivalent circuit. 33
Figure 2.25 A symmetrical antiparallel-coupled line and its equivalent circuit. 33
Figure 2.26 Circuit configuration of the second-order gap coupling filter. 34
Figure 2.27 The overall equivalent circuit of the second-order gap coupling filter. 35
Figure 2.28 Circuit configuration of the second-order gap coupling filter. 37
Figure 2.29 The overall equivalent circuit of the second-order gap coupling filter. 37
Figure 3.1 The stepped-impedance resonator and tapped line 42
Figure 3.2 The short-end type SIR and tapped line 44
Figure 3.3 The general case of tapping with SIR. 45
Figure 3.4 The equivalent circuit of tapping with SIR. 45

Figure 3.5 The SIR feeding structure with a matching network..... 46

Figure 3.6 The overall equivalent circuit of the second-order tapped coupling filter. .. 47

Figure 3.7 Circuit configuration of the second-order tapped coupling filter. (Type III) 48

Figure 3.8 The circuit simulation result..... 48

Figure 3.9 Circuit configuration of the second-order tapped coupling filter. (Type IV) 49

Figure 3.10 Two-section dual-band transformer..... 50

Figure 4.1 The overall circuit diagram. (a) In circuit simulation tool, ADS. (b) In EM simulation tool, Sonnet. 52

Figure 4.2 The circuit layout of the proposed Filter A. 54

Figure 4.3 Photograph of Filter A..... 55

Figure 4.4 Simulated and measured results of Filter A. (a) Simulated $|S_{11}|$ and $|S_{21}|$ for 2~4 GHz. (b) Simulated $|S_{11}|$ and $|S_{21}|$ for 1~7 GHz. (c) Measured $|S_{11}|$ and $|S_{21}|$ for 2~4 GHz. (d) Measured $|S_{11}|$ and $|S_{21}|$ for 1~7 GHz. (e) Measured isolation between two modes. 58

Figure 4.5 The overall circuit scheme of Filter B. (a) The circuit structure in ADS. (b) The circuit layout in Sonnet..... 58

Figure 4.6 Photograph of Filter B..... 60

Figure 4.7 Simulated and measured results of Filter B. (a) Simulated $|S_{11}|$ and $|S_{21}|$ for 2~4 GHz. (b) Simulated $|S_{11}|$ and $|S_{21}|$ for 1~7 GHz. (c) Measured $|S_{11}|$ and $|S_{21}|$ for 2~4 GHz. (d) Measured $|S_{11}|$ and $|S_{21}|$ for 1~7 GHz. (e) Measured isolation between two modes. 63

Figure 4.8 The overall circuit configuration of Filter C. (a) The overall layout. (b) The part of resonators. (c) The part of transformers. 65

Figure 4.9 Photograph of Filter C..... 66

Figure 4.10 Simulated and measured results of Filter C (a) Simulated $|S_{11}|$ and $|S_{21}|$ for 2~4 GHz. (b) Simulated $|S_{11}|$ and $|S_{21}|$ for 1~7 GHz. (c) Measured $|S_{11}|$ and $|S_{21}|$ for 2~4 GHz. (d) Measured $|S_{11}|$ and $|S_{21}|$ for 1~7 GHz. (e) Measured isolation between two modes..... 69

Figure 4.11 The overall circuit topology of Filter D. 70

Figure 4.12 Photograph of Filter D. 71

Figure 4.13 Simulated and measured results of Filter D. (a) Simulated $|S_{11}|$ and $|S_{21}|$ for 2~4 GHz. (b) Simulated $|S_{11}|$ and $|S_{21}|$ for 1~7 GHz. (c) Measured $|S_{11}|$ and $|S_{21}|$ for 2~4 GHz. (d) Measured $|S_{11}|$ and $|S_{21}|$ for 1~7 GHz. (e) Measured isolation between two modes..... 74

Figure 4.14 The overall circuit topology of the Filter E. (a) The circuit scheme in ADS. (b) The circuit scheme in Sonnet..... 76

Figure 4.15 Photograph of proposed Filter E. 79

Figure 4.16 Photograph of proposed Filter F. 79

Figure 4.17 Simulated and measured results of Filter E. (a) Simulated $|S_{11}|$ and $|S_{21}|$ for 2~4 GHz. (b) Simulated $|S_{11}|$ and $|S_{21}|$ for 1~7 GHz. (c) Measured $|S_{11}|$ and $|S_{21}|$ for 2~4 GHz. (d) Measured $|S_{11}|$ and $|S_{21}|$ for 1~7 GHz. (e) Measured isolation between two modes..... 82

Figure 4.18 Simulated and measured results of Filter F. a) Simulated $|S_{11}|$ and $|S_{21}|$ for 2~4 GHz. (b) Simulated $|S_{11}|$ and $|S_{21}|$ for 1~7 GHz. (c) Measured $|S_{11}|$ and $|S_{21}|$ for 2~4 GHz. (d) Measured $|S_{11}|$ and $|S_{21}|$ for 1~7 GHz. (e) Measured isolation between two modes..... 85

Figure 4.19 The circuit configuration of Filter G. 86

Figure 4.20 Photograph of proposed Filter G. 88

Figure 4.21 Simulated and measured results of Filter F. (a) Simulated $|S_{11}|$ and $|S_{21}|$ for 2~4 GHz. (b) Simulated $|S_{11}|$ and $|S_{21}|$ for 1~7 GHz. (c) Measured $|S_{11}|$ and $|S_{21}|$ for 2~4 GHz. (d) Measured $|S_{11}|$ and $|S_{21}|$ for 1~7 GHz. (e) Measured isolation between two modes..... 91

Figure 5.1 The comparison of four circuits. (a) Hairpin-resonator filter. (b) Type I filter in Seciton 2.6. (c) Type III filter in Section 3.2. (d) Parallel-coupled line resonator filter. (e) Simulated results for S11 and S21. 94

List of Tables

Table 2.1 Parameters of coupling coefficients and Qext's with N=2, Lr=0.1dB. 22

Table 2.2 Parameters of coupling coefficients and Qext's with N=3, Lr=0.1dB 22

Table 4.1 Initial parameters for the odd-mode filter in Filter A. 53

Table 4.2 Physical dimensions of the proposed Filter A. (Unit: mil) 54

Table 4.3 Physical dimensions of the proposed Filter B. (Unit: mil) 59

Table 4.4 Initial parameters of the even-mode filter in Filter B. 59

Table 4.5 Initial parameters of the even-mode filter in Filter C. 64

Table 4.6 Physical dimensions of the proposed Filter C. (Unit: mil) 66

Table 4.7 Physical dimensions of the proposed Filter D. (Unit: mil) 71

Table 4.8 Physical dimensions of the proposed Filter E. (Unit: mil) 76

Table 4.9 Initial parameters of the odd-mode filter in Filter E. 77

Table 4.10 Initial parameters of the two-section transformer in Filter E. 78

Table 4.11 Physical dimensions of the proposed Filter G. (Unit: mil) 87

Table 4.12 Initial parameters of the odd-mode filter in Filter G. 87

Table 4.13 Initial parameters of the two-section transformer in Filter G. 87

Chapter 1

Introduction

With the rapid expansion and growth of wireless communication systems for military and commercial applications, implementation of microwave and mm-wave systems is increasing dramatically due to their advantages over conventional architectures. Commercial applications of these systems include short-haul line-of-sight transmission links for personal communication networks , wireless cable, wireless local area networks (LANs) and mobile broadband systems.

In modern wireless and mobile communication systems, filters are always playing important and essential roles. Planar filters are particularly popular structures because they can be fabricated using printed circuit technology and are suitable for commercial applications due to their compact size and low-cost integration [1]. Moreover, planar filters using the structures of parallel-coupled and cross-coupled resonators are preferable and extensively used in communication systems because of their high practicality and high performance [2]-[6].

To design a planar filter, it is necessary to select proper resonator types since resonators are basic components of a filter. To reduce the resonator size, several types of resonators such as the U-shaped hairpin resonators [4], the open-loop resonators [5], and the folded open-line resonators [6], [7] have been proposed to design different kinds of bandpass filters. However, all of them are always too large. Among these popular resonators, the most frequently used is the stepped impedance resonator (SIR) because it was originally presented not only to reduce the resonator size, but also to control the spurious resonant frequencies by properly adjusting its structural parameters [8],[9].

In multiservice and multiband communications, diplexers are one of the key components in the transceiver. They are often needed to have some capabilities of high compactness, light weight, and high isolation. Microwave diplexers are typically employed to connect the RX and TX filters of a transceiver to a single antenna through a suitable three-port junction. Basically, a diplexer is composed of bandpass filters and associated matching networks. Thus, a reduction of the filter size is essential in reducing the size of a diplexer. To reduce the circuit size, the diplexers based on the slow-wave open-loop resonators with high-impedance resonators[6], the folded coupled-line resonators [7], the miniaturized open-loop resonators [8], and stepped-impedance resonators [9] were proposed. However, all of them required two filters in realizing the diplexer. Figure 1.1 shows the general structure of a diplexer.

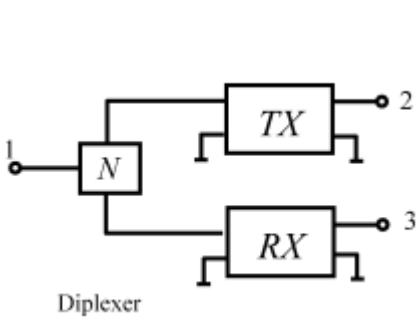

Figure 1.1 The general scheme of a diplexer.

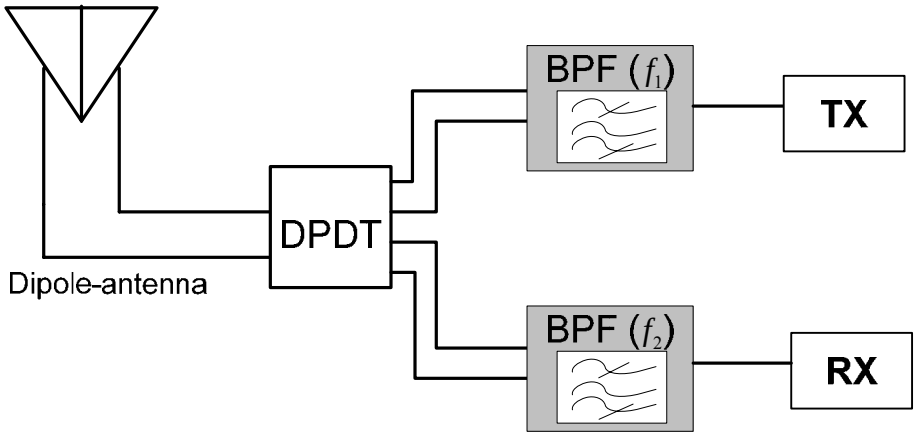

(a) Simplified architecture of the diplexer in a balanced transceiver.

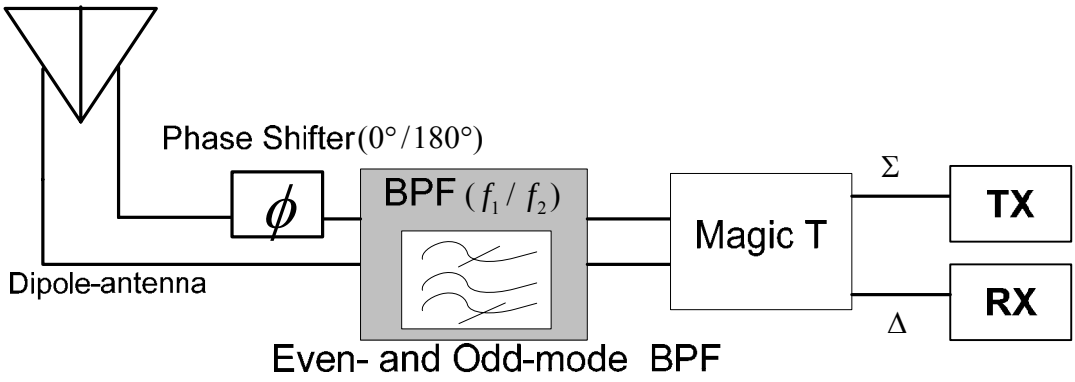

(b) Modified architecture of the diplexer in a balanced transceiver.

Figure 1.2 The diplexer structures in a balanced transceiver system. (a) The original Structure. (b) The modified structure with the proposed even and odd-mode bandpass filter.

Moreover, consider the importance of balanced circuits in modern communication system. It's necessary to figure out a solution to decrease the circuit size in the balanced transceiver as shown in Figure 1.2(a).

In this thesis, a new four-port bandpass filter is proposed. Unlike the operation of the four-port balanced-to-balanced bandpass filter in [10], the proposed bandpass filter based on SIRs can operate at two different passbands while exciting differential- or common-mode signal respectively. This filter can be used to develop a compact microstrip diplexer by adding additional passive components, e.g. a $0^o/180^o$ phase shifter and a magic T, as illustrated in Figure 1.2(b). With the number of filters reduced by half, the size of the proposed diplexer may be made compact when compared with that of the conventional diplexer consisting of two single-passband filters.

On the other hand, another application is for a two-channel system. For example, Figure 1.3(a) depicts a conventional two-channel balanced system. Using the proposed filter design, the number of filters can be reduced by half as presented in Figure 1.3(b). The two channels are selected with the switch of two kinds of phase delay.

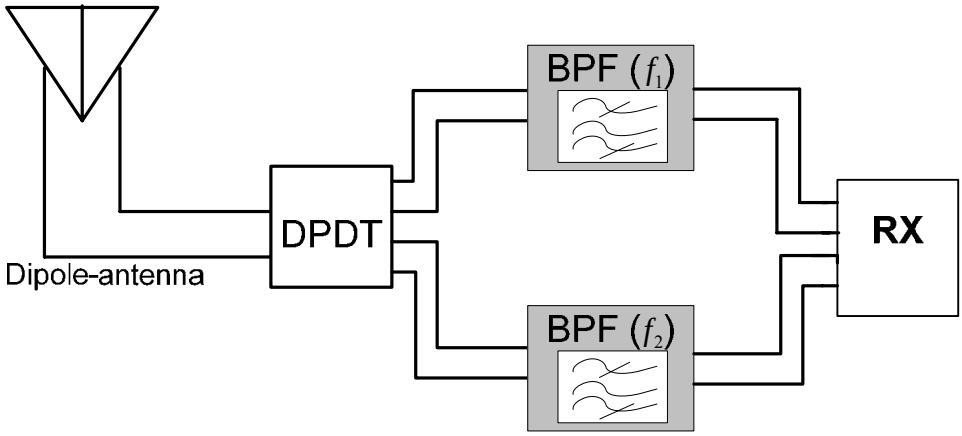

(a) The general structure of a two-channel system in a balanced receiver.

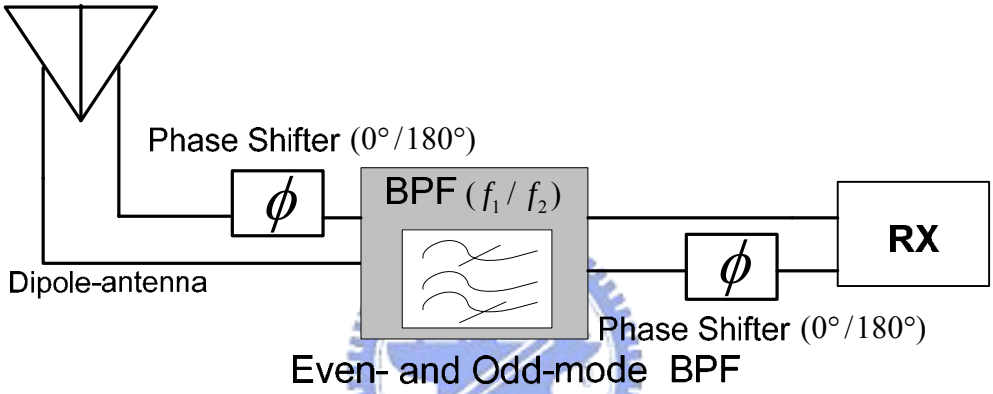

(b) The modified structure of a two-channel system in a balanced receiver.

Figure 1.3 The structures of a two channel system in a balanced receiver. (a) The general structure. (b) The modified structure with the proposed even and odd-mode bandpass filter.

Chapter 2

Basic Theory

2.1 Analysis and Characteristics of SIR

Because we want to fabricate a bandpass filter with SIR and UIR, the basic structure of λ/4- and λ/2-type SIR are presented in this part [11], followed by the introduction and definition of the impedance ratio R. In addition, basic properties such as resonant conditions, resonator length, and spurious resonance frequencies are systematically discussed using R.

2.1.1 Resonance condition and resonator electrical length

The SIR is a TEM or quasi-TEM mode resonator composed of more than two transmission lines with different characteristic impedance. Figure 2.1 shows typical examples of its structural variation, where figures (a) and (b) are examples of λ/4 and λ/2 resonators.

Characteristic impedance and corresponding electrical length of the transmission lines between the open- and short-circuited ends in Figure 2.1 are defined as Z_a and Z_b, θ_a and θ_b, respectively. The structural fundamental building element of a SIR comprises a composite transmission line possessing both open- and short-circuited ends and a step

junction in between. After defining this fundamental building element, λ/4- and λ/2-type of SIR can be looked as a combination of one and two fundamental building elements respectively. An electrical parameter which characterizes the SIR is the ratio of the two transmission line impedances Z_a and Z_b, which we define by the following equation.

$$R \equiv \frac{Z_b}{Z_a} \tag{2.1}$$

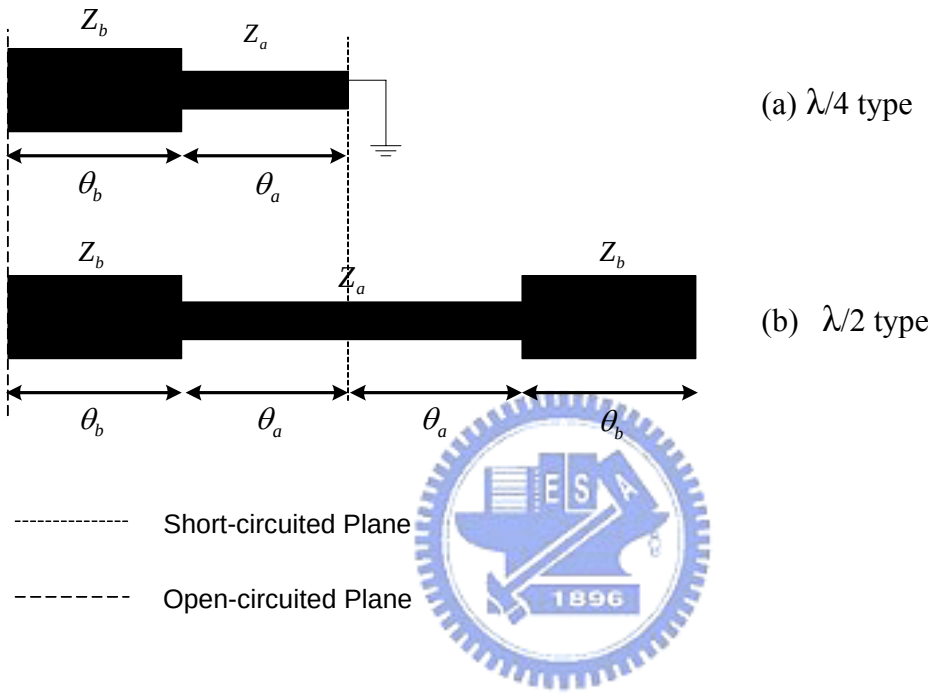

Figure2.1 Basic structure of SIR. (a) Quarter-wavelength type. (b) Half-wavelength type.

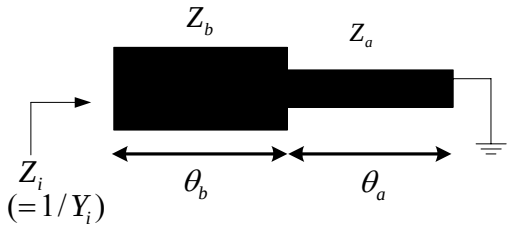

Figure 2.2 Electrical parameters of fundamental building element of a SIR.

Figure 2.2 shows the fundamental building element of a SIR with an open-end, short-end and an impedance step. When ignoring the influences of step discontinuity and

edge capacitance at the open end, the input impedance and admittance defined as Z_i and $Y_i\,(=1/Z_i)$ can be expressed as

$$Z_i = jZ_b \frac{Z_a \tan\theta_a + Z_b \tan\theta_b}{Z_b - Z_a \tan\theta_a \tan\theta_b} \tag{2.2}$$

Let $Y_i = 0$, and then the parallel resonance can be obtained as follows:

$$\tan\theta_a \tan\theta_b = \frac{Z_b}{Z_a} \equiv R \tag{2.3}$$

Define the overall electrical length of the SIR as θ_T. With (2.3), θ_{TA} can be expressed as

$$\begin{aligned}\theta_{TA} &= \theta_a + \theta_b \\ &= \theta_a + \tan^{-1}(R/\tan\theta_a)\end{aligned} \tag{2.4}$$

Normalized resonator length is defined by the following equation with respect to the electrical length of the corresponding UIR measuring $\pi/2$.

$$L_n = \theta_{TA}/(\pi/2) = 2\theta_{TA}/\pi\,. \tag{2.5}$$

Following the resonant condition (2.3), Figure 2.3 shows the relationship between θ_a and L_n, taking R as a parameter.

With Figure 2.3, we can choose a curve which represents an impedance ratio R, and then decide the electrical length θ_a to get a specific L_n which means the overall electrical length of the SIR is:

$$\theta_{TA} = L_n \times (\pi/2)\,. \tag{2.6}$$

Similarly, for $\lambda/2$- and λ-type SIR, overall electrical lengths are defined as θ_{TB} and θ_{TC} which can be normalized as follows:

$$\theta_{TB}/\pi = 2\theta_{TA}/\pi = L_n\,, \tag{2.7}$$

$$\theta_{TC}/2\pi = 4\theta_{TA}/\pi = L_n\,. \tag{2.8}$$

Figure 2.3 shows that when

(1) $R>1$, the total electrical length of the resonator is longer than $\lambda/4$ and a maximum value exists.

(2) $R=1$, represents a uniform impedance resonator (UIR). The total electrical length

ofthe resonator equals $\lambda/4$.

(3) $R<1$, the total electrical length of the resonator is shorter than $\lambda/4$ and a minimum value exists.

That is, applying a smaller impedance ratio R and choosing the electrical length properly, the resonator length can be shortened effectively.

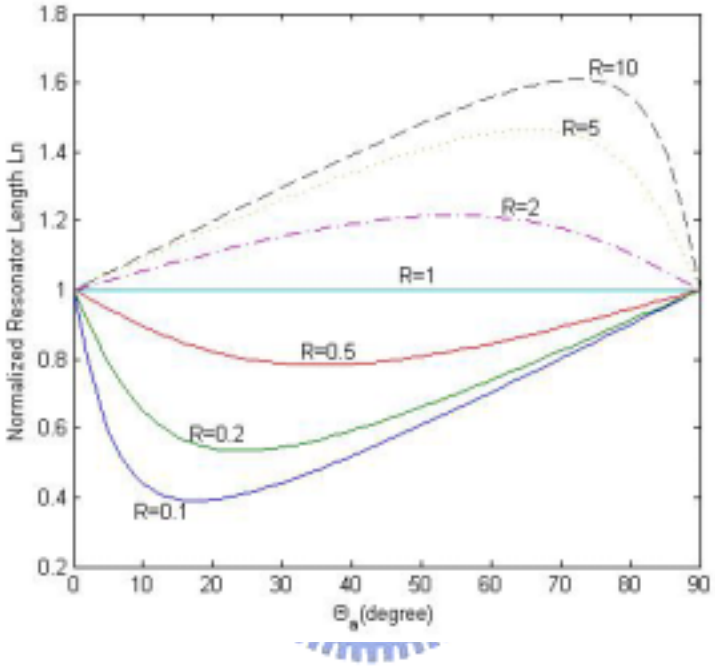

Figure 2.3 Resonance condition of SIR.

2.1.2 Basic structure of the Half-wavelength Type SIR

The proposed bandpass filters are mainly composed by λ/2-type UIR or SIR. Figure 2.4 shows the open-end type SIR. For the direct analysis, input admittance Yi seen from an open-end is given as

$$Y_i = jY_b \frac{2(R\tan\theta_a + \tan\theta_b)(R - \tan\theta_b \tan\theta_a)}{R(1-\tan^2\theta_b)(1-\tan^2\theta_a) - 2(1+R^2)\tan\theta_b \tan\theta_a} = jB_s \qquad (2.9)$$

Resonance conditions are obtained by taking $Y_i = 0$, which is the same as (2.3).

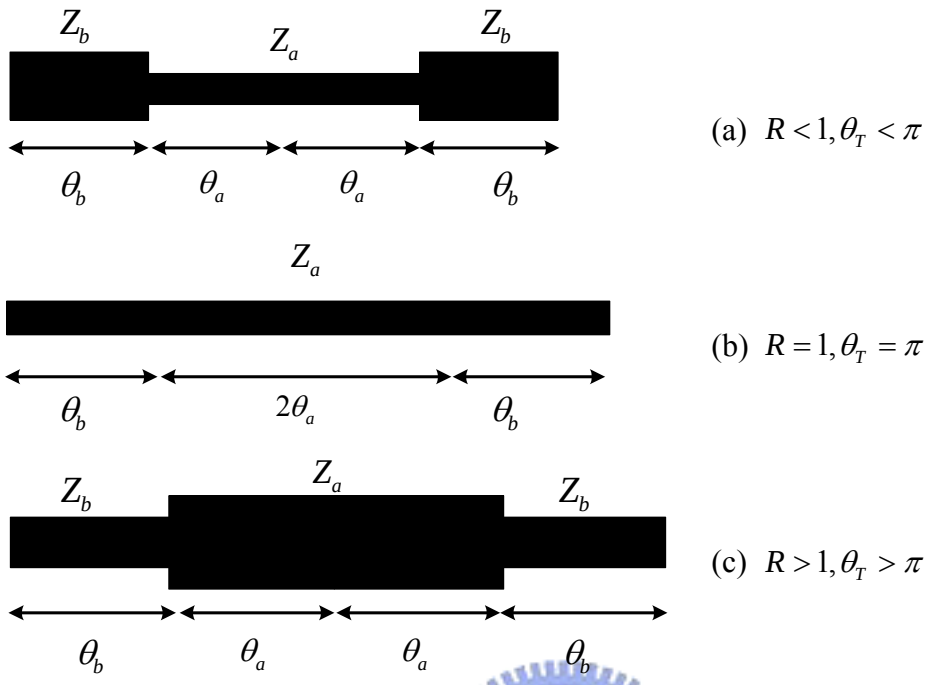

Figure 2.4 Basic structure of λ/2-type open-end SIRs. (a) $R<1$. (b) $R=1$. (c) $R>1$.

The slope parameter b_s can be obtained from its definition as follows:

$$b_s = \frac{\omega_0}{2} \frac{dB_s}{d\omega}\bigg|_{\omega=\omega_0} \tag{2.10}$$

where w_0 is the angular resonance frequency and B_s is the total susceptance of the resonator.

In addition, a lower impedance ratio R can obtain a shorter length of SIR which is similar with the λ/4-type mentioned in Section 2.1.1.

Similarly, for the short-end type shown in Figure 2.5, the resonance condition can be obtained which is identified with (2.3). On the contrary, the higher the impedance ratio R is, the shorter the electrical length can be.

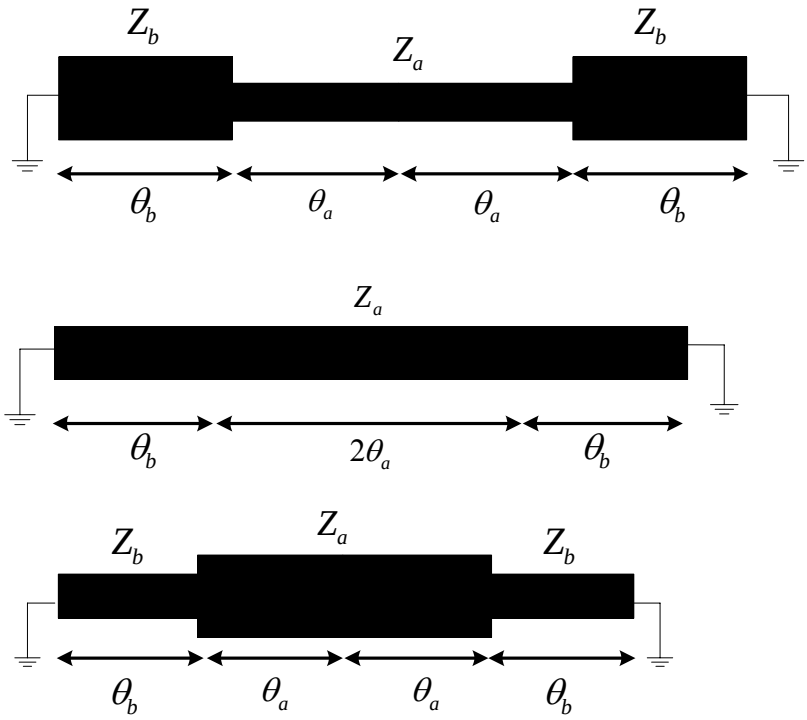

Figure 2.5 Basic structure of λ/2-type short-end SIRs. (a) $R<1$. (b) $R=1$. (c) $R>1$.

2.1.3 Spurious Resonance Frequency

A distinct feature of the SIR is that the resonator length and corresponding spurious resonance frequencies can be adjusted by changing the impedance ratio R [9]. In the following discussion, the fundamental resonance frequency is represented as f_0, while the lowest spurious frequencies of $\lambda/4$- and $\lambda/2$-type SIR are represented as f_{SA1} and f_{SB1}. Now consider the TEM mode as the dominant resonant mode and neglect the effect of the step junction. We assume $\theta_a = \theta_b = \theta_0$, and resonator electrical lengths corresponding to spurious frequencies f_{SA1} and f_{SB1} are expressed as θ_{SA1} and θ_{SB1}.

From (2.3), the following equation is obtained for f_{SA1}.

$$\tan\theta_{SA} = \tan(\pi - \theta_0) = -\tan^{-1}\sqrt{R}\,. \tag{2.11}$$

And then,

$$\frac{f_{SA1}}{f_0} = \frac{\theta_{SA}}{\theta_0} = \frac{\pi - \theta_0}{\theta_0} = \frac{\pi}{\tan^{-1}\sqrt{R}} - 1. \tag{2.12}$$

As previously described , the resonance condition for $\lambda/2$-type SIR can be derived. In the case of $\theta_a = \theta_b = \theta_0$, (2.9) is simplified as [8],

$$Y_i = jY_b \frac{2(R+1)(R-\tan^2\theta_0)}{R-2(1+R+R^2)\tan^2\theta_0 + R\tan^4\theta_0}. \tag{2.13}$$

Thus, resonance conditions are expressed as,

$$\theta_0 = \tan^{-1}\sqrt{R}. \tag{2.14}$$

Expressing the spurious resonance frequencies as $f_{SB1}, f_{SB2}, f_{SB3}$, the corresponding electrical lengths θ_{S1}, θ_{S2} and θ_{S3} can be obtained from (2.13) as [8],

$$\begin{aligned} &\tan\theta_{S1} = \infty, \\ &\tan^2\theta_{S2} - R = 0, \\ &\tan\theta_{S3} = 0. \end{aligned} \tag{2.15}$$

So,

$$\begin{aligned} &\theta_{S1} = \pi/2, \\ &\theta_{S2} = \tan^{-1}(-\sqrt{R}) = \pi - \theta_0, \\ &\theta_{S3} = \pi. \end{aligned} \tag{2.16}$$

Thus,

$$\begin{aligned} &\frac{f_{SB1}}{f_0} = \frac{\theta_{S1}}{\theta_0} = \frac{\pi}{2\tan^{-1}\sqrt{R}}, \\ &\frac{f_{SB2}}{f_0} = \frac{\theta_{S2}}{\theta_0} = 2(\frac{f_{SB1}}{f_0}) - 1, \\ &\frac{f_{SB2}}{f_0} = \frac{\theta_{S3}}{\theta_0} = 2(\frac{f_{SB1}}{f_0}). \end{aligned} \tag{2.17}$$

Figure 2.6 illustrates the relationship between impedance ratio and normalized spurious resonance frequencies from (2.12) and (2.17a). Figure 2.7 [18] describes the relationship between resonant frequencies including the fundamental, first, second, and third higher order modes against the ratio of electrical lengths for impedance ratio $R =$ 0.2, 0.8, and 2.5. It shows that the smaller the ratio R is, the larger the maximum ratio of

$\frac{f_s}{f_0}$ is. It's a critical characteristic that can be employed for a bandpass filter with a wide stopband. It's noted that Figure 2.6 and 2.7 are for the λ/2-type SIRs in Figure 2.4. For the λ/2-type short-end SIRs in Figure 2.5, the same situation holds while the high-Z and the low-Z segments interchange.

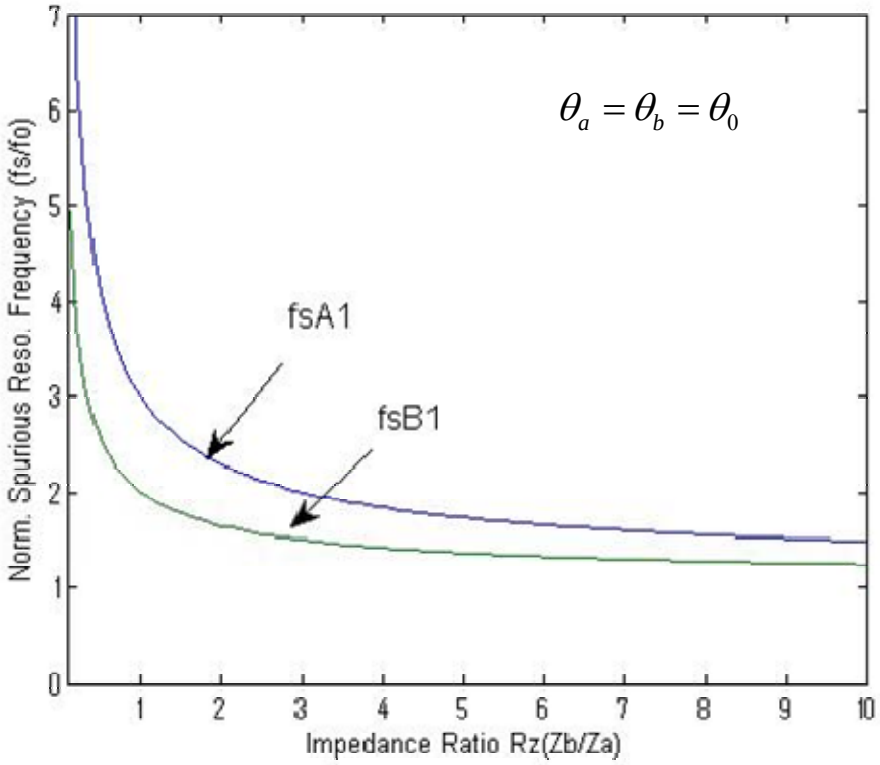

Figure 2.6 The relationship between impedance ratio and normalized spurious resonance frequencies

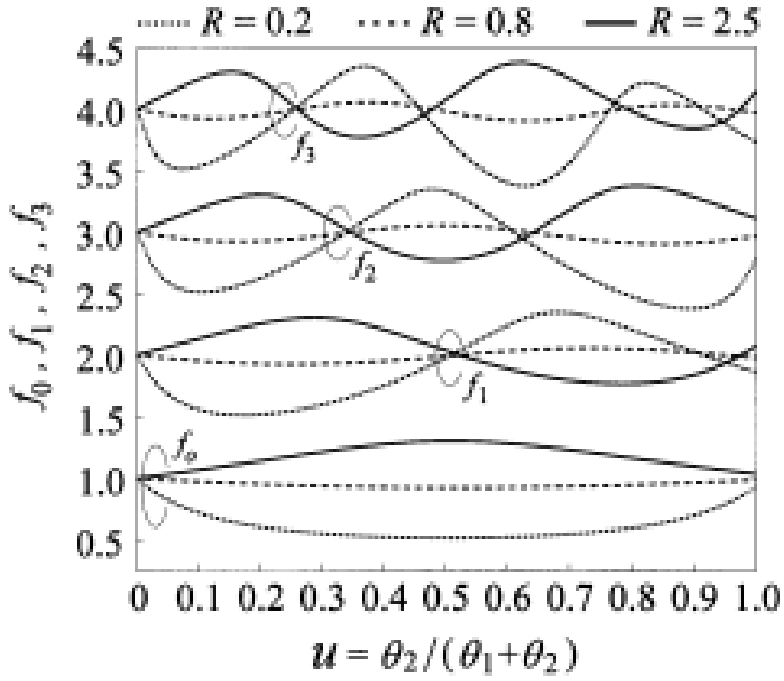

Figure 2.7 Normalized resonant frequencies of an SIR.

2.2 Lowpass Prototype Circuit and the transformation from lowpass prototype to bandpass filter

There are many methods to generate element values for the filter design. The insertion loss method allows a high degree of control of the passband and stopband responses [1]. In our design, the element values for Chebyshev prototypes are used. For the filter prototypes to be discussed below, the order of the filter is equal to the number of reactive elements.

2.2.1 The Lowpass Prototype

The lowpass prototype which may be of lumped or distributed realization is a building block from which real filters may be constructed. Various transformations may be used to convert it into a bandpass or other types filter responses with arbitrary centre frequency and bandwidth. The doubly terminated lowpass prototype circuits, connected to their terminating impedances or admittances, are depicted in Figure 2.8. The element values in the network are termed with the "g-parameters" [5], which may be the value of a shunt capacitor or a series inductor. The source termination g_0 is resistive if g_1 is a capacitor, and conductive if g_1 is an inductor, and similarly for the load termination g_{N+1}.

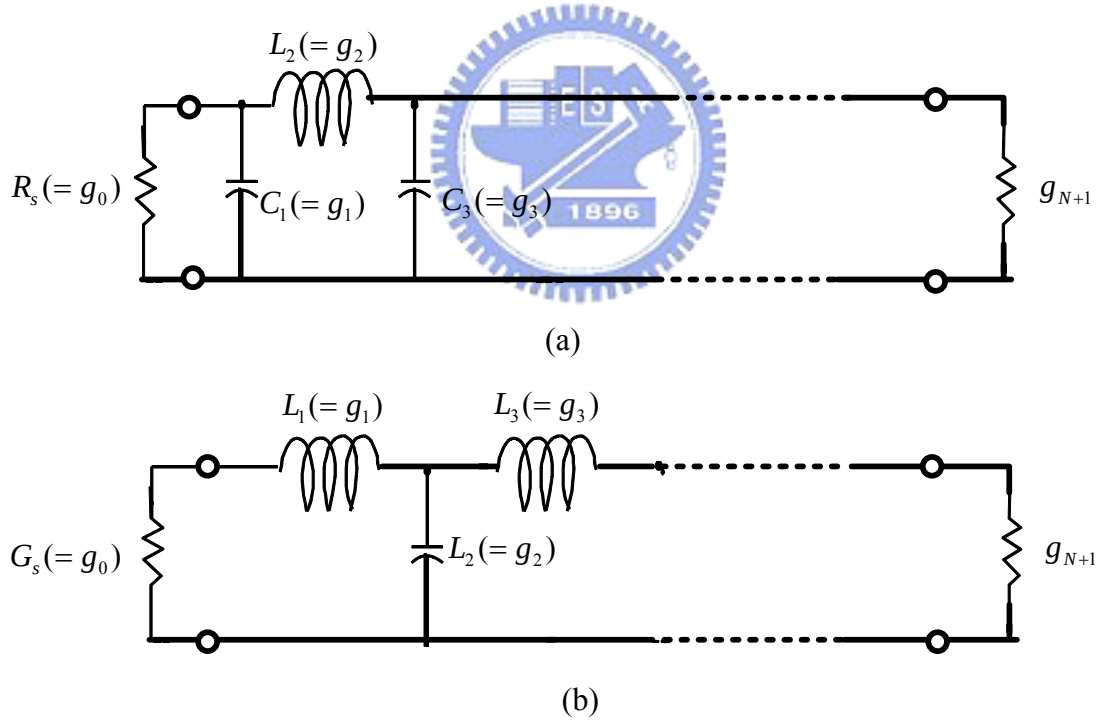

Figure 2.8 Lowpass prototype ladder networks. (a) The leading component is a shunt capacitor; (b) The dual of the network in (a).

The circuits of Figure 2.8 can be considered as the dual of each other, and both will give the same response. When the filter specification is given, the "g parameters" are decided.

2.2.2 Transformation of elements by J- or K-inverter

Simply to say, J and K inverters are admittance and impedance inverters which are similar to the ideal quarter-wavelength transformers shown in Figure 2.9.

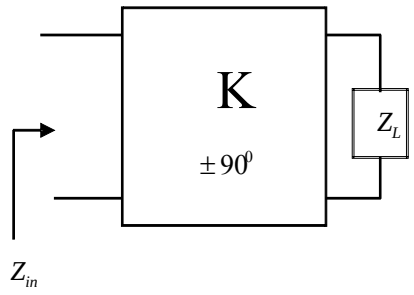

$$Z_{in} \cdot Z_L = K^2 \quad (2.18)$$

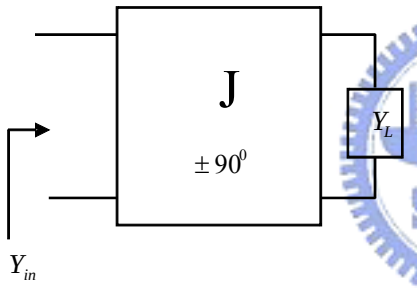

$$Y_{in} \cdot Y_L = J^2 \quad (2.19)$$

Figure 2. 9 Admittance and impedance inverters

There would be a phase delay of ±90 degrees when the wave passes through the inverters for all frequency. That is, the inverters don't exist in reality. Figure 2.10 illustrates that with K- or J-inverters, we can transform a series component to a shunt component and transform oppositely as well.

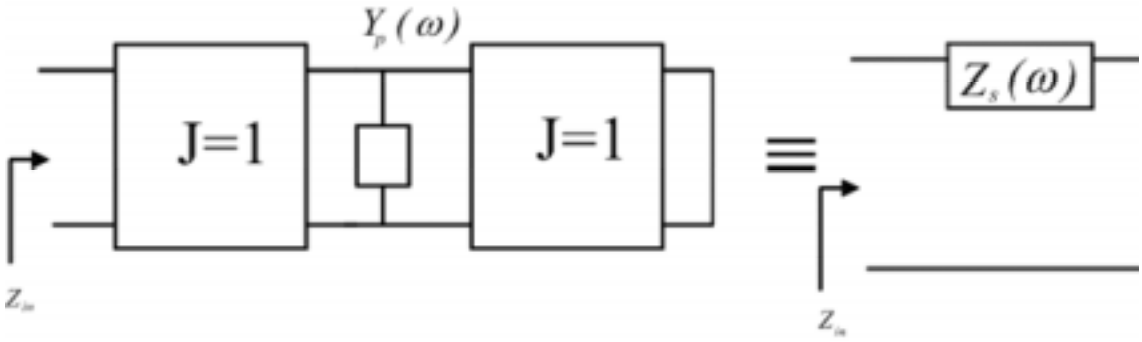

(a)

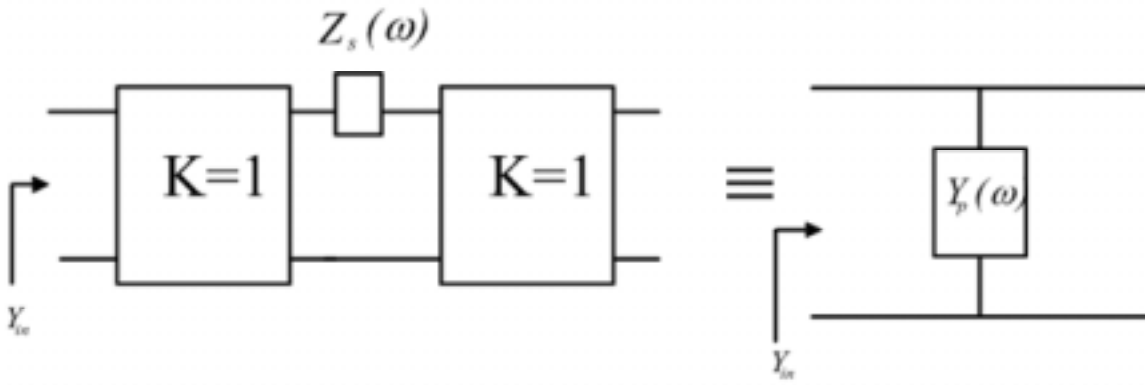

(b)

Figure2.10 The transformation between series and shunt components. (a) Transformation of series to shunt components. (b) Transformation of shunt to series components.

In Figure 2.10(a), the input impedance Z_{in} should be identified. Likewise, the analysis is derived as follows. At first, the J inverter in Figure 2.10(a) can transform the short-circuit termination to an open-circuit as shown in Figure 2.11.

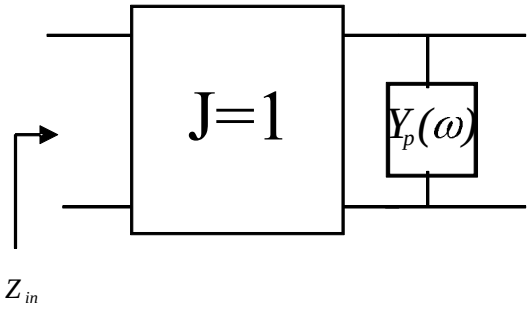

Figure 2.11 Transformation of J inverter.

For the circuit of parallel resonance, Y_p can be derived as

$$Y_p = j\omega C - \frac{j}{\omega L} = j\omega C\left(1 - \frac{\omega_o^2}{\omega^2}\right) \tag{2.20}$$

And if the circuit in Figure 2.10(a) is of series resonance, we can attain

$$Z_s = j\omega L'\left(1 - \frac{\omega_o^2}{\omega^2}\right) \tag{2.21}$$

where $\omega_0 = \frac{1}{\sqrt{LC}} = \frac{1}{\sqrt{L'C'}}$ is the center angular frequency.

For J=1, the input impedance in Figure 2.11 is

$$Z_{in} = \frac{1}{Y_{in}} = \frac{Y_p}{J^2} = Y_p. \tag{2.22}$$

The equivalence in Figure 2.10(a) holds. That is,

$$Z_{in} = Y_p = Z_s. \tag{2.23}$$

which means

$$j\omega C\left(1 - \frac{\omega_o^2}{\omega^2}\right) = j\omega L'\left(1 - \frac{\omega_o^2}{\omega^2}\right)$$

$$L' = C \tag{2.24}$$

Similarly, for Figure 2.10(b),

$$Y_{in} = \frac{1}{Z_{in}} = \frac{Z_s}{K^2} = Z_s = Y_p. \tag{2.25}$$

Thus,

$$L = C' \tag{2.26}$$

Notice that (2.24) and (2.26) exists only when J=1. When it comes to practical realization, using all shunt or series connected resonators can be more convenient.

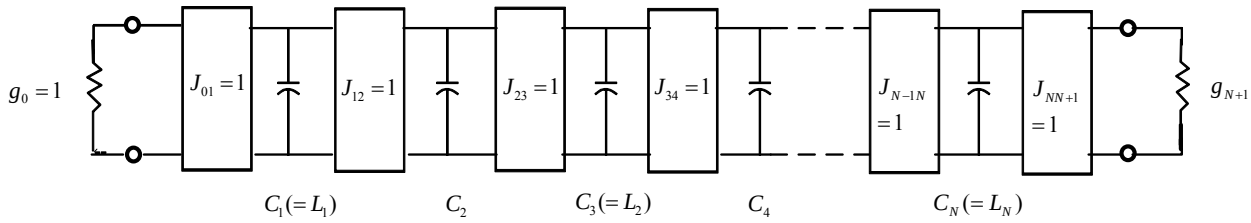

Figure 2.12 The series inductors can be transformed to shunt capacitor.

At this stage, the dual-network theorem is applied to add unit inverters to the network to transform the series inductors to shunt capacitors. Assuming N is odd, Figure 2.12 shows the series inductors in Figure 2.8(a) can be transformed to shunt capacitor. From (2.23) and (2.25), indeed, the transformed capacitance would be the same as the inductance before transformation. Now the network is composed of parallel resonant resonators and is known as a lowpass prototype circuit. In addition, these inverters have a one-to-one relationship with the physical coupling elements in the final realized filter structure.

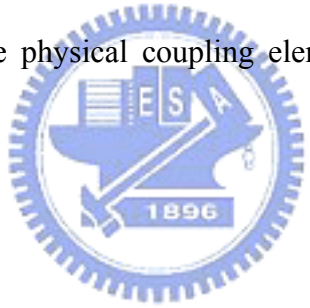

2.2.3 Lowpass to Bandpass Transformation

Now we require a transformation to convert the lowpass prototype into a bandpass filter with arbitrary center frequency and bandwidth. This can be achieved by the following transformation.

$$\Omega \to \frac{1}{W}\left(\frac{\omega}{\omega_0} - \frac{\omega_0}{\omega}\right) = \omega' . \tag{2.27}$$

$\omega_0 = 2\pi \times f_0$, f_0 corresponds to the center frequency of the bandpass filter.

$W = \dfrac{\omega_2 - \omega_1}{\omega_0}$ is the fractional bandwidth.

Ω is the frequency referring to the low-pass filter response which normalizes to its cutoff

frequency.

From Figure 2.13, the resulting admittance for one of the parallel resonators should be as follows:

For $j = 1, 2, 3...N$,

$$Y_{jr} = jB_{jr} = j\omega C_{jr} + \frac{1}{j\omega L_{jr}}. \tag{2.28}$$

On the other hand, Figure 2.12 shows that

$$jB_{jr} = j\omega' C_j = jC_j \frac{1}{W}\left(\frac{\omega}{\omega_0} - \frac{\omega_0}{\omega}\right). \tag{2.29}$$

From (2.28) and (2.29), we acquire

$$\begin{aligned} C_{jr} &= \frac{C_j}{\omega_0 W} = \frac{g_j}{\omega_0 W}, \\ L_{jr} &= \frac{W}{\omega_0 C_j} = \frac{W}{\omega_0 g_j}. \end{aligned} \tag{2.30}$$

which is the bandpass transformation for the circuit in Figure 2.8(a).

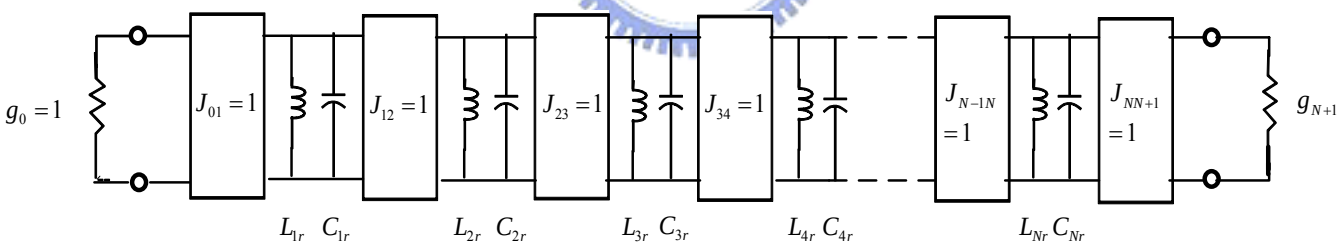

Figure 2.13 Lowpass to bandpass transformation.

2.2.4 Slope Parameters

In this part, we introduce the susceptance slope parameter "b" to represent the parallel resonant resonators. The definition is the same as (2.10). As Figure 2.14 depicted, we obtain the admittance inverter parameters presented with the slope parameters,

normalized source and load impedances, R_S and R_L.

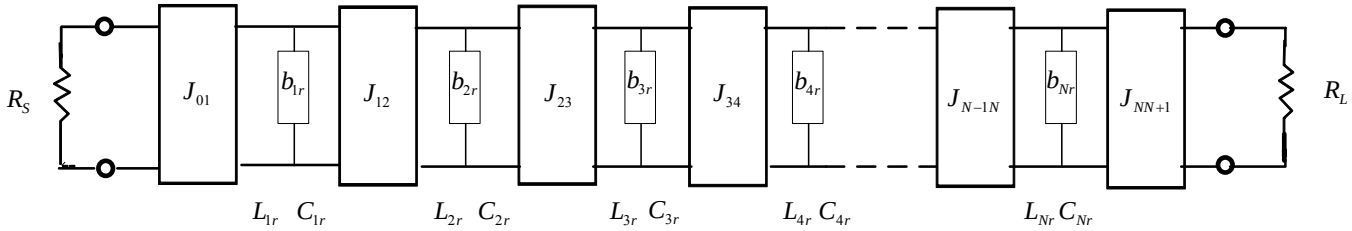

Figure 2.14 Parallel resonances are represented with slope parameters.

The admittance inverter parameters J_S are

$$J_{01} = \sqrt{\frac{b_{1r} G_S}{g_0 g_1}} \cdot \sqrt{W},$$

$$J_{N,N+1} = \sqrt{\frac{b_{Nr} G_L}{g_N g_{N+1}}} \cdot \sqrt{W},$$

$$J_{j,j+1} = \sqrt{\frac{b_j b_{j+1}}{g_j g_{j+1}}} \cdot \sqrt{W}, \quad \text{for} \quad j = 1,2,3\ldots N-1 \tag{2.31}$$

where

$$G_S = \frac{1}{R_S}, G_L = \frac{1}{R_L}, b_{jr} = \frac{\omega_0}{2} \frac{dB_{jr}}{d\omega}\bigg|_{w=w_0} = \omega_0 C_{jr}. \tag{2.32}$$

Similarly, for any resonator exhibits a series-resonance type, we calculate the reactance slope parameter "x" as the definition

$$x = \frac{\omega_0}{2} \frac{dX}{d\omega}\bigg|_{w=w_0} \tag{2.33}$$

where X is the total reactance of the resonant circuit, and we can obtain the K inverters as follows:

$$K_{01} = \sqrt{\frac{x_{1r} R_S}{g_0 g_1}} \cdot \sqrt{W},$$

$$K_{N,N+1} = \sqrt{\frac{x_{Nr} R_L}{g_N^{20} g_{N+1}}} \cdot \sqrt{W},$$

$$K_{j,j+1} = \sqrt{\frac{x_j x_{j+1}}{g_j g_{j+1}}} \cdot W. \qquad \text{for} \quad \text{j = 1,2,3…N-1} \qquad (2.34)$$

2.3 Dishal's Method

Any narrow-band, lumped-element, or distributed bandpass filter could be described by three fundamental variables: the synchronous tuning frequency of each resonator f_0, the coupling coefficient between adjacent resonators k, and the singly loaded or external Q of the first and last resonators, Q_{ex}, as shown in Figure 2.15.

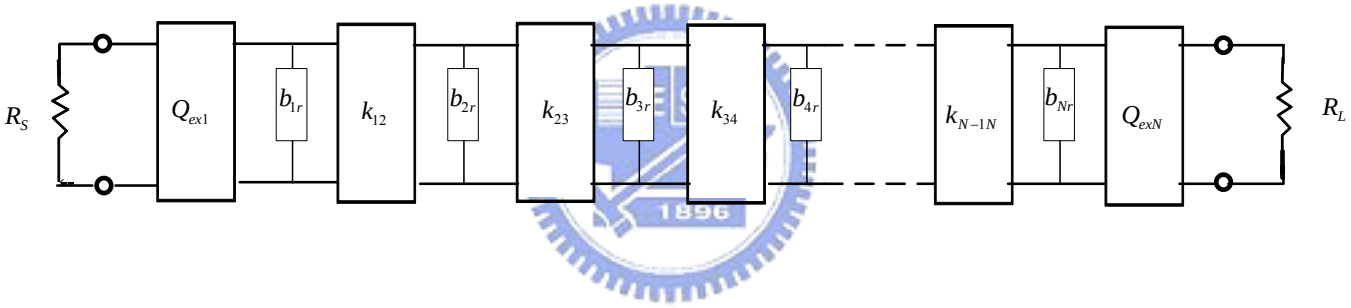

Figure 2.15 Parameters Q_{ex} and coupling coefficients k.

When the bandpass filter specification including fractional bandwidth, maximum insertion loss in the passband are decided, we can derive the required k_S and Q_{exs} from a few simple equations [13].

$$k_{j,j+1} = \frac{J_{j,j+1}}{\sqrt{b_{jr} b_{j+1r}}} = \frac{W}{\sqrt{g_j g_{j+1}}} \quad \text{for} \quad j = 1,2,3...N-1 \qquad (2.35)$$

$$Q_{ex1} = \frac{b_{j1}}{\frac{J^2_{01}}{G_S}} = \frac{g_0 g_1}{W}, \qquad (2.36)$$

$$Q_{exN} = \frac{b_{N+1}}{\frac{J^2_{N,N+1}}{G_L}} = \frac{g_N g_{N+1}}{W}. \tag{2.37}$$

where W is the fractional bandwidth. Q_{ex1} represents the coupling between R_S and the first resonator whereas Q_{exN} is similar but for the last resonator. $k_{j,j+1}$ corresponds to the coupling between the j_{th} and $j+1_{th}$ resonators. For example, Table 2.1 and 2.2 can be constructed with ripple level 0.1 dB ,

Table 2.1 Parameters of coupling coefficients and Qext's with N=2, Lr=0.1dB.

Fractional bandwidth	*k12*	*Qext*
0.04	0.0552	21.0767
0.05	0.069	16.8614
0.06	0.0829	14.0511
0.07	0.0967	12.0438
0.08	0.1105	10.5384
0.09	0.1243	9.3674
0.1	0.1381	8.4307

Table 2.2 Parameters of coupling coefficients and Qext's with N=3, Lr=0.1dB

Fractional bandwidth	k12	k12	*Qext*
0.04	0.0368	0.0368	25.7896
0.05	0.046	0.046	20.6317
0.06	0.0551	0.0551	17.1931
0.07	0.0643	0.0643	14.7369
0.08	0.0735	0.0735	12.8948
0.09	0.0827	0.0827	11.4621
0.1	0.0919	0.0919	10.3159

2.4 Coupled Line Theory

A “coupled line” configuration consists of two transmission lines placed parallel to each other and in close proximity. In such a configuration, there is a continuous coupling between the electromagnetic fields of the two lines. Coupled lines are utilized extensively as basic elements for directional couplers, filters, and a variety of other useful circuits.

Because of the coupling of electromagnetic fields, a pair of coupled lines can support two different modes of propagation. These modes have different characteristic impedances. The velocity of propagation of these two modes is equal when the lines are embedded in a homogeneous dielectric medium (as, for example, in a triplate stripline structure). This is a desirable property for the design of circuits such as directional couplers and filters. However, for transmission lines such as coupled microstrip lines, the dielectric coupled microstrip lines, the dielectric medium is not homogeneous since part of the field extends into the air above the substrate. This fraction is different for the two modes of coupled lines. Consequently, the effective dielectric constants as well as the phase velocities are not equal for two modes. This unequal modal phase velocities may deteriorate the performance of circuits using these types of coupled lines.

When two conductors of a coupled line pair are identical we have a symmetrical configuration. This symmetry is very useful for simplifying the analysis and design of such coupled lines. If the two lines do not have the same impedance, the configuration is called asymmetric.

Coupled transmission lines are usually assumed to operate in the TEM mode, which is rigorously valid for stripline structures and approximately valid for microstrip structures. For that reason, the properties of coupled lines can be determined from the self- and mutual inductors and capacitances for the lines.

2.4.1 even-and odd- mode approach[17]

Coupled microstrip structures are characterized by the characteristic impedances (or admittances) and phase velocities for the two modes. For simplicity, we will restrict our attention to the case of symmetric coupled lines, that is, identical lines of equal characteristic impedances. The analysis of coupled microstrip lines for these characteristics can be carried out by the even- and odd-mode method which is the most convenient way of describing the behavior of symmetrical coupled lines. In this method, wave propagation along a coupled pair of lines is expressed in terms of two modes corresponding to an even or an odd symmetry about a plane that can, therefore, be replaced by a magnetic or electric wall for the purpose of analysis.

Furthermore, static capacitances for the coupled line geometry may be used to give simpler equations for the mode impedances and effective dielectric constants. Therefore, even- and odd-mode capacitances for the symmetric coupled lines are obtained first.

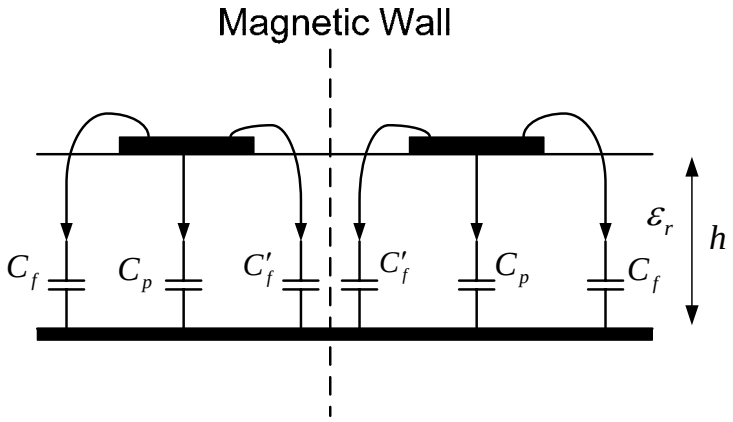

(a)

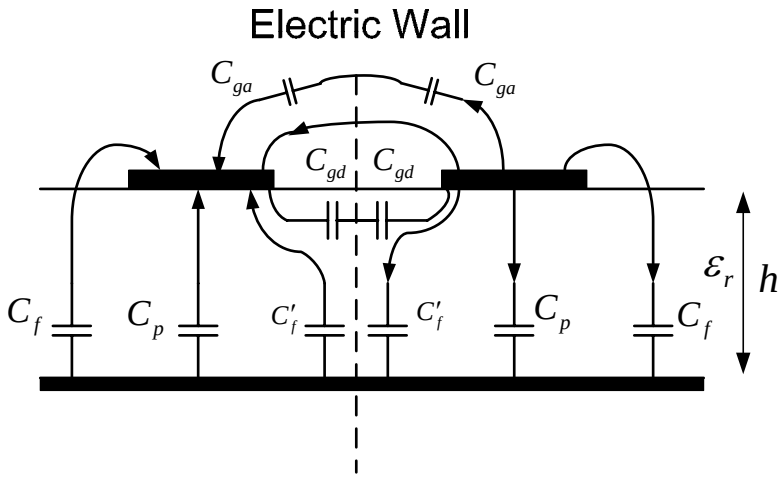

(b)

Figure 2.16 Analysis of coupled microstrip lines in terms of capacitances: (a) even-mode capacitance. (b) odd-mode capacitance.

As shown in Figure 2.16(a) the even-mode capacitance C_e can be divided into three capacitance; that is,

$$C_e = C_p + C_f + C'_f \tag{2.38}$$

C_p denotes the parallel plate capacitance between the strip and the ground plane. C_f is the fringe capacitance at the outer edge of the strip. It is the fringe capacitance of a single microstrip line and can be evaluated from the capacitance of the microstrip line and the value of C_p. The term C'_f accounts for the modification of fringe capacitance C_f of a single line due to the presence of another line.

The odd-mode capacitance C_o can be decomposed into five constituents $C_{f,}$ $C_{p,}$ $C'_{f,}$ C_{gd} and C_{ga} as shown in Figure 2.16(b) ; that is,

$$C_o = C_p + C_f + C'_f + C_{gd} + C_{ga} \tag{2.39}$$

Expressions for $C_{p,}$ $C_{f,}$ and $C'_{f,}$ are the same as those given earlier in the case of even mode. The capacitance C_{gd} may be calculated from the corresponding coupled

stripline geometry with the spacing between the ground planes given by $2h$. The capacitance C_{ga} describes the gap capacitance in air.

Effective dielectric constants $\varepsilon^e{}_{re}$ and $\varepsilon^o{}_{re}$ for even and odd modes, respectively, can be obtained from C_e and C_o by using the relations

$$\varepsilon^e{}_{re} = \frac{C_e}{C^a{}_e}, \tag{2.40}$$

$$\varepsilon^e{}_{re} = \frac{C_o}{C^a{}_o}. \tag{2.41}$$

$C^a{}_e$ and $C^a{}_o$ are the capacitances for the even- and odd-mode capacitances for the coupled microstrip line with air as dielectric. Further, Accurate closed-form expressions for $\varepsilon^e{}_{re}$ and $\varepsilon^o{}_{re}$ are also available in [17].

On the other hand, self-and mutual inductors and capacitances can be derived with $C_e(\varepsilon_r)$, $C_o(\varepsilon_r)$, $C^a{}_e$ and $C^a{}_o$. The characteristic impedances Z_{oe}, Z_{oo} can be written as [17]

$$Z_{oe} = \frac{\omega}{\beta_e}\frac{\mu_0\varepsilon_0}{C^a_e}, \tag{2.42}$$

$$Z_{oe} = \frac{\omega}{\beta_o}\frac{\mu_0\varepsilon_0}{C^a_o}. \tag{2.43}$$

with

$$\beta_{e,o} = \omega\sqrt{\mu_0\varepsilon_0}\sqrt{\frac{C_{e,o}(\varepsilon_r)}{C^a{}_{e,o}}}. \tag{2.44}$$

or

$$Z_{oe} = (v\sqrt{C^a_e C_e}) \tag{2.45}$$

$$Z_{oe} = (v\sqrt{C^a_o C_o}) \tag{2.46}$$

where v is the velocity of light.

2.5 J- and K-inverters with distributed circuits

This section considers several types of coupled transmission lines with arbitrary lengths and their equivalent circuits. For designing bandpass filters with SIR in which lines are coupled in parallel or antiparallel, it's necessary to find the relationship between even and odd mode impedance/admittance in the coupled lines and the impedance/admittance inverter parameters. With the equivalent circuits, we can design the bandpass filter more easily. In this section, the equivalent transmission-line circuit will be represented by two-wire lines. In each case, the characteristic impedance or admittance of the transmission line is shown, together with the electrical length θ. Meanwhile, the unsymmetrical-coupled line with different widths is also discussed [12].

2.5.1 Equivalent Circuit of Parallel-Coupled Line

Figure 2.18(a) shows the parallel-coupled section generalized to cover the case where the two lines may be of different widths and its equivalent circuit is shown in Figure 2.18(b) [14], [15]. The parameter v refers to propagation velocity in media while C_a, C_b, and C_{ab} are the line capacitances per unit length as defined in Figure 2.17. Note that C_a is the capacitance per unit length between Line a and ground. C_b is the capacitance per unit length between Line b and ground while C_{ab} is the capacitance per unit length between Line a and Line b. The definition of L_a, L_b are the self-inductances per unit length of Line a and b, while L_{ab} is the mutual inductance per unit length between the parallel-coupled lines. Since the line capacitances are more convenient to deal with, the line impedances of the equivalent open-wire circuit are also given in terms of C_a, C_b, and C_{ab}. From Figure 2.18(b), it's apparent that when θ is 90 degrees, the series stubs act like the series resonant resonators.

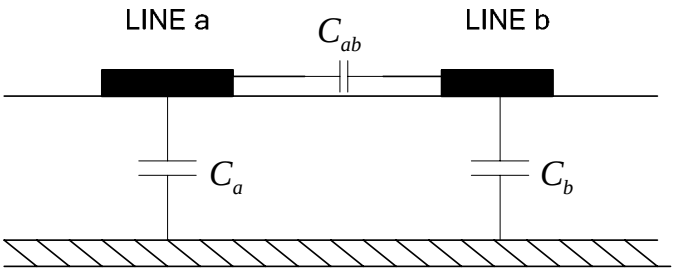

Figure 2.17 An unsymmetrical pair of parallel-coupled lines. C_a, C_b and C_{ab} are line capacitances per unit length.

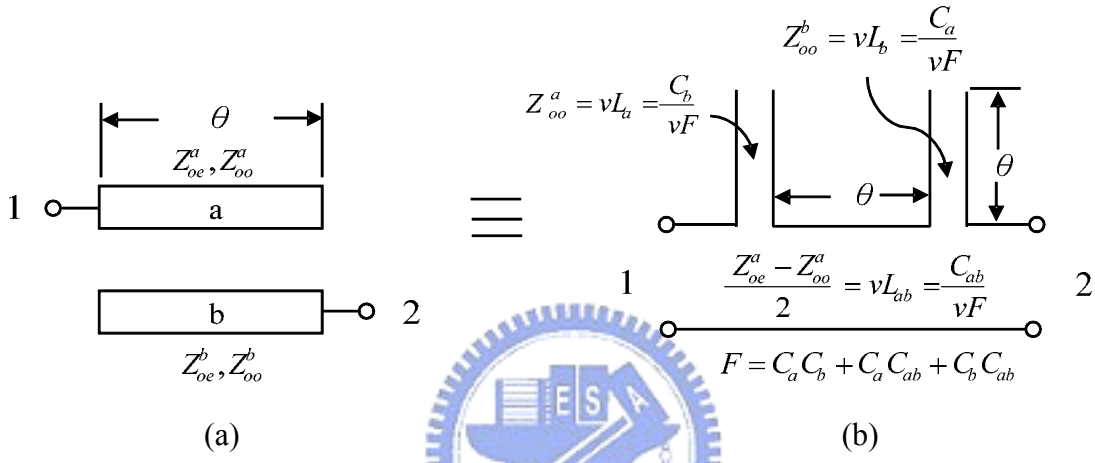

Figure 2.18 An unsymmetrical parallel-coupled line and its equivalent circuit.

On the other hand, the symmetric parallel-coupled line relating to the lines with the same width is depicted in Figure 2.19(a). In this case, $Y_{oe}^{\ a} = Y_{oe}^{\ b} = Y_{oe}$ and $Y_{oo}^{\ a} = Y_{oo}^{\ b} = Y_{oo}$. It's clear to see that the even- and odd-mode admittance can be simplified as Y_{oe}, Y_{oo}, and the equivalent circuit is expressed by two single transmission lines of electrical length θ, admittance Y_0 and admittance inverter parameter J, as shown in Figure 2.19(b) .

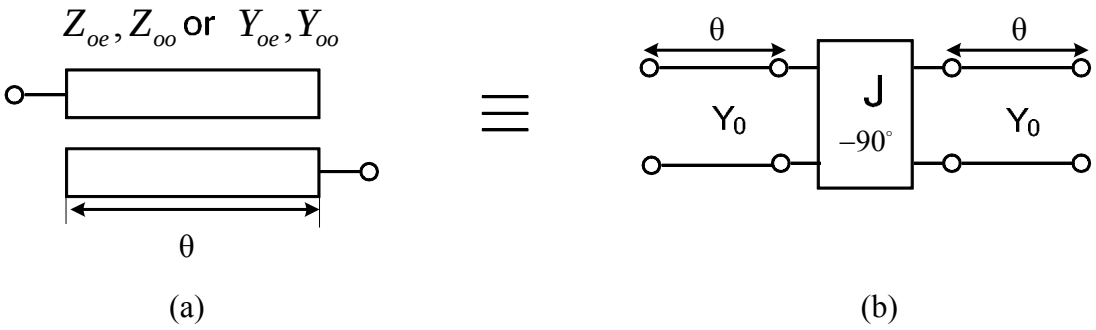

Figure 2.19 A symmetrical parallel-coupled line and its equivalent circuit.

The ABCD matrix for Figure 2.19(a) and (b) can be expressed as

$$[F_a]=\begin{bmatrix} \dfrac{Y_{oo}+Y_{oe}}{Y_{oo}-Y_{oe}}\cos\theta & j\dfrac{(Y_{oo}-Y_{oe})^2+(Y_{oo}+Y_{oe})^2\cos^2\theta}{2(Y_{oo}-Y_{oe})\sin\theta}\cdot\dfrac{1}{Y_{oo}Y_{oe}} \\ j\dfrac{2\sin\theta}{Y_{oo}-Y_{oe}}\cdot Y_{oo}Y_{oe} & \dfrac{Y_{oo}+Y_{oe}}{Y_{oo}-Y_{oe}}\cdot\cos\theta \end{bmatrix}, \tag{2.47}$$

$$[F_b]=\begin{bmatrix} \left(\dfrac{J}{Y_0}+\dfrac{Y_0}{J}\right)\sin\theta\cos\theta & j\dfrac{1}{Y_0}\left(\dfrac{J}{Y_0}\sin^2\theta-\dfrac{Y_0}{J}\cos\theta\right) \\ jY_0\left(\dfrac{Y_0}{J}\sin^2\theta-\dfrac{J}{Y_0}\cos^2\theta\right) & \left(\dfrac{J}{Y_0}+\dfrac{Y_0}{J}\right)\sin\theta\cos\theta \end{bmatrix}. \tag{2.48}$$

Then equalizing each corresponding matrix element, we can obtain [8]

$$\frac{Y_{oe}}{Y_0}=\frac{1-\left(\dfrac{J}{Y_0}\right)^2\cot^2\theta}{1+\left(\dfrac{J}{Y_0}\right)^2\csc\theta+\left(\dfrac{J}{Y_0}\right)^2}, \tag{2.49}$$

$$\frac{Y_{oo}}{Y_0}=\frac{1-\left(\dfrac{J}{Y_0}\right)^2\cot^2\theta}{1-\left(\dfrac{J}{Y_0}\right)^2\csc\theta+\left(\dfrac{J}{Y_0}\right)^2}. \tag{2.50}$$

In Figure 2.20, placing short-circuits on diagonal ports instead, the dual situation of the circuit in Figure 2.18 holds. Similarly, the even- and odd-mode admittances are

depicted and the electrical length is θ. The equivalent two-wire circuit is shown in Figure 2.20(b) accordingly with the parameters defined in Figure 2.18 [14],[15]. In this case, when θ is 90 degrees, each of the series stub acts like a resonator of parallel resonance.

Meanwhile, in the case of symmetrical coupled lines, the circuit schematic diagram is simplified as Figure 2.21(a) while the even- and odd-mode impedances are represented as Z_{oe}, Z_{oo}. This section can be approximately modeled by the equivalent circuit shown in Figure 2.21(b) including an impedance inverter parameter K together with two single transmission lines of electrical length θ and impedance Z_0, connected in series on both sides [12].

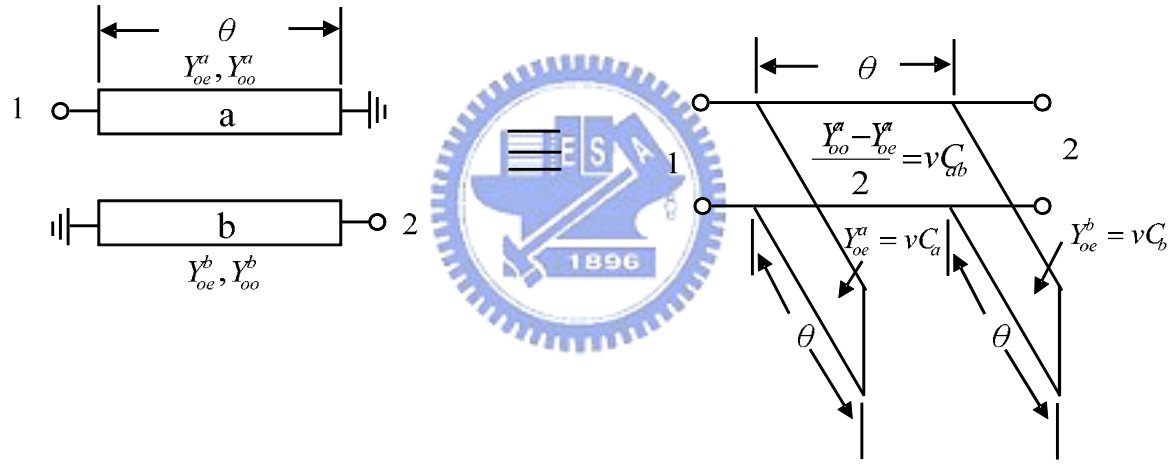

(a) (b)

Figure 2.20 An unsymmetrical parallel-coupled line and its equivalent circuit.

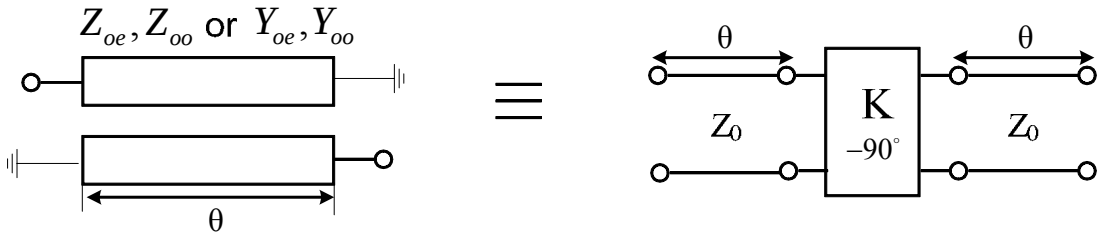

(a) (b)

Figure 2.21 A symmetrical parallel-coupled line and its equivalent circuit.

Similar, equating the ABCD matrixes in Figure 2.21, design formulas correspond to Z_{oe}, Z_{oo} can be derived as

$$\frac{Z_{oe}}{Z_0} = \frac{1-\left(\frac{K}{Z_0}\right)^2 \cot^2\theta}{1-\left(\frac{K}{Z_0}\right)\csc\theta+\left(\frac{K}{Z_0}\right)^2}, \tag{2.51}$$

$$\frac{Z_{oo}}{Z_0} = \frac{1-\left(\frac{K}{Z_0}\right)^2 \cot^2\theta}{1+\left(\frac{K}{Z_0}\right)\csc\theta+\left(\frac{K}{Z_0}\right)^2}. \tag{2.52}$$

2.5.2 Equivalent Circuit of Antiparallel-Coupled Line

Different from the parallel-coupled lines described in previous section 2.4.1, we introduce the antiparallel coupled-line circuits which are terminated with short circuits or open circuits on the same side. The circuit scheme shown in Figure 2.22(a) is the asymmetrical coupled line with an open-circuit termination on the same side while the equivalent two-wire circuit is shown in Figure 2.22(b). The even- and odd-mode impedance with electrical length θ are depicted. When θ is 90 degrees, the circuit operates like an all-stop structure.

For a symmetrical case, Figure 2.23(a) illustrates even- and odd-mode admittance Y_{oe}, Y_{oo} of the antiparallel coupled-line section with electrical length θ. The equivalent circuit is shown in Figure 2.23(b) which is expressed by an admittance inverter parameter J as well as two open stubs with electrical length θ and impedance Z_0 which shunted on both of its sides [12].

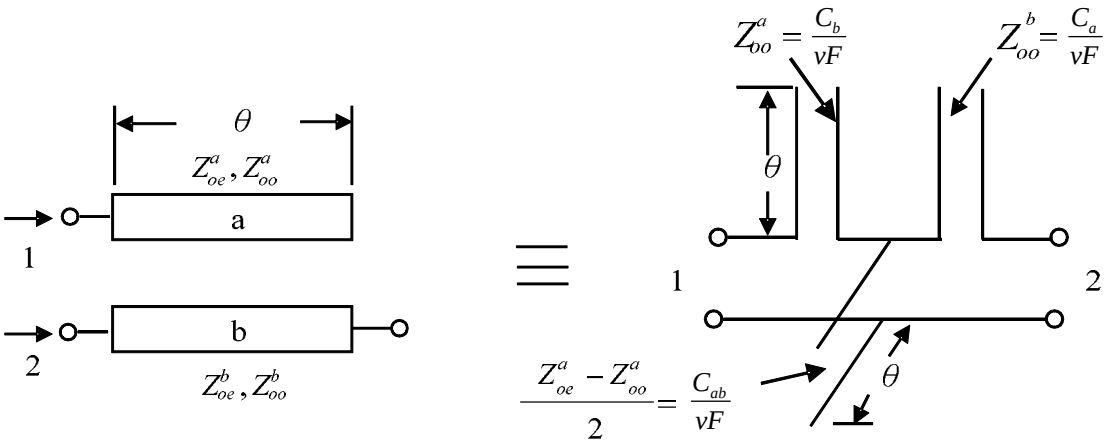

(a) (b)

Figure 2.22 An unsymmetrical parallel-coupled line and its equivalent circuit.

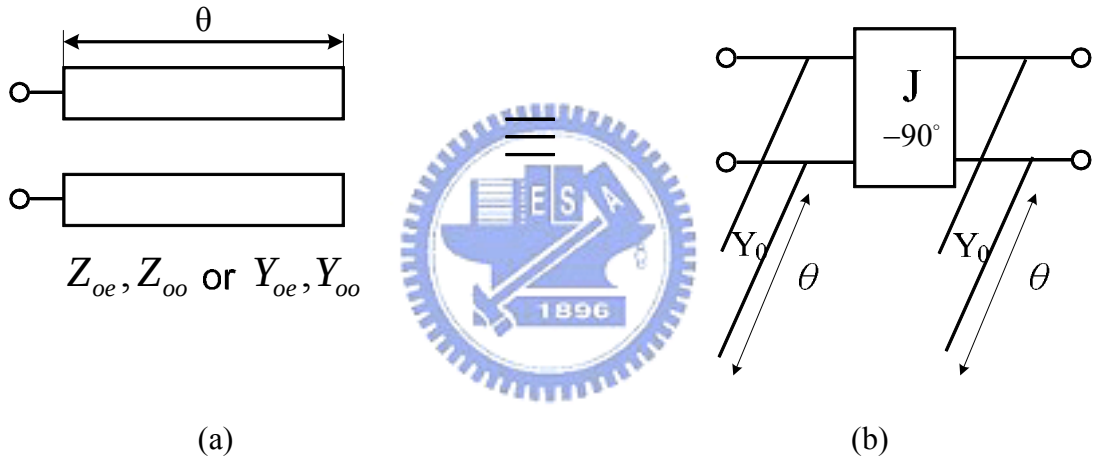

(a) (b)

Figure 2.23 A symmetrical parallel-coupled line and its equivalent circuit.

Similar with the previous section, we can derive the formulas relate to Y_{oe} and Y_{oo} as follows:

$$\frac{Y_{oo}}{Y_0} = 1 + \frac{J}{Y_0}\cot\theta, \tag{2.53}$$

$$\frac{Y_{oe}}{Y_0} = 1 - \frac{J}{Y_0}\cot\theta. \tag{2.54}$$

It's noted that when θ is equal to 90 degrees that means $Y_{oe} = Y_{oo}$, no coupling exists in the coupled line. Therefore, (2.53) and (2.54) are applicable except that θ is 90 degrees.

On the other hand, in Figure 2.24(a), the coupled line shows two ports on the same

side are shorted which is the dual of the circuit in Figure 2.22. The equivalent circuit is expressed as Figure 2.24(b). In this case, when θ is 90 degrees, the circuit operates like an all-stop structure which is similar with that in Figure 2.22.

Futhermore, if the coupled line is symmetric , it's obvious that $Y_{oe}{}^{a} = Y_{oe}{}^{b} = Y_{oe}$ and $Y_{oo}{}^{a} = Y_{oo}{}^{b} = Y_{oo}$ as shown in Figure 2.25(a). The corresponding equivalent circuit shown in Figure 2.25(b) consists of two shunt stubs with short-circuit terminations on both sides and an admittance inverter between them. [12]

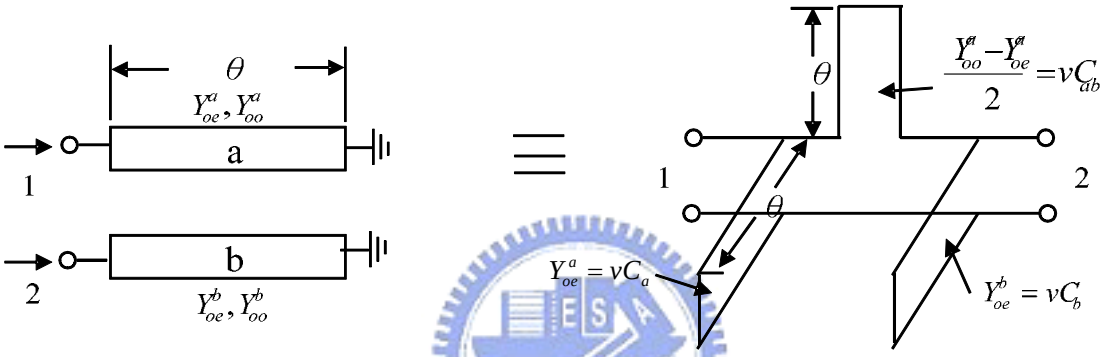

(a) (b)

Figure 2.24 An unsymmetrical antiparallel-coupled line and its equivalent circuit.

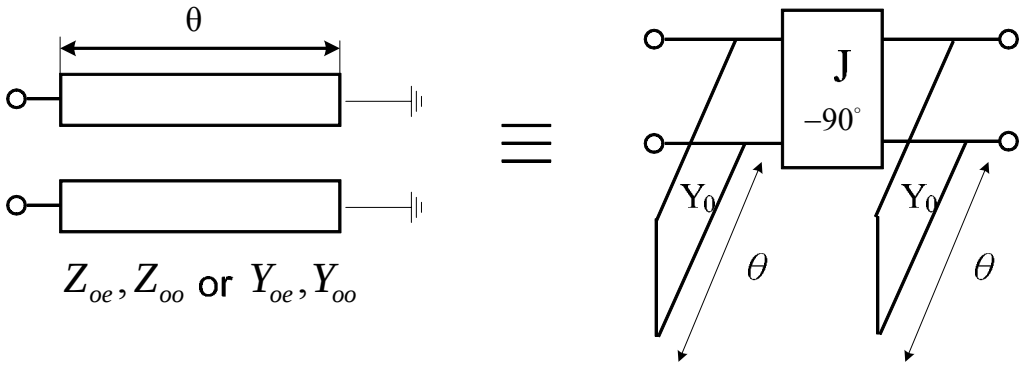

(a) (b)

Figure 2.25 A symmetrical antiparallel-coupled line and its equivalent circuit.

Finally, we can acquire the formulas relating to Y_{oo} and Y_{oe},

$$\frac{Y_{oo}}{Y_0} = 1 + \frac{J}{Y_0}\tan\theta, \tag{2.55}$$

$$\frac{Y_{oe}}{Y_0} = 1 - \frac{J}{Y_0}\tan\theta. \tag{2.56}$$

When θ is equal to 90 degrees, Y_{oo} and Y_{oe} tend to be infinite. Therefore, the design formulas in Figure 2.25 is not suitable for the case $\theta = \pi/2$.

2.6 Second-Order Gap Coupling Bandpass Filter

In this section, we introduce an example for the second-order bandpass filter using the theory discussed in previous sections. First, utilizing the theory about $\lambda/2$ SIR described in Section 2.1.2, we can easily design the SIR by giving an impedance ratio R and the electrical length θ_b. For example, choose $Z_b = 50ohm$, $Z_a = 70ohm$ ($R<1$) and $\theta_b = 60^o$ with center frequency 3GHz, 6% bandwidth and 0.1 dB ripple. From (2.3), we can obtain $\theta_a = 22.41^o$.

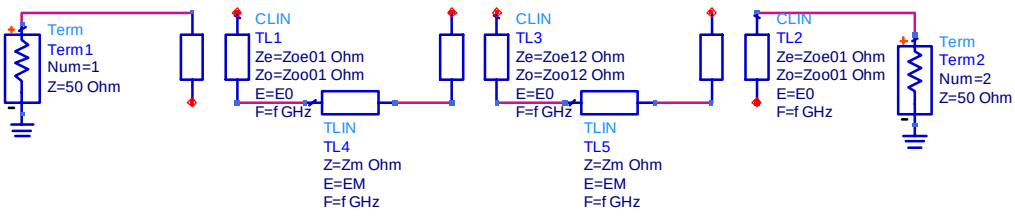

Figure 2.26 Circuit configuration of the second-order gap coupling filter.

Figure 2.26 shows the circuit scheme of the filter in ADS. The first and third sections

correspond to open-circuited parallel coupled-line. Therefore, we can approximately utilize the equivalence shown in Figure 2.19. On the other hand, the second coupled section belongs to the open-circuited antiparallel coupled-line discussed in Section 2.5.2, so that the equivalence shown in Figure 2.23 can be used here. The consideration about θ_b relating to the antiparallel and parallel coupled-line sections in the bandpass filter is that θ_b should be shorter then $\pi/2$ due to the accuracy about design equations. Now, we can construct the equivalent circuits with admittance inverters as depicted in Figure 2.27. The second-order coupled-line filter is equivalent to several admittance inverters separated by transmission-line sections which is actually the $\lambda/2$-type SIR shown in Figure 2.4(a).

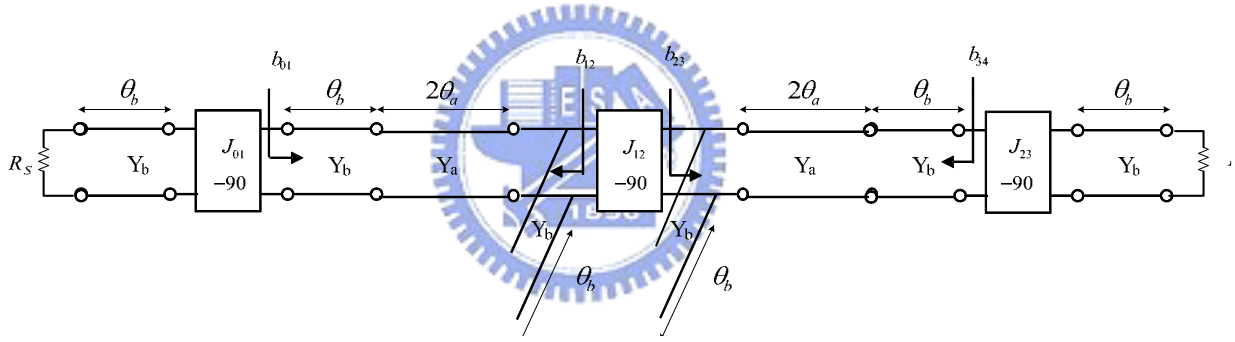

Figure 2.27 The overall equivalent circuit of the second-order gap coupling filter.

Since the SIR structure exists the parallel type of resonance physically, we can then use the theory introduced in Section 2.2 that all the resonators can be represented by the susceptance slope parameter "b". Thus, we are going to calculate the parameters b. Figure 2.27 shows that b_{01} and b_{34} are the slope parameters seen by J_{01} and J_{34} looking into the resonator whereas b_{12} and b_{23} are those seen by J_{12} looking into the resonator on both of its sides. Obviously, $b_{01} = b_{34}$ and $b_{12} = b_{23}$. Therefore we only need to derive b_{01} and b_{12}. From (2.9) and (2.10), b_{01} can be obtained easily as follows,

for $R = \frac{Z_b}{Z_a}$, the input admittance seen by inverter J_{01} looking into the resonator is,

$$Y_{01} = jY_b \frac{2(R\tan\theta_a + \tan\theta_b)(R - \tan\theta_b \tan\theta_a)}{R(1-\tan^2\theta_b)(1-\tan^2\theta_a) - 2(1+R^2)\tan\theta_b \tan\theta_a} = jB_{01} \tag{2.57}$$

$$b_{01} = \frac{\omega_0}{2}\frac{dB_{01}}{d\omega}\bigg|_{\omega=\omega_0}$$

$$= \frac{Y_b}{2}\frac{\theta_b \tan 2\theta_a \times (R^2 \csc^2\theta_b + \sec^2\theta_b) + 2\theta_a \sec^2 2\theta_a \times (-R^2\cot\theta_b + \tan\theta_b)}{\tan 2\theta_a \times (1+R^2) + R(\tan\theta_b - \cot\theta_b)}. \tag{2.58}$$

where B_{01} is the susceptance component of the input admittance. In the case of UIR (uniform impedance resonator), (2.58) can be simplified as follows:

$$b_{01} = \frac{\pi Y_b}{2}. \tag{2.59}$$

Next, assume the input admittance seen from J_{12} towards left is Y_{12} derived as

$$Y_{12} = jY_b \frac{R^2 - \tan^2\theta_b + 2R\tan\theta_b \cot 2\theta_a}{R\cot 2\theta_a - \tan\theta_b} = jB_{12} \tag{2.60}$$

Then,

$$b_{12} = \frac{\omega_0}{2}\frac{dB_{12}}{d\omega}\bigg|_{\omega=\omega_0}$$

$$= \frac{Y_b}{2}\frac{\theta_b \sec^2\theta_b (2R\cot 2\theta_a - 2\tan\theta_b) - 4R\theta_a \tan\theta_b \csc^2 2\theta_a}{R\cot 2\theta_a - \tan\theta_b} \tag{2.61}$$

Also, in the case of UIR, (2.61) can be simplified as follows:

$$b_{01} = \frac{\pi Y_b}{2}\sec^2\theta_b. \tag{2.62}$$

Therefore, given the impedance ratio and electrical length of SIR, the slope parameters from b_{01} to b_{34} shown in Figure 2.27 can be obtained definitely.

From (2.31) and (2.32), choose R_S and R_L to be port impedance $50ohm$, with the calculated slope parameters b, we can find the inverter parameters J_{01}, J_{12} and J_{23}.

By symmetry, $J_{12}=J_{23}$. While J_{01}, J_{12} and J_{23} are available and $Y_0=\frac{1}{50}\Omega^{-1}$, with (2.49) , (2.50) , (2.53) and (2.54), the even- and odd-mode impedances for each of the coupled-line section can then be derived.

On the other hand, similar procedure can be used to design the bandpass filter using the coupled-line section with short-circuit terminations shown in Figure 2.21 and Figure 2.25. That is, the first and third coupled-line sections are replaced with the parallel coupled line depicted in Figure 2.21(a). Meanwhile, the second coupled-line section is substituted for the antiparallel coupled-line circuit in Figure 2.25(a). Furthermore, the $\lambda/2$ SIR is considered as the short-end type SIR in Figure 2.5 which is different from the SIR used in Type I filter. Figure 2.28 illustrates the overall circuit scheme.

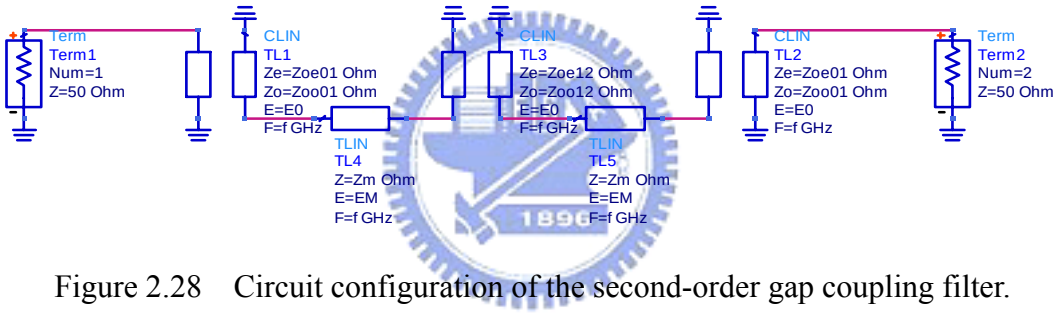

Figure 2.28 Circuit configuration of the second-order gap coupling filter.

Finally, cascading the equivalent circuits of parallel and antiparallel coupled lines, the complete equivalent circuits of the filter can be constructed as Figure 2.29.

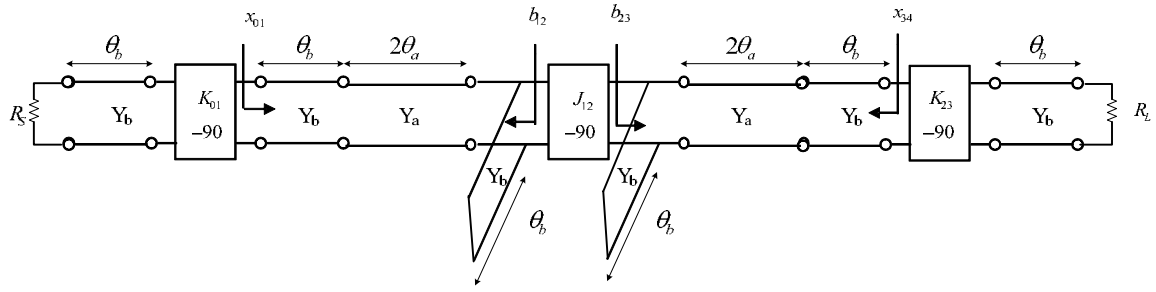

Figure 2.29 The overall equivalent circuit of the second-order gap coupling filter.

Different from Type I filter, the structure consists of two impedance inverters K_{01}

and K_{34} for the first and third coupling as well as an admittance inverter J_{12} in the centre. When looking into the resonator by K_{01}, the resonator performs series resonance; therefore, it's reasonable to use the reactance slope parameter x mentioned in (2.33) to represent the resonator. The same situation occurs when looking towards the resonator on the right-hand side by K_{34}. On the contrary, seen by the inverter J_{12} into the left or right till the K inverters, the parallel resonance exists where the slope parameter is utilized. Figure 2.29 shows that x_{01} and x_{34} are the reactance parameters seen by K_{01} and K_{34} whereas b_{12} and b_{23} are seen by J_{12} looking into the resonator on both of its sides. By symmetry, $x_{01} = x_{34}$ and $b_{12} = b_{23}$. Therefore, we only need to calculate x_{01} and b_{12} respectively. From (2.9) and (2.10), x_{01} can be obtained easily as follows,

for $R = \dfrac{Z_b}{Z_a}$, the input impedance seen by K_{01} looking towards the resonator is

$$\begin{aligned} Z_{01} &= jZ_b \frac{-2R\tan\theta_b - \tan 2\theta_a + R^2 \tan^2\theta_b \tan 2\theta_a}{R - R^2 \tan\theta_b \tan 2\theta_a - R\tan^2\theta_b - \tan\theta_b \tan 2\theta_a} \\ &= jZ_b \frac{-2R\tan\theta_b - \tan 2\theta_a + R^2 \tan^2\theta_b \tan 2\theta_a}{R(1-\tan^2\theta_b) - (1+R^2)\tan\theta_b \tan 2\theta_a} \\ &= jX_{01} \end{aligned} \tag{2.63}$$

Thus,

$$x_{01} = \frac{\omega_0}{2}\frac{dX_{01}}{d\omega}\bigg|_{\omega=\omega_0}$$

$$= \frac{Z_b}{2}\frac{2\theta_a \sec^2 2\theta_a (1 - R^2\tan^2\theta_b) + 2\theta_b R\sec^2\theta_b (1 - R\tan\theta_b \tan 2\theta_a)}{R(1-\tan^2\theta_b) - \tan\theta_b \tan 2\theta_a (1+R^2)} \tag{2.64}$$

where X_{01} is the reactance component of the input impedance X_{01} seen by inverter J_{01} looking into the resonator.

Further, in the case of UIR, (2.64) can be simplified as follows:

$$x_{01} = \frac{\pi Z_b}{2}. \tag{2.65}$$

Accordingly, assume the input admittance seen by inverter J_{12} looking into the

resonator on the left is Y_{12}.

$$Y_{12} = jY_b \frac{-2R + R^2 \tan\theta_b \tan 2\theta_a - \tan 2\theta_a \cot\theta_b}{R\tan\theta_b + \tan 2\theta_a} = jB_{12} \tag{2.66}$$

Then,

$$b_{12} = \frac{\omega_0}{2} \frac{dB_{12}}{d\omega}\bigg|_{\omega=\omega_0}$$

$$= \frac{Y_b}{2} \frac{\theta_b \tan 2\theta_a (\csc^2\theta_b + R^2 \sec^2\theta_b) - 2\theta_a \sec^2 2\theta_a (\cot\theta_b - R^2 \tan\theta_b)}{R\tan\theta_b + \tan 2\theta_a} \tag{2.67}$$

For the case of UIR, (2.67) can be simplified as

$$b_{12} = \frac{\pi Z_b}{2} \csc^2\theta_b. \tag{2.68}$$

Therefore, given the impedance ratio and electrical length of SIR, x_{01} to x_{34} shown in Figure 2.29 can be calculated. From (2.31) and (2.34), choose R_S and R_L as port impedance $50ohm$, with the parameters b and x, we can find the inverter parameters K_{01}, J_{12} and K_{23}. By symmetry, $K_{01} = K_{23}$.

So far, with K_{01}, J_{12} and K_{23} obtained, the even and odd mode impedance for each coupled-line section can therefore be easily derived from (2.51) , (2.52) , (2.55) and (2.56).

In the following sections, we name the filters discussed above to be the Type I and the Type II filter respectively for convenience.

Chapter3

Second-Order Tapped Coupling Bandpass Filter

3.1 Input/Output Tapping

The coupling between the feed lines and the resonators of a bandpass filter can be performed with gap or tapped coupling. For Type I and Type II filter, the coupling realized with gap coupling. However, it's easy to reach physical limit for gap coupling. Therefore, tapped coupling is proposed in our design. In this case, the singly loaded $Q(Q_{si})$ of a resonator should be calculated. The value of Q_{si} should be determined by the filter specification, which specifies the in-band response. For a tapped resonator, the Q_{si} value is given as [15]

$$Q_{si} = R_L \frac{\omega_0}{2} \frac{dB}{d\omega}\bigg|_{\omega=\omega_0} \tag{3.1}$$

where R_L is the load impedance seen by the resonator looking into the load at the tap point, ω_0 is the center angular frequency, and B is the total susceptance of the resonator seen by the feed line at the tap point.

From the definition of slope parameter b, it's rational that (3.1) can be rewritten as

$$Q_{si} = \frac{b}{G_L} \tag{3.2}$$

where $G_L = 1/R_L$ is the load admittance. It's to be noted that the variation of tapped positions can influence the slope parameter b greatly. To simplify the question, we fix the position of the feed line at the step junction shown in Figure 3.1 and 3.2 so that the

parameter b becomes a specific value when the SIR is designed. From Section 2.3, if both conductors and dielectric substrate are assumed loss free, for the first and last SIRs, the external Q's are given by (2.36) and (2.37). That is, Q_{si} in (3.2) should be in accordance with these external Q's if the SIRs are considered lossless. In other words, given the tapped position, the load impedance of feed lines at the first and last resonator should be determined by the external Q's. That is, in our design, the problem is mainly to find an appropriate load impedance to satisfy (3.2).

In order to obtain the parameter b, it's necessary to derive the total input admittance Y_{in} looking into the resonator at the tap point. Figure 3.1 illustrates the circuit scheme for calculating the parameter Y_{in}. Notice that we fix the tap point at the stepped impedance junction to simplify the calculation.

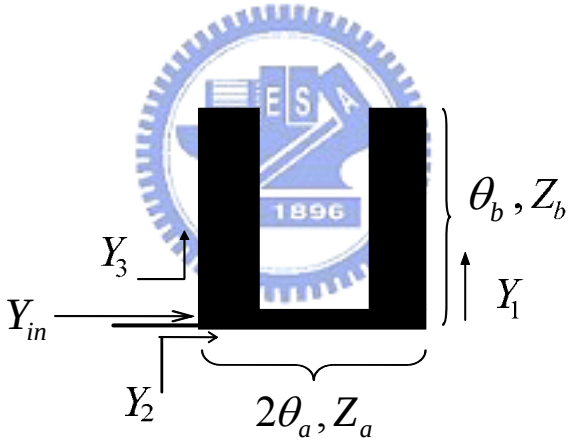

Figure 3.1 The stepped-impedance resonator and tapped line .

First, the input admittances looking into one stub of the SIR resonator terminated with open-circuits are defined as Y_1 and Y_3. It is easily derived as

$$Y_1 = Y_3 = j\frac{1}{Z_b}\tan\theta_b \tag{3.3a}$$

Next, we defined the input admittance seen from the tap point to the open end is Y_2 which includes two sections with a step junction between. It can be calculated as follows,

$$Y_2 = \frac{1}{Z_a}\left(\frac{Z_a + Z_b\cot\theta_b\tan 2\theta_a}{-jZ_b\cot\theta_b + jZ_a\tan 2\theta_a}\right) = \frac{j}{Z_a}\left(\frac{Z_a + Z_b\cot\theta_b\tan 2\theta_a}{Z_b\cot\theta_b - Z_a\tan 2\theta_a}\right) \tag{3.3b}$$

And then, the total input admittance Y_{in} is

$$Y_{in} = Y_2 + Y_3 = \frac{j}{Z_a}\left(\frac{2Z_aZ_b + {Z_b}^2 \cot\theta_b \tan 2\theta_a - {Z_a}^2 \tan\theta_b \tan 2\theta_a}{Z_b(Z_b \cot\theta_b - Z_a \tan 2\theta_a)}\right)$$

$$= \frac{j}{Z_b}\left(\frac{2R + R^2 \cot\theta_b \tan 2\theta_a - \tan\theta_b \tan 2\theta_a}{R\cot\theta_b - \tan 2\theta_a}\right) = jB \tag{3.4}$$

where $R \equiv \frac{Z_b}{Z_a}$.

Finally, the slope parameter can be achieved,

$$b = \frac{\omega_0}{2}\frac{dB}{d\omega}\bigg|_{\omega=\omega_0}$$

$$= \frac{\theta_b}{2}\frac{dB}{d\theta}\bigg|_{\theta=\theta_b}$$

$$= \frac{\theta_b}{2Z_b}\left(\frac{-R^2 \csc^2\theta_b \tan 2\theta_a + 2mR^2 \cot\theta_b \sec^2 2\theta_a - 2m\tan\theta_b \sec^2 2\theta_a - \tan\theta_a \sec^2\theta_b}{R\cot\theta_b - \tan 2\theta_m}\right)$$

$$= \frac{\theta_b}{2Z_b}\left(\frac{2m\sec^2\theta_a(R^2\cot\theta_b - \tan\theta_b) - \tan 2\theta_a(R^2\csc^2\theta_b + \sec^2\theta_b)}{R\cot\theta_b - \tan 2\theta_a}\right) \tag{3.5}$$

During the derivation, we utilize the parameter m which is equal to $\frac{\theta_a}{\theta_b}$.

Similarly, for short-ended λ/2 SIR, the slope parameter can be derived as follows. The total input admittance Y_{in}, seen at the tap point is shown in Figure 3.2. To find the parameter b, we need to calculate Y_{in} firstly.

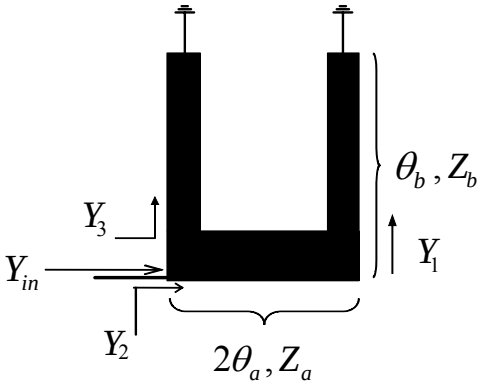

Figure 3.2 The short-end type SIR and tapped line .

Figure 3.2 depicts that the input admittances of the short stubs are Y_1 and Y_3 that can be obtained as

$$Y_1 = Y_3 = -j\frac{1}{Z_b}\cot\theta_1 \tag{3.6}$$

Meanwhile, the input admittance Y_2 in Figure 3.2 becomes

$$Y_2 = \frac{1}{Z_a}\left(\frac{Z_a - Z_b\tan\theta_1\tan 2\theta_m}{jZ_b\tan\theta_1 + jZ_a\tan 2\theta_m}\right) = \frac{j}{Z_a}\left(\frac{Z_b\tan\theta_1\tan 2\theta_m - Z_a}{Z_b\tan\theta_1 + Z_a\tan 2\theta_m}\right) \tag{3.7}$$

Likewise, it's easily to derive Y_{in} as follows

$$Y_{in} = Y_2 + Y_3 = \frac{j}{Z_a}\left(\frac{{Z_b}^2\tan\theta_1\tan 2\theta_m - 2Z_aZ_b - {Z_a}^2\cot\theta_1\tan 2\theta_m}{Z_b(Z_b\tan\theta_1 + Z_a\tan 2\theta_m)}\right)$$

$$= \frac{j}{Z_b}\left(\frac{R^2\tan\theta_1\tan 2\theta_m - 2R - \cot\theta_1\tan 2\theta_m}{R\cot\theta_1 + \tan 2\theta_m}\right) = jB \tag{3.8}$$

Finally, the formulas for the slope parameter b becomes

$$b = \frac{\omega_0}{2}\left.\frac{dB}{d\omega}\right|_{\omega=\omega_0}$$

$$= \frac{\theta_1}{2Z_b}\left(\frac{R^2\sec^2\theta_1\tan 2\theta_m + 2mR^2\tan\theta_1\sec^2 2\theta_m - 2m\cot\theta_1\sec^2 2\theta_m + \tan\theta_m\csc^2\theta_1}{R\tan\theta_1 + \tan 2\theta_m}\right)$$

$$= \frac{\theta_1}{2Z_b}\left(\frac{2m\sec^2\theta_m(R^2\tan\theta_1 - \cot\theta_1) + \tan 2\theta_m(R^2\sec^2\theta_1 + \csc^2\theta_1)}{R\tan\theta_1 + \tan 2\theta_m}\right) \tag{3.9}$$

So far, from (3.5) and (3.9), it's observed that the parameter b is a specific value if the electrical length as well as the impedance ratio of SIRs are available.

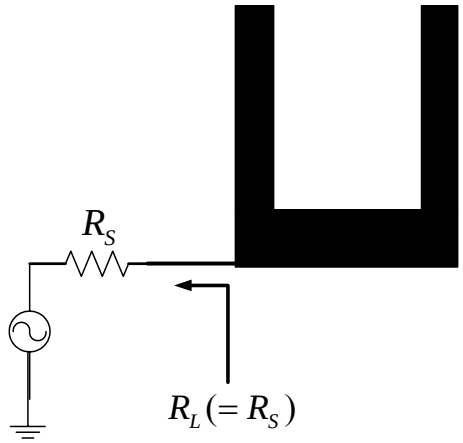

Figure 3.3 The general case of tapping with SIR.

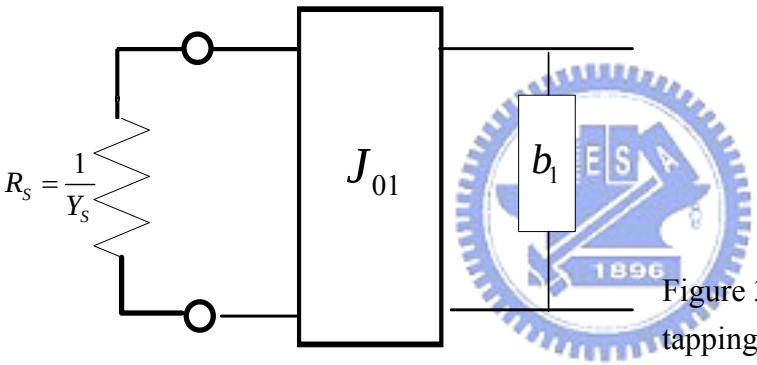

Figure 3.4 The equivalent circuit of tapping with SIR.

Figure 3.3 illustrates the schematic diagram for the general case of tapping where the source impedance is R_s and the SIR is tapped with a feed line directly from the source to the resonator without any transformation. That circuit can be verified as Figure 3.4 where the resonator is represented by the slope parameter b_1 while the function of tapping simply performs as an admittance inverter J_{01}. In fact, the circuit in Figure 3.4 corresponds to the first stage of the circuit in Figure 2.13. Likewise, we already know that from (2.31), J_{01} can be rewritten as

$$J_{01} = \sqrt{\frac{b_1 Y_0}{g_0 g_1}} \cdot \sqrt{W}. \tag{3.10}$$

where W is the fractional bandwidth and Y_0 is the admittance of the resonator.

We now assume the admittance inverter parameter J_{01} is equivalent to the source admittance Y_S which means

$$J_{01} = \sqrt{\frac{b_1 Y_0}{g_0 g_1}} \cdot \sqrt{W} = Y_S \tag{3.11}$$

It turns out that when the filter specification as well as the size of SIR are given, Y_S can be obtained from (3.11) as long as the image impedance $Z_0 (=1/Y_0)$ is chosen. In that way, the source admittance Y_S relates to the load admittance G_L seen at the tap point in (3.2).

However, in most practical cases, the condition is more complicated. The source admittance Y_S cannot be chosen arbitrarily. For that reason, (3.11) should be modified as

$$J_{01} = \sqrt{\frac{b_1 Y_0}{g_0 g_1}} \cdot \sqrt{W} = G_L = \frac{1}{R_L} \tag{3.12}$$

Hence, an additional matching network to transform the load impedance R_L to the source impedance R_S is required as illustrated in Figure 3.5. Actually, if an appropriate load impedance can be realized with a matching circuit at the operating frequency, the coupling required can be achieved at I/O which also corresponds to the physical meaning of external Q introduced in Dishal's method in Section 2.3.

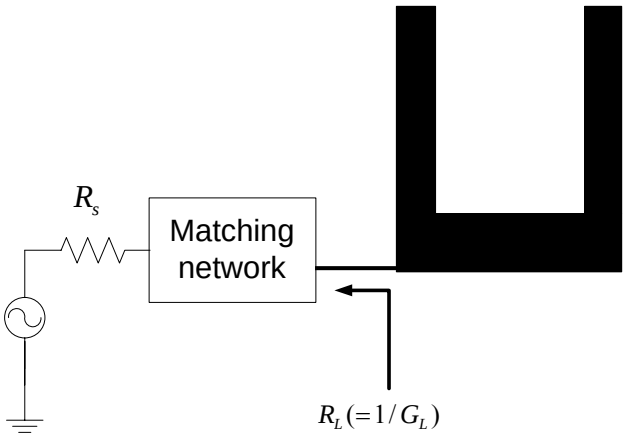

Figure 3.5 The SIR feeding structure with a matching network.

3.2 Second-Order Bandpass Filter with Tapped Line

In this section, we now try to give design steps for a bandpass filter similar with Type I filter but using tapped lines at input and output stage instead of gap coupling. In that way, the theory introduced in section 3.1 will be employed. First, the open-circuited λ/2 SIR is chosen. For the theory of $\lambda/2$ SIR described in Section 2.1.2, we can easily design the SIR or UIR by giving the impedance ratio R and the electrical length θ_b. For example, choose $Z_b = 50ohm$, $Z_a = 70ohm$ ($R<1$) and $\theta_b = 60^o$ with center frequency at 3GHz, 6% bandwidth and 0.1-dB ripple. From (2.3), we can obtain $\theta_a = 22.41^o$. Second, it is rational that the equivalent circuit for tapping in Figure 3.4 is then considered in the first and last stage in our design. Therefore, the overall equivalent structure can be verified as Figure 3.6.

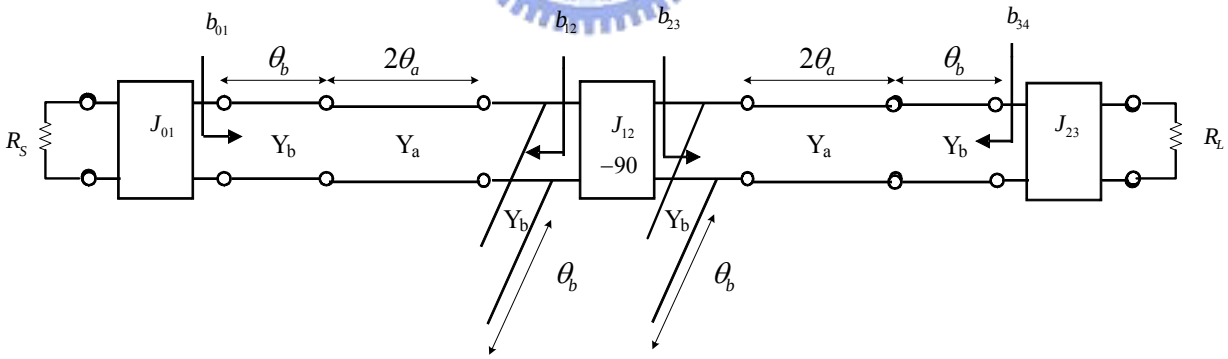

Figure 3.6 The overall equivalent circuit of the second-order tapped coupling filter.

Obviously, the value of the admittance inverter as well as the characteristic impedances of the coupled-line section in the center of the circuit can be found by following the derivation in Section 2.5. In that way, the coupling required for the filter response can be achieved. Thus, in the next step, the only problem is to find the proper

load impedance seen by the resonator looking into the load at the tap point of the feed line as well as the matching network to transform the source impedance R_s to the load impedance R_L. In order to find R_L, we utilize (3.12) where the slope parameter b for the resonator seen at the tap point can be calculated in (3.5). The admittance Y_0 of the resonator depends on the characteristic impedance in our design. Here, we set Y_0 is equal to 1/50 S. In addition, the element values g_0, g_1 are available from the filter specification. Consequently, with (3.12), the load impedance can be derived.

After that, the last step is to design an impedance matching network at center frequency. Here, in our design, we choose a quarter-wave transformer to realize the matching circuit. Figure 3.7 represents the complete circuit scheme of our design and the circuit simulation is shown in Figure 3.8.

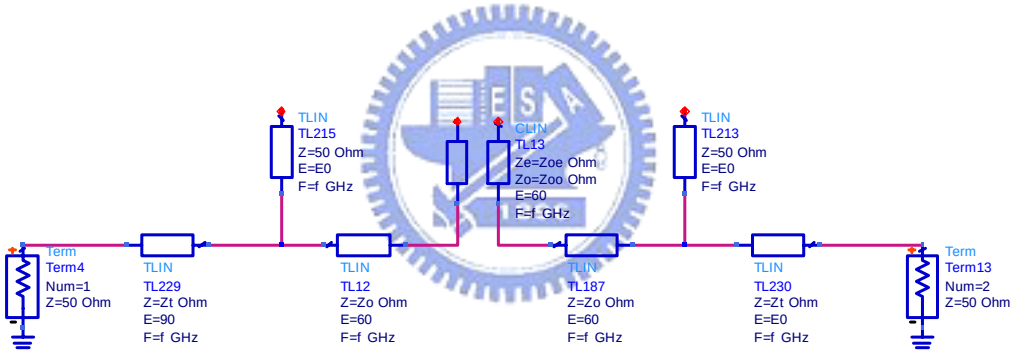

Figure 3.7 Circuit configuration of the second-order tapped coupling filter. (Type III)

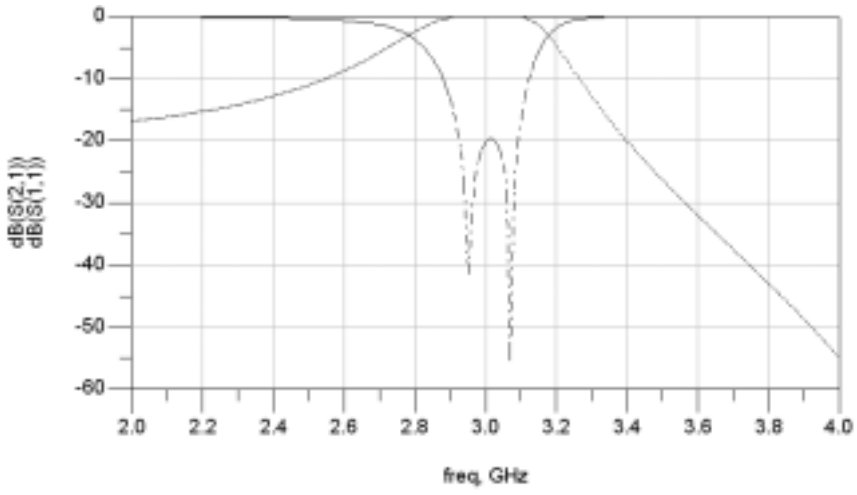

Figure 3.8 The circuit simulation result.

Accordingly, the same procedure can be applied if we want to modify Type II filter in Figure 2.29 that the gap coupling in I/O stage can be replaced by tapped coupling respectively. Given the design specification, we firstly design the SIR or UIR where both ends are short circuited. After that, the characteristic impedance Z_{oe}, Z_{oo} of the coupled line in the second stage can be decided to fit the required coupling. Finally, the slope parameter for the SIR seen at tap point can be derived using (3.9). By (3.12), we can obtain the load impedance Z_L. With a quarter wavelength transformer, the tapped line can be realized. The new schematic model is depicted in Figure 3.9.

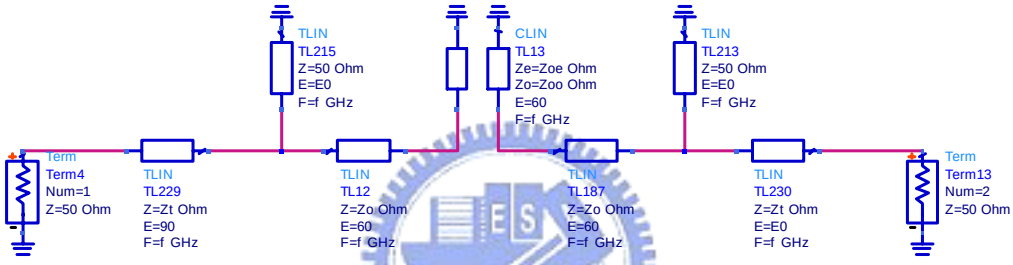

Figure 3.9 Circuit configuration of the second-order tapped coupling filter. (Type IV)

Let's call the filters introduced in this section as Type III and IV filter respectively in later discussions for convenience.

3.3 Dual-Frequency Transformer[19]

Impedance transformers have traditionally been broadly divided into two groups; those with a continuously tapered impedance distribution and those with a stepped piece-wise impedance distribution. The latter being considerably shorter than the broad-band tapered transformers perhaps because they tend to mimic a traditional lumped-element design.

The feasibility of an electrically small transformer with two sections and capable of achieving ideal impedance matching at two arbitrary frequencies is demonstrated

analytically. The parameters of the transformer are presented in explicit closed form.

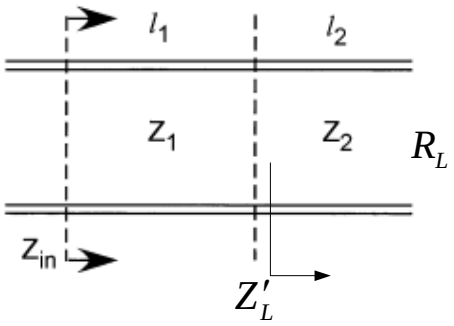

Figure 3.10 Two-section dual-band transformer.

The input impedance is given by

$$Z_{\text{in}} = Z_1 \frac{Z'_L + jZ_1 \tan(\beta\ell_1)}{Z_1 + jZ'_L \tan(\beta\ell_1)} \tag{3.13}$$

$$Z'_L = Z_2 \frac{R_L + jZ_2 \tan(\beta\ell_2)}{Z_2 + jR_L \tan(\beta\ell_2)}. \tag{3.14}$$

We want the input impedance to be equal to source impedance Z_0 at the two frequencies of interest f_1 and f_2. Equating Z_{in} to Z_0 and solving for Z'_L from (3.13) leads to

$$Z'_L = Z_1 \frac{Z_0 \quad jZ_1 \tan(\beta\ell_1)}{Z_1 - jZ_0 \tan(\beta\ell_1)}. \tag{3.15}$$

From (3.14) and (3.15), after some complicated calculation and we can obtain

$$Z_1 = \sqrt{\frac{Z_0}{2\alpha}(R_L - Z_0) + \sqrt{\left[\frac{Z_0}{2\alpha}(R_L - Z_0)\right]^2 + Z_0^3 R_L}} \tag{3.16}$$

$$Z_2 = \frac{Z_0 R_L}{Z_1}. \tag{3.17}$$

where

$$\alpha = (\tan(\beta_1 \ell_1))^2 \tag{3.18}$$

Chapter 4

The Proposed Dual-Band Bandpass Filter

We want to design the second and third-order bandpass filters with the function that can operate at two different frequencies corresponding to even- or odd-mode signals respectively. The design procedure and circuit realization as well as the simulation and measurement results will be presented. In the following sections, the filters are classified according to the type of tapping. In addition, the tool we used for circuit simulation is conducted by ADS from Agilent and the EM simulation is completed by Sonnet. All the measurements are obtained by four-port network analyzer E5070. All the filters are fabricated on Rogers RO4003 with a relative dielectric constant of 3.38 and thickness of 20 mil. For the short-end type SIR, the diameter of via hole is chosen as 40mil.

4.1 Design Procedure and Realization with Type I tapping

4.1.1 Second-Order Filter with Open-Ended $\lambda/2$ SIR

In this design, we choose the specification that the center frequencies for the higher pass and the lower passband are 3GHz and 2.8GHz respectively. The fractional bandwidth

is about 4~6% and the ripple level is 0.1 dB.

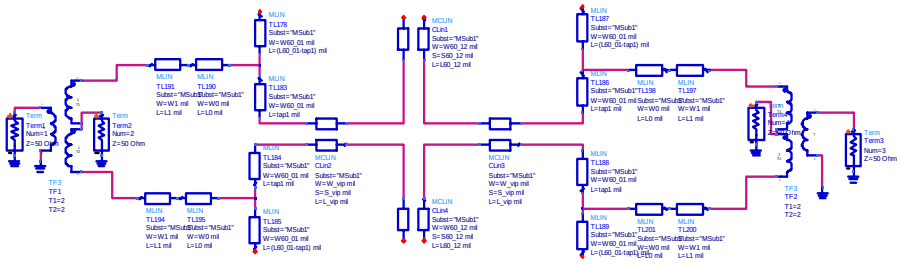

(a)

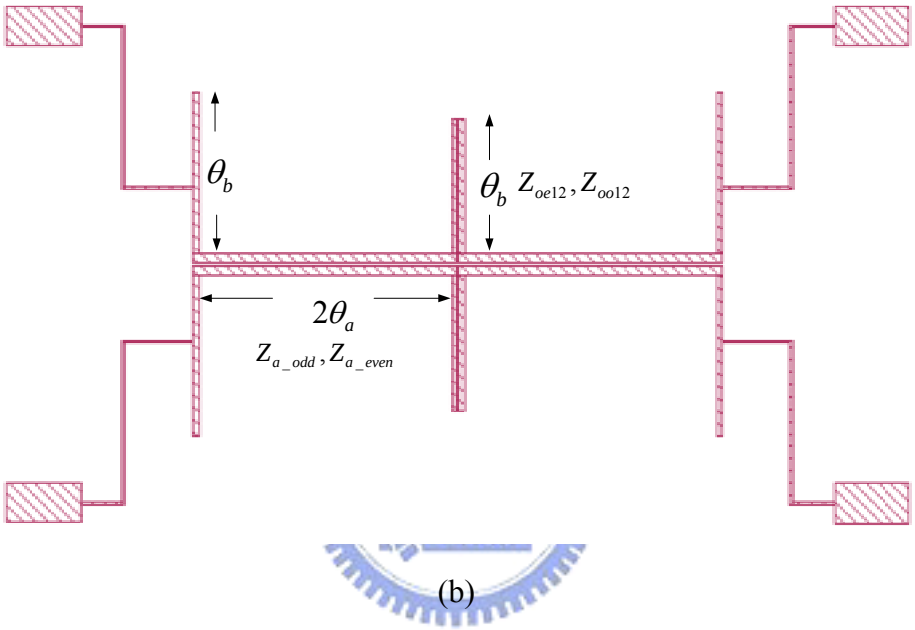

(b)

Figure 4.1 The overall circuit diagram. (a) In circuit simulation tool, ADS. (b) In EM simulation tool, Sonnet.

The overall circuit diagram in ADS and Sonnet are shown in Figure 4.1. We utilize the same design procedure as Type III filter in Figure 3.8. First, the filter is considered as two sections consisting of the resonators and the feeding structure at input and output stages. For the resonators, the center frequency depends on the resonant frequency of the SIR structure while the bandwidths are mainly controlled by the coupling between the resonators. We first design a second-order bandpass filter with the operating frequency 3GHz, fractional bandwidth 5%. The initial parameters for the filter are shown in Table

4.1. In our case, a higher characteristic impedance is used to avoid the physical limit in microstirp coupled lines but not deteriorate the coupling required. In Table 4.1, Z_{oe12} and Z_{oo12} represent the characteristic impedances of the coupled line between the resonators. After that, we design another filter with all the dimensions fixed as previous filter except for the impedance Z_a, which is replaced with a higher impedance Z_{a_high}. In our case, the impedance is chosen to be 70 ohm. For the characteristics of SIRs mentioned in Section 2.1.3, it's observed that the fundamental frequency is changeable with the variation of impedance ratio. The smaller the impedance ratio is, the lower the fundamental frequency becomes. That is, the fundamental resonant frequency of the latter filter will be lower than the former one. In our design, a coupled line is employed to realize the segment in the center of each SIR. When excited with even- and odd-mode signals, the segment can perform characteristic impedances Z_{oe} and Z_{oo} relating to Z_{a_high} and Z_{a_low} for the two filters respectively. From the coupled line theory, it's reasonable that $Z_{oe} > Z_{oo}$ for microstrip coupled lines. In conclusion, when a differential signal is applied, the filter will operate at the high-frequency band whereas the low-frequency band will only perform with a common mode source.

f_0 (GHz)	Z_a (ohm)	Z_b (ohm)	θ_b	θ_a	Z_{oe12} (ohm)	Z_{oo12} (ohm)
3	46	95	60^o	47.647^o	133.68	73.67

Table 4.1 Initial parameters for the odd-mode filter in Filter A.

So far, the circuit parameters for the resonators are decided. Therefore, the final problem is to find a proper feeding structure to realize the needed coupling between the tapped lines and end resonators. Following Section 3.1, the tapped position should be

evaluated to give the desired load impedances R_{L1} , R_{L2} at two designed center frequencies. The load impedances R_{L1} and R_{L2} may be different. For convenience, it is assumed that $R_{L1} = R_{L2}$. In this case, the dual frequency transformer in Section 3.3 can be utilized to carry out the matching circuit. Finally, we use Table 2.1 as a reference to fine tune the full circuit in EM simulation tool, and the total filter is completed which we call Filter A. The circuit layout of Filter A with physical dimensions are shown in Figure 4.2 and listed in Table 4.2. The photograph and measured results are shown in Figure 4.3. and 4.4.

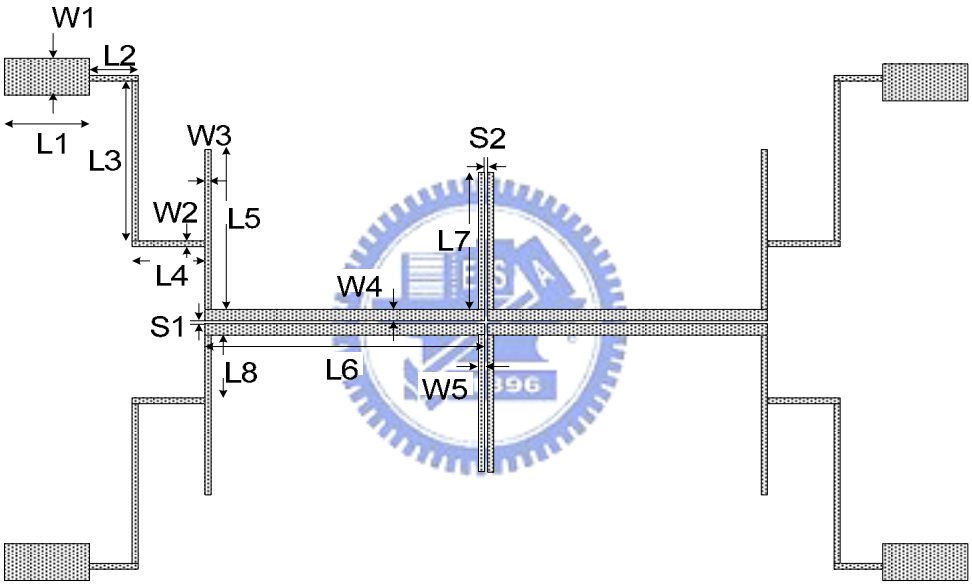

Figure 4.2 The circuit layout of the proposed Filter A.

W1	W2	W3	W4	W5
95	6	12	23	12
L1	L2	L3	L4	L5
180	106	388	170	435
L6	L7	L8	S1	S2
632	328	156	6	5

Table 4.2 Physical dimensions of the proposed Filter A. (Unit: mil)

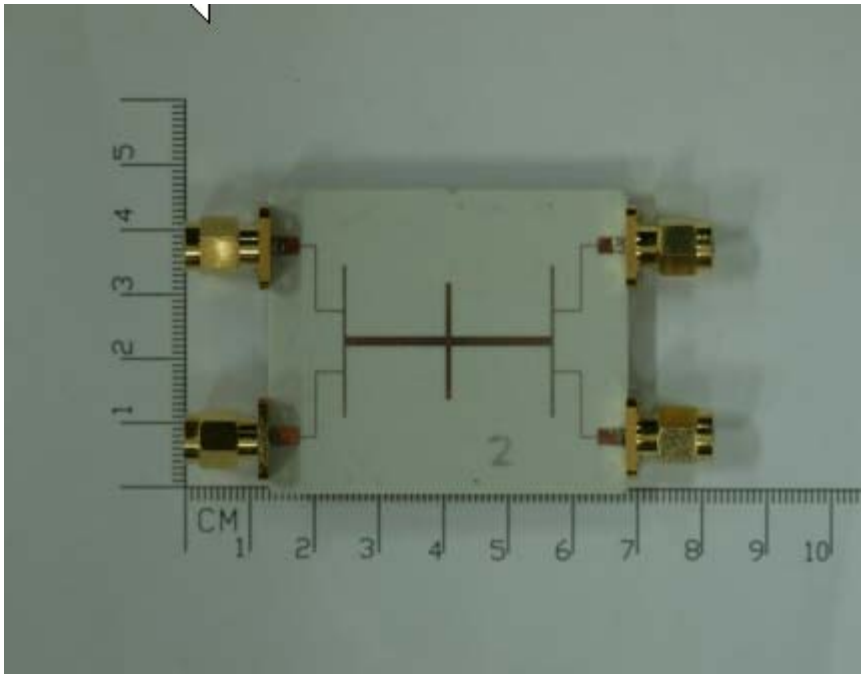

Figure 4.3 Photograph of Filter A

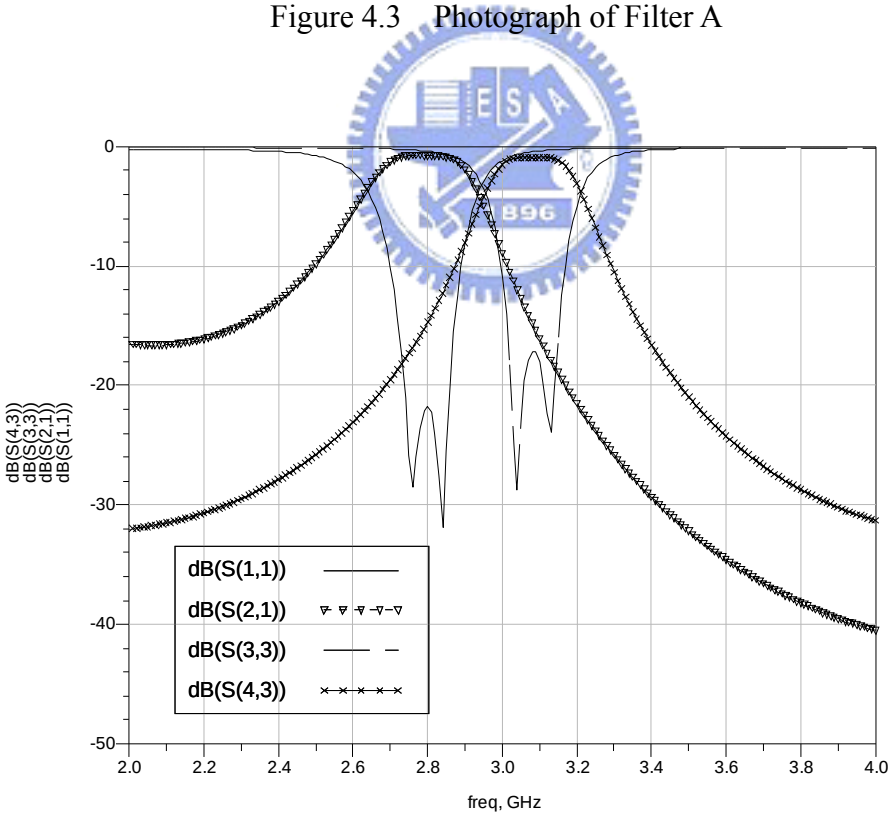

(a)

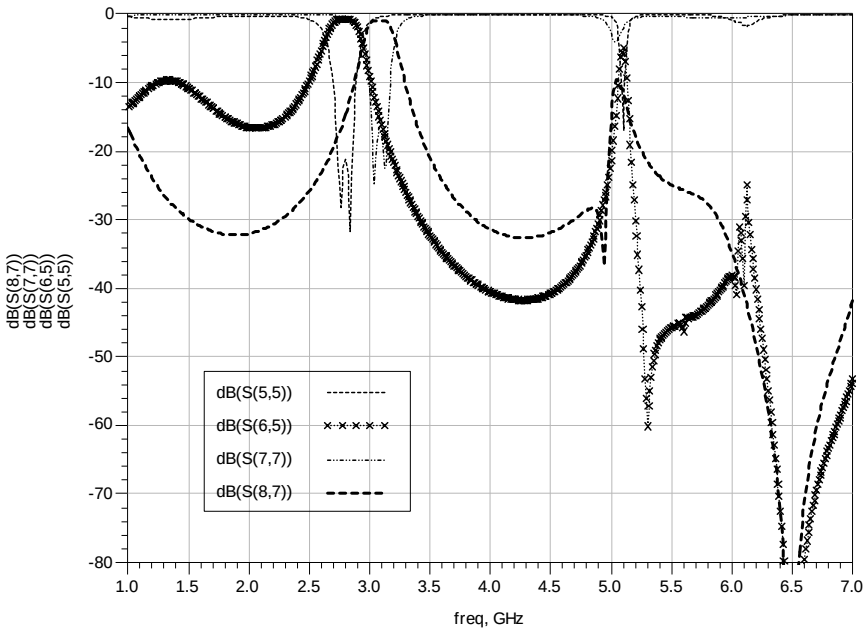
dB(S(8,7))
dB(S(7,7))
dB(S(6,5))
dB(S(5,5))
0
-10
-20
-30
-40
-50
-60
-70
-80
1.0
1.5
2.0
2.5
3.0
3.5
4.0
4.5
5.0
5.5
6.0
6.5
7.0
freq, GHz
dB(S(5,5))
dB(S(6,5))
dB(S(7,7))
dB(S(8,7))

(b)

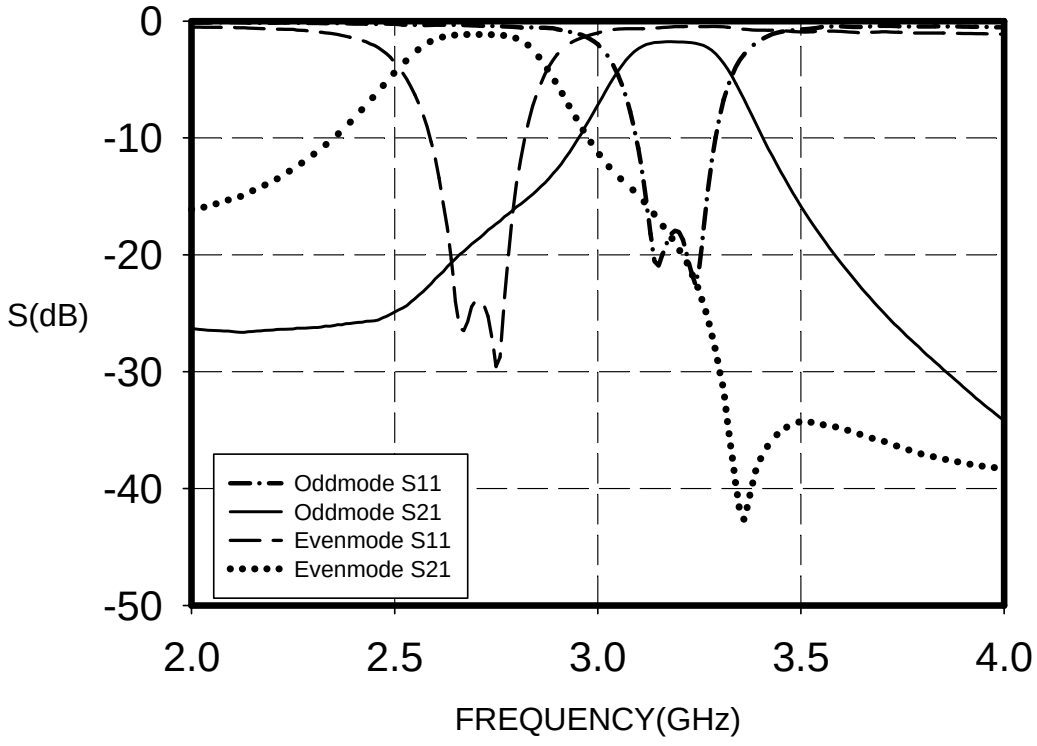
0
-10
-20
-30
-40
-50
S(dB)
2.0
2.5
3.0
3.5
4.0
FREQUENCY(GHz)
Oddmode S11
Oddmode S21
Evenmode S11
Evenmode S21

(c)

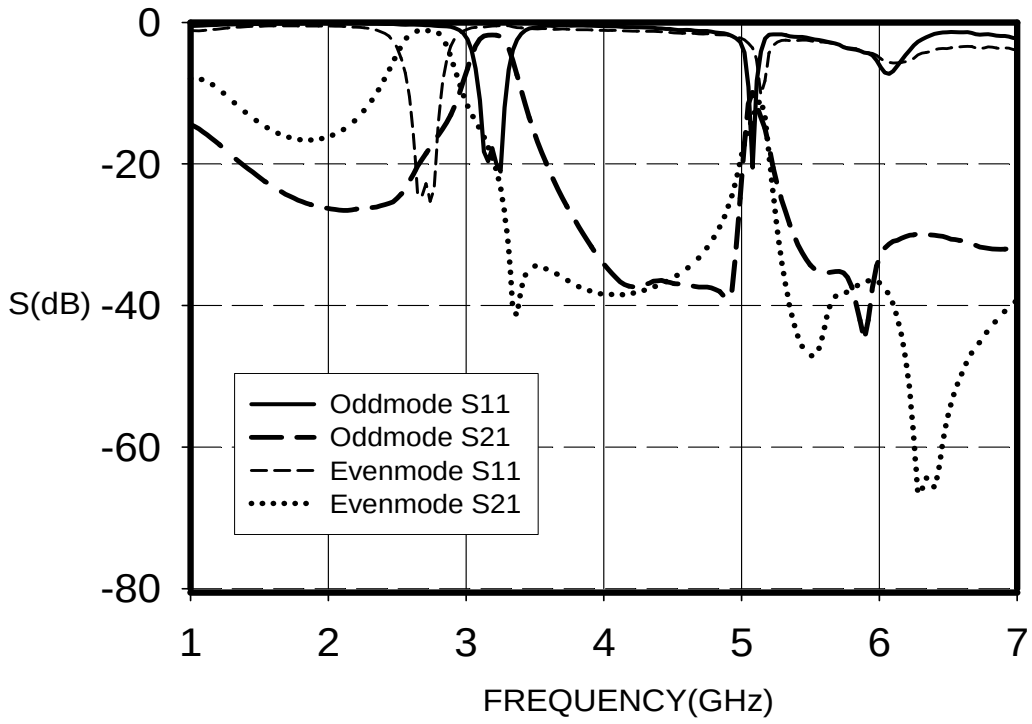
0
-20
-40
-60
-80
S(dB)
1
2
3
4
5
6
7
FREQUENCY(GHz)
Oddmode S11
Oddmode S21
Evenmode S11
Evenmode S21

(d)

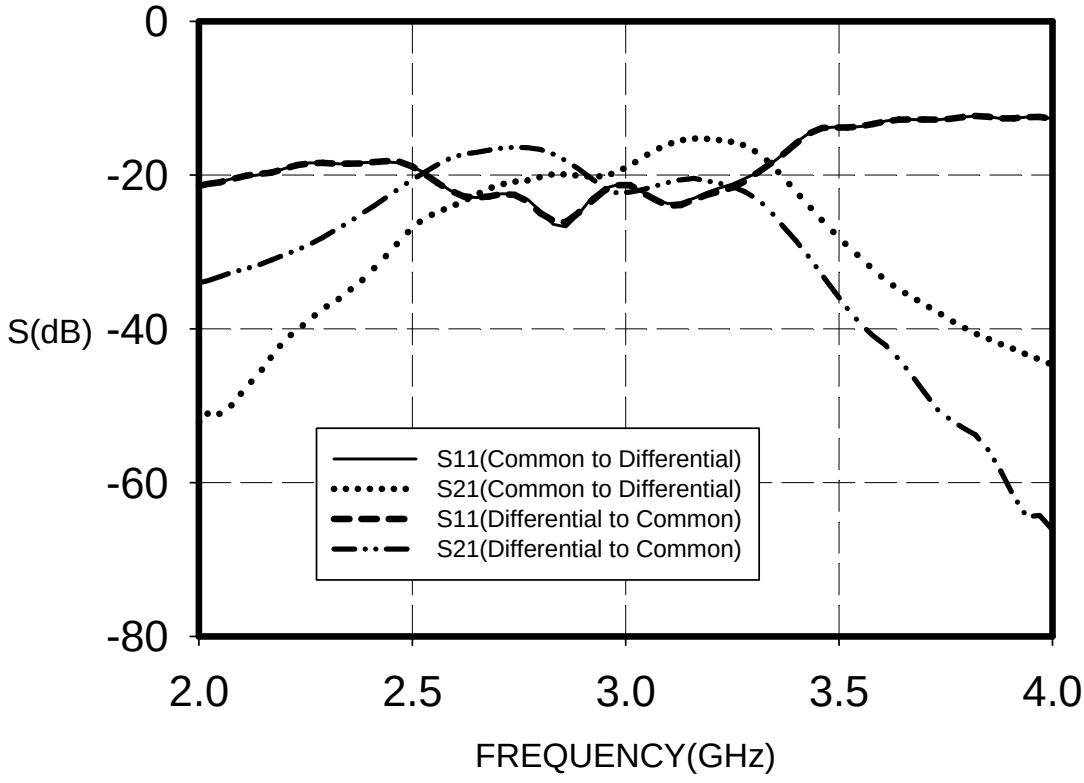
0
-20
-40
-60
-80
S(dB)
2.0
2.5
3.0
3.5
4.0
FREQUENCY(GHz)
S11(Common to Differential)
S21(Common to Differential)
S11(Differential to Common)
S21(Differential to Common)

(e)

Figure 4.4 Simulated and measured results of Filter A. (a) Simulated $|S_{11}|$ and $|S_{21}|$ for 2~4 GHz. (b) Simulated $|S_{11}|$ and $|S_{21}|$ for 1~7 GHz. (c) Measured $|S_{11}|$ and $|S_{21}|$ for 2~4 GHz. (d) Measured $|S_{11}|$ and $|S_{21}|$ for 1~7 GHz. (e) Measured isolation between two modes.

Figure 4.4 shows the measured return loss in the passband is better than 15dB and the insertion loss is about 1.5~2 dB. The fractional bandwidths are 6% and 4.7% at 2.7 GHz and 3.19 GHz respectively. The first spurious resonance happens at about 5GHz. The results confirm to the simulation approximately.

4.1.2 Second-Order Filter with Short-Ended λ/2 SIR

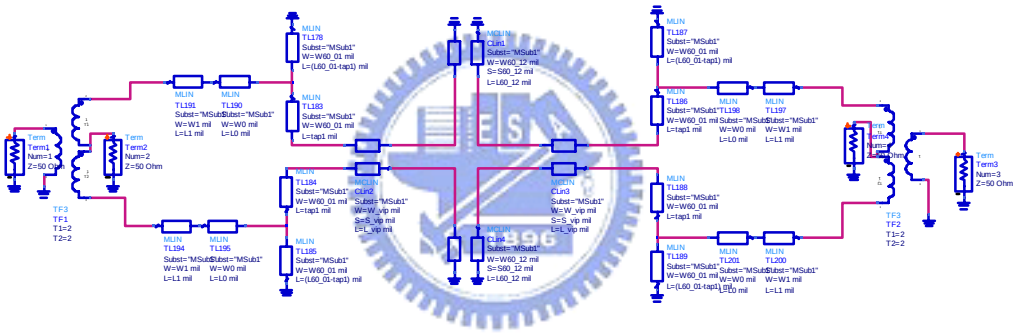

(a)

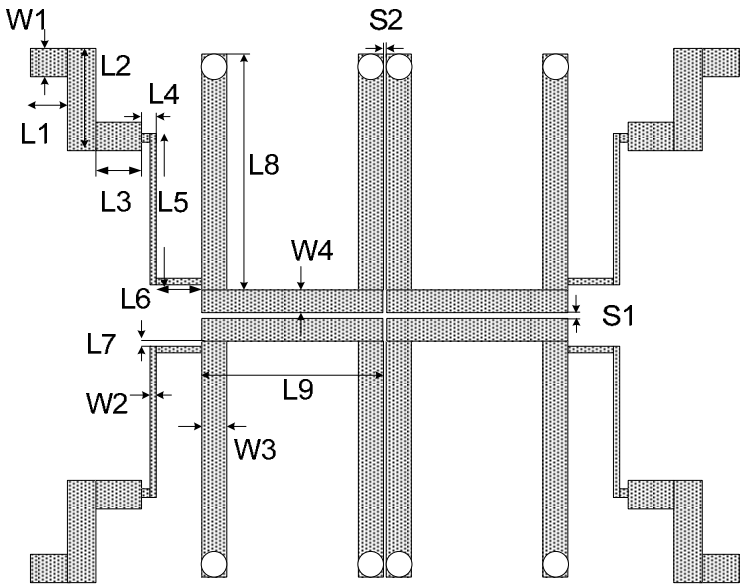

(b)

Figure 4.5 The overall circuit scheme of Filter B. (a) The circuit structure in ADS. (b)

The circuit layout in Sonnet.

W1	W2	W3	W4	L1
46	8	44	40	76
L2	L3	L4	L5	L6
200	100	28	300	96
L7	L8	L9	S1	S2
6	472	360	6	6

Table 4.3 Physical dimensions of the proposed Filter B. (Unit: mil)

On the other hand, we can also employ the filter in Figure 3.9 as a main structure to build a second-order bandpass filter with similar function as Filter A. The overall circuit configuration with physical dimensions are depicted in Figure 4.5 in Table 4.3. The filter which we'll call Filter B is designed with the specification that the two passbands are at 3.3 GHz and 2.9 GHz with ripple level 0.1 dB, and the fractional bandwidth is about 4~6%. Likewise, the structure are partitioned into two parts. The first section corresponds to the SIRs. The same as Filter A, the filter for the higher passband is constructed first. The initial parameters are shown in Table 4.2.

f_0 (GHz)	Z_a (ohm)	Z_b (ohm)	θ_b	θ_a	Z_{oe12} (ohm)	Z_{oo12} (ohm)
3.3	60	50	60^o	25.69^o	58.9298	43.4204

Table 4.4 Initial parameters of the even-mode filter in Filter B.

Later, for the second filter with a lower passband, we choose a lower impedance Z_{a_low}, 37 ohm, to reach the center frequency 2.9 GHz. The decision of Z_a is different from that in Filter A. This is because the characteristics of the short-ended λ/2 SIR discussed in Section 2.1 for which the same properties with the open-ended λ/2 SIR

can perform while the high-Z and low-Z segments are interchanged.

Finally, we choose a coupled line with the characteristic impedances Z_{oe} and Z_{oo} related to Z_{a_high}, Z_{a_low}. In the end, the filter will operate at higher passband when applying a common-mode signal. With a differential-mode signal, the lower band can be performed.

Following Section 3.1, we can calculate the load impedance needed of the tapped line when fixing the tapping point. In this case, we choose the tapped position to obtain the same load impedances so that the dual frequency transformer can be utilized to realize the matching circuit. Consequently, we use Table 2.1 as a reference to fine tune the circuit in EM simulation tool. The photograph and measured results are shown in Figure 4.5. and 4.6.

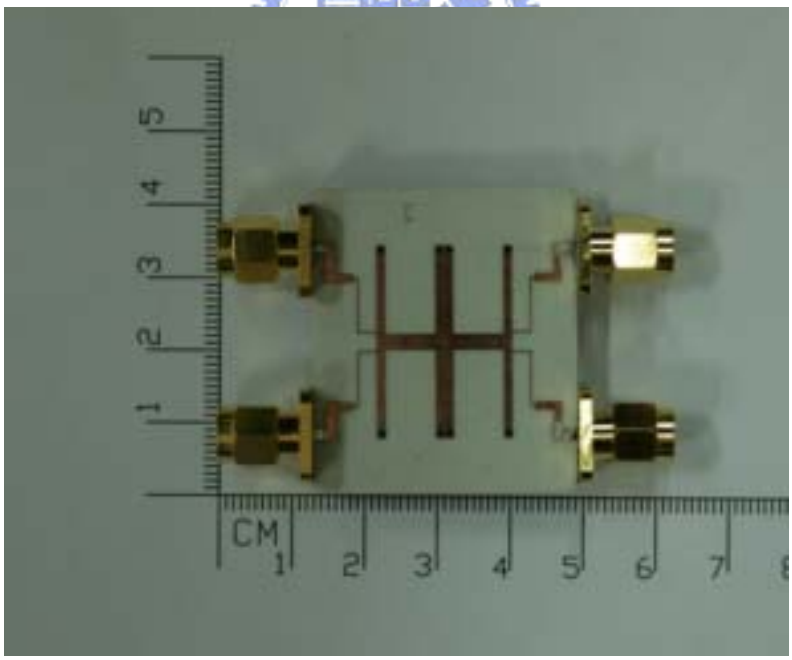

Figure 4.6 Photograph of Filter B.

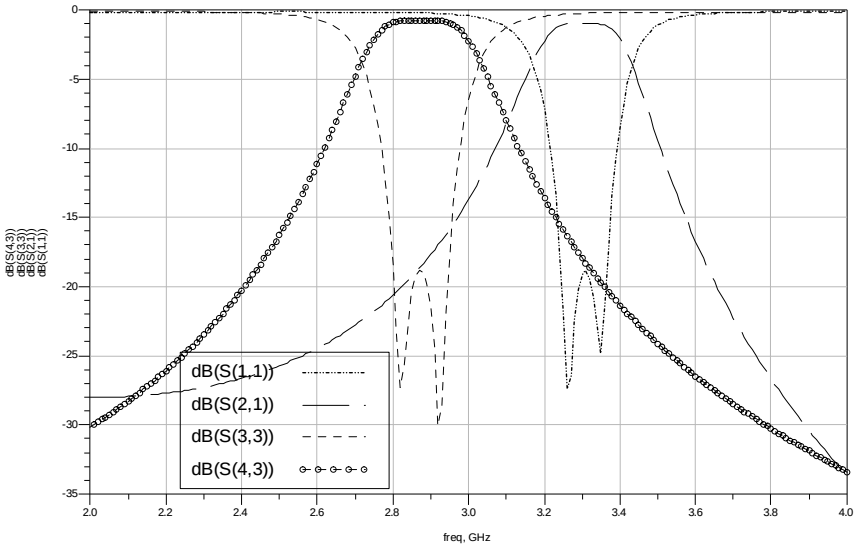
dB(S(1,1))
dB(S(2,1))
dB(S(3,3))
dB(S(4,3))
freq, GHz

(a)

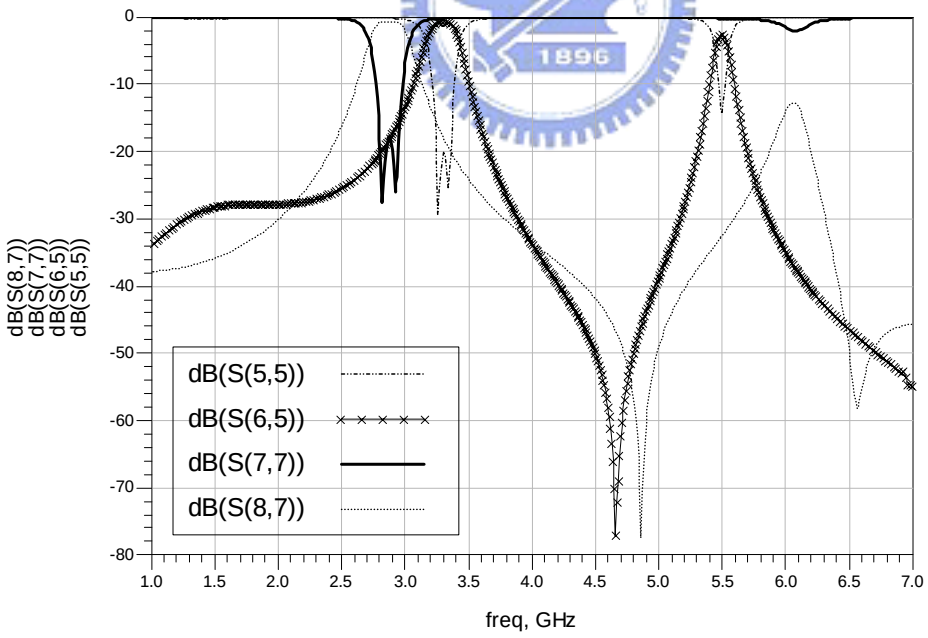
dB(S(5,5))
dB(S(6,5))
dB(S(7,7))
dB(S(8,7))
freq, GHz

(b)

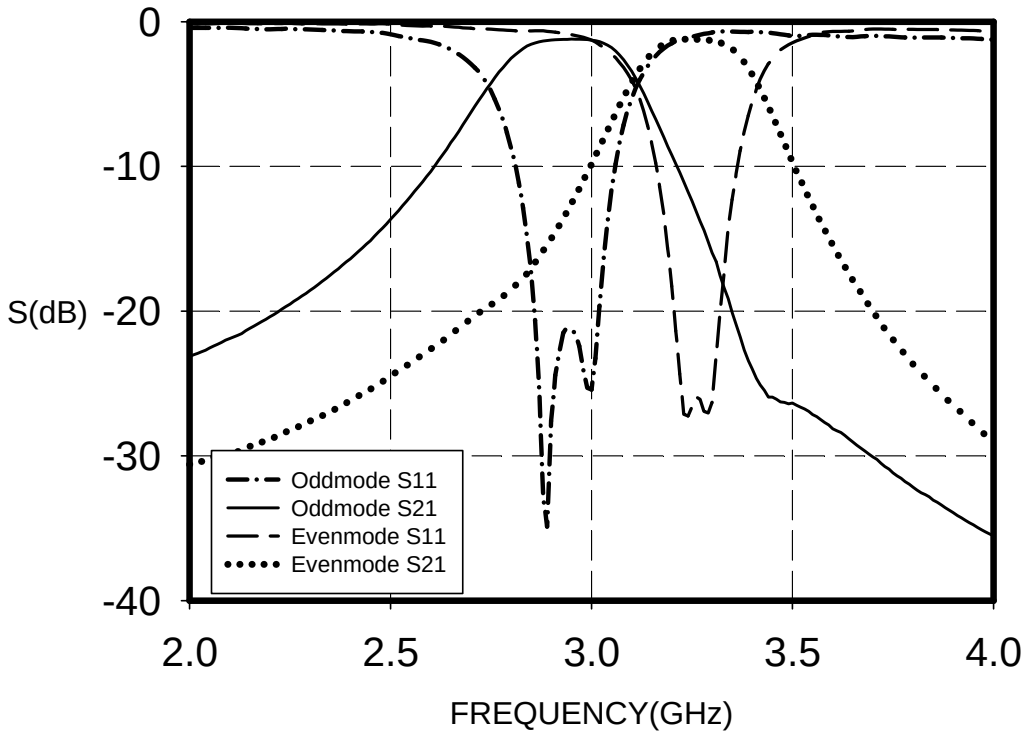
0
-10
-20
-30
-40
S(dB)
2.0
2.5
3.0
3.5
4.0
FREQUENCY(GHz)
Oddmode S11
Oddmode S21
Evenmode S11
Evenmode S21

(c)

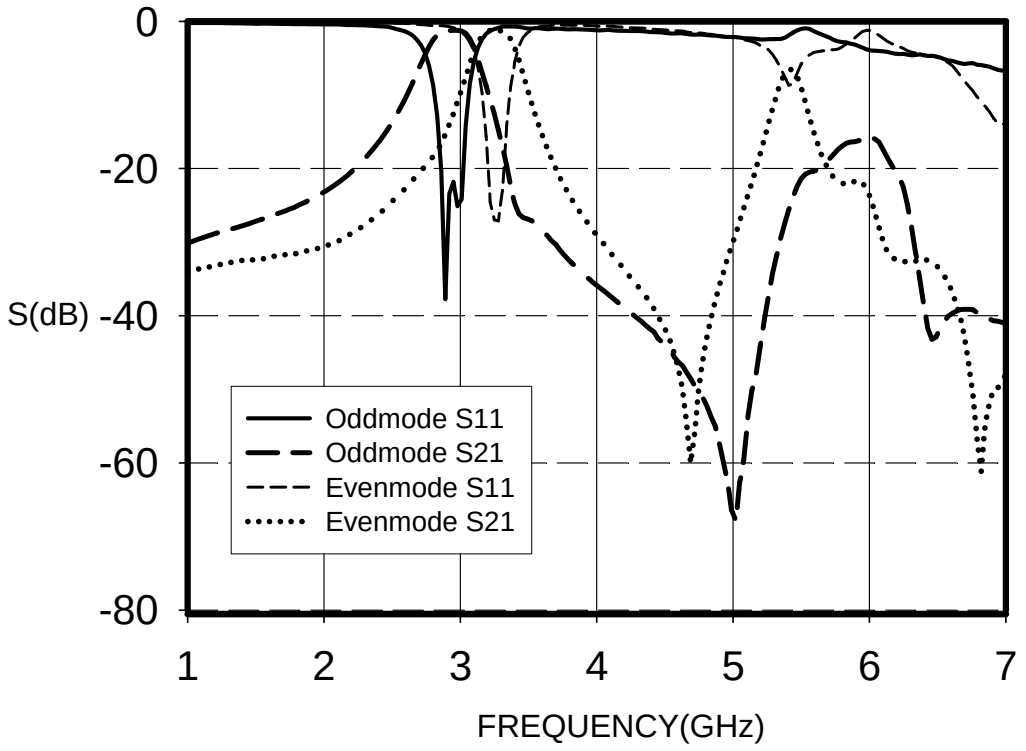
0
-20
-40
-60
-80
S(dB)
1
2
3
4
5
6
7
FREQUENCY(GHz)
Oddmode S11
Oddmode S21
Evenmode S11
Evenmode S21

(d)

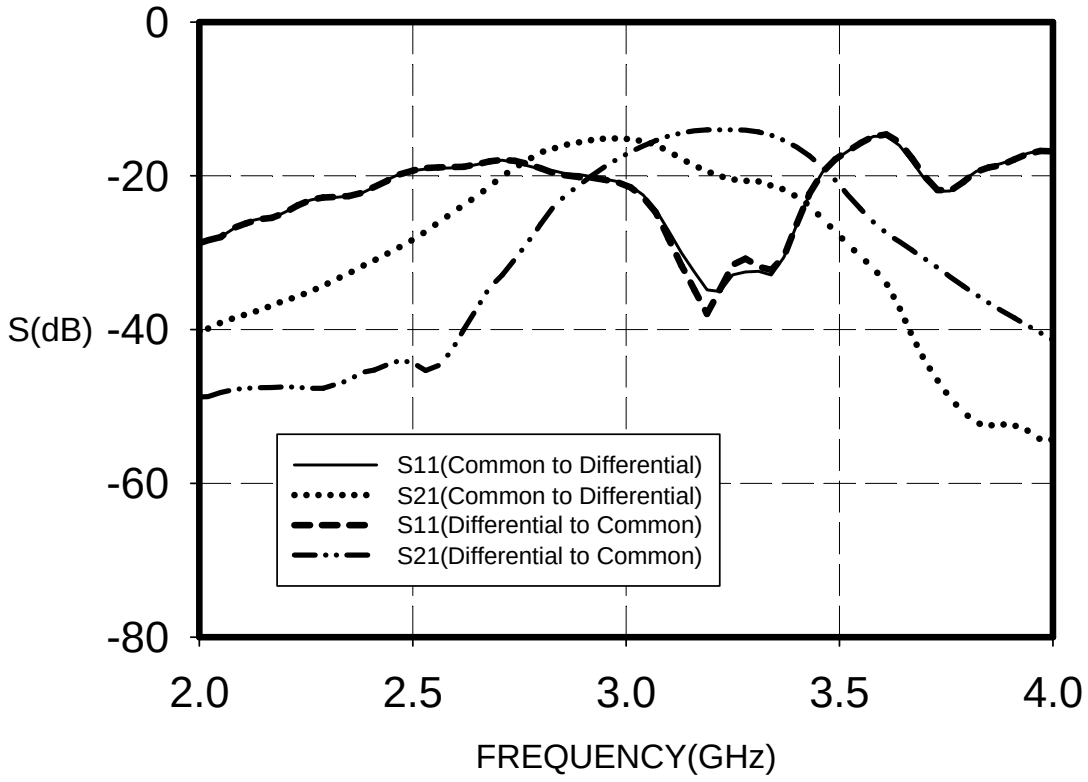

(e)

Figure 4.7 Simulated and measured results of Filter B. (a) Simulated $|S_{11}|$ and $|S_{21}|$ for 2~4 GHz. (b) Simulated $|S_{11}|$ and $|S_{21}|$ for 1~7 GHz. (c) Measured $|S_{11}|$ and $|S_{21}|$ for 2~4 GHz. (d) Measured $|S_{11}|$ and $|S_{21}|$ for 1~7 GHz. (e) Measured isolation between two modes.

Figure 4.7 shows the measured in-band return loss is better than 20 dB and the insertion loss is about 1.2~1.5 dB. The fractional bandwidths are 6.6% and 4.6% at 2.93 GHz and 3.27 GHz. The first spurious occurs at 5.5 GHz. These results consist with the simulated results approximately.

4.1.3 Third-Order Filter with Short-Ended λ/2 SIR

The same procedure in Section 4.1.2 can be utilized to design a higher order bandpass filter. In our case, we try to manipulate a third-order design. The specification of the filter are about 2.9 GHz and 3.2 GHz for center frequencies and 3~5% for the bandwidth with

ripple level 0.1 dB . First, focus on the section of the resonators and the coupling causes different resonant frequencies. We use the element values for third-order Chebyshev response to synthesize the initial circuit parameters for the filter with higher passband. Furthermore, considering the lowest spurious resonance. we choose the impedance ratio of the filter with higher passband is nearly unity which means a UIR filter while the ratio R of the other one is smaller than unity. It's for the reason that the SIR filter possesses the advantage that the first spurious can be much higher than $2f_0$; meanwhile, the first spurious of the UIR filter will resonate at $2f_0$. Thus, we utilize a coupled line to realize Z_{a_high}, Z_{a_low}. And finally, we can obtain the filter with a higher upper stopband. The initial parameters are presented in Table 4.5.

f_0 (GHz)	Z_a (ohm)	Z_b (ohm)	θ_b	θ_a	Z_{oe12} (ohm)	Z_{oo12} (ohm)
3.3	37	50	60^o	25.69^o	55.6	45.4189

Table 4.5 Initial parameters of the even-mode filter in Filter C.

For more degrees of freedom, we utilize the transmission line with three sections to accomplish the impedance matching. In addition, Table 2.2 provides a reference to fine tune the circuit during EM simulation. We name the design Filter C. The overall circuit configuration with parameters of physical dimensions are shown in Figure 4.8 and Table 4.6. The photograph and measured results of Filter C are shown in Figure 4.9. and 4.10.

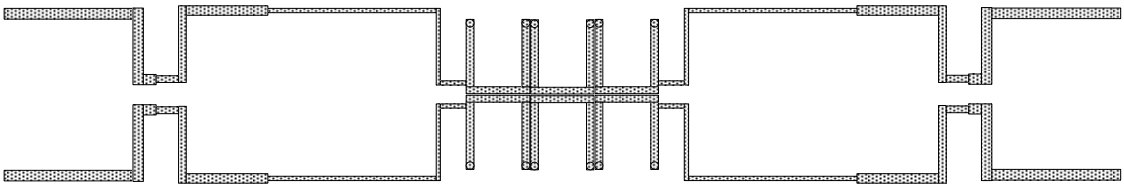

(a)

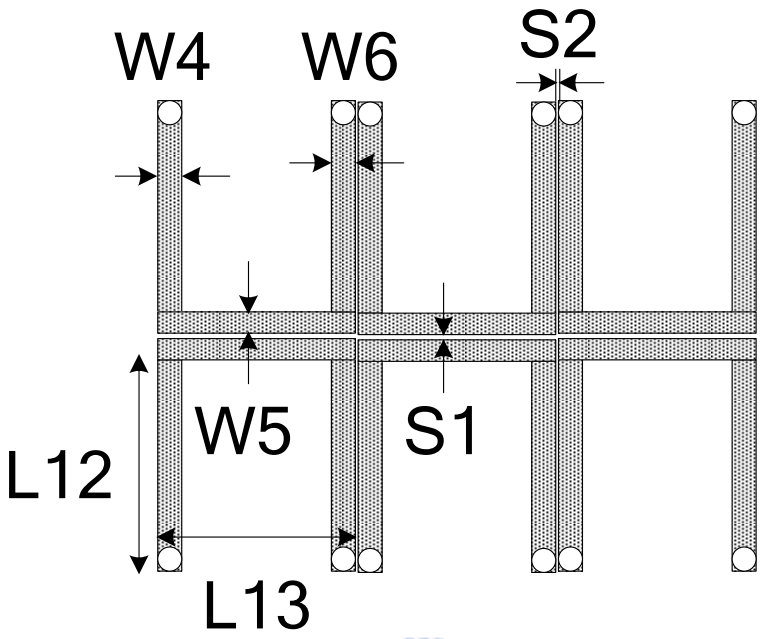

(b)

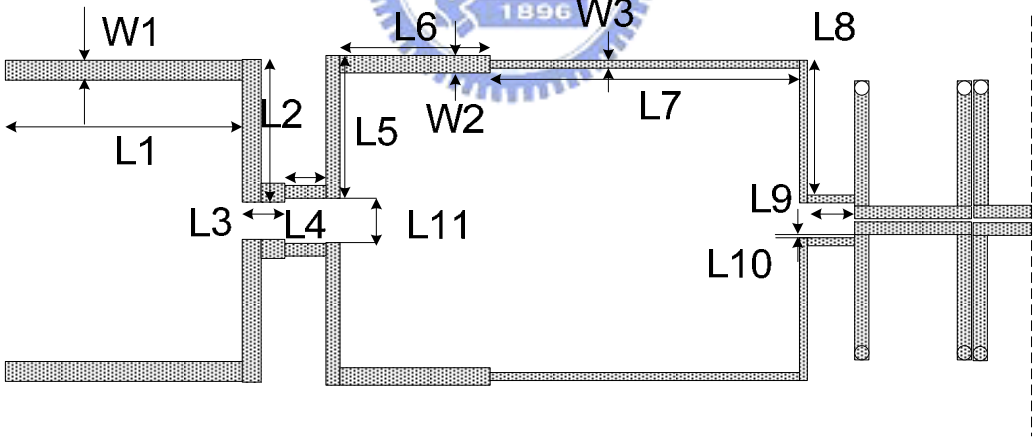

(c)

Figure 4.8 The overall circuit configuration of Filter C. (a) The overall layout. (b) The part of resonators. (c) The part of transformers.

W1	W2	W3	W4	W5	W6
54	52	30	44	40	44
L1	L2	L3	L4	L5	L6
900	500	127	151	500	529
L7	L8	L9	L10	L11	L12
1100	470	160	5	151	420
L13	S1	S2			
410	6	12			

Table 4.6 Physical dimensions of the proposed Filter C. (Unit: mil)

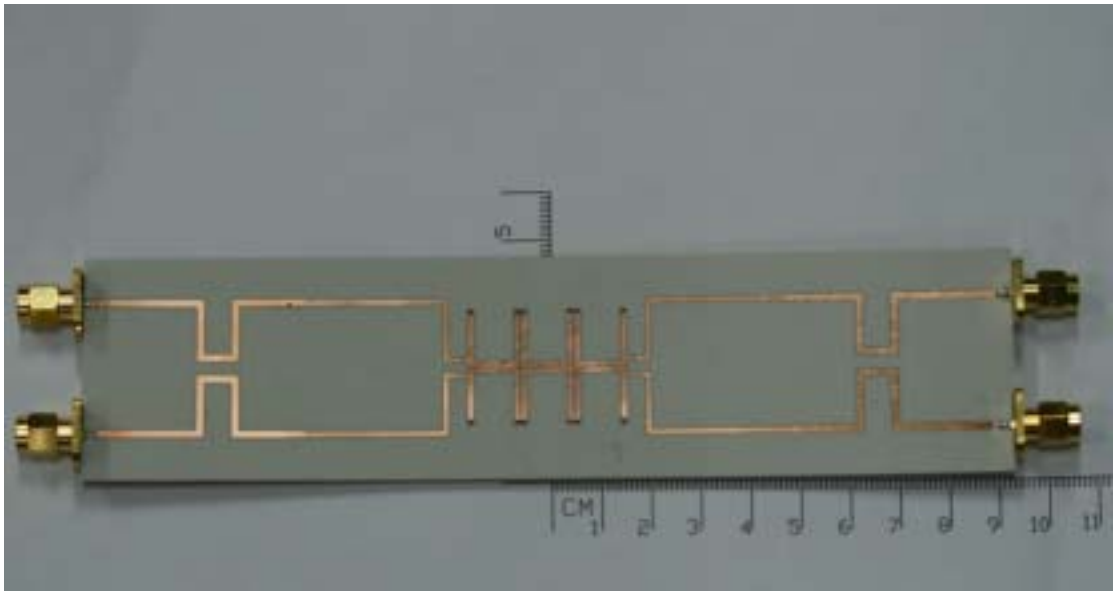

Figure 4.9 Photograph of Filter C.

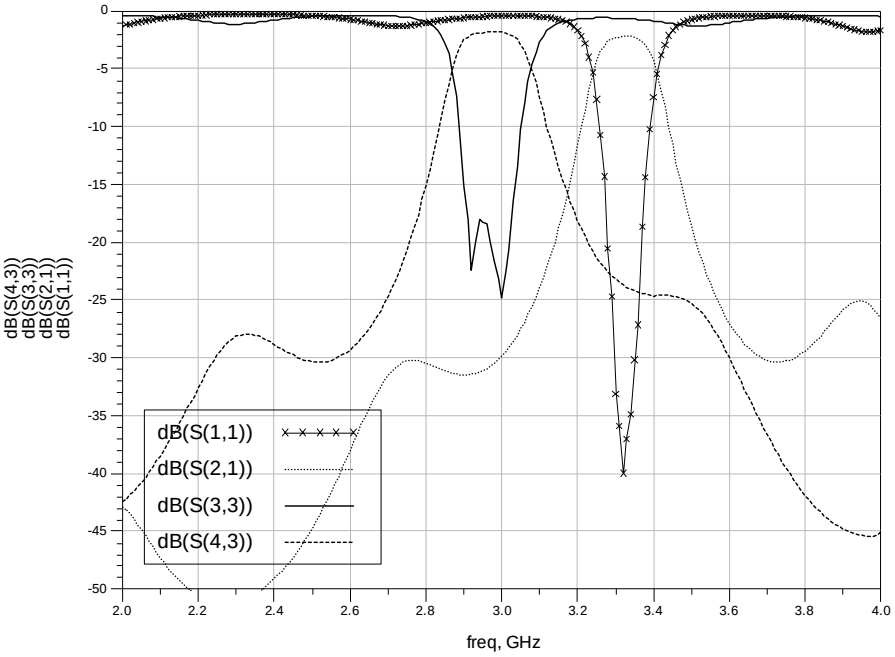
dB(S(4,3))
dB(S(3,3))
dB(S(2,1))
dB(S(1,1))
freq, GHz

(a)

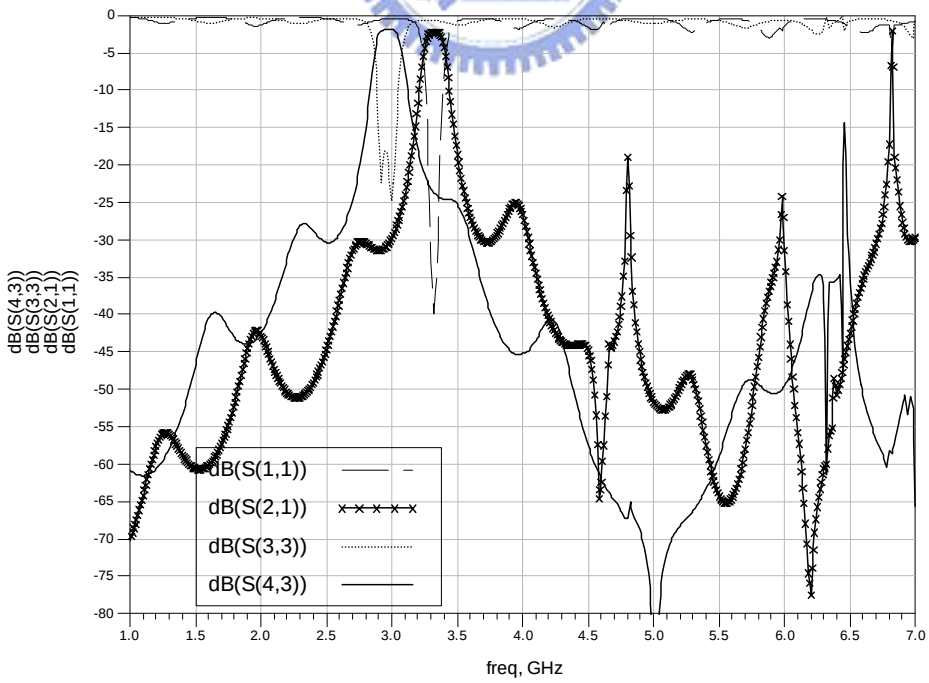
dB(S(4,3))
dB(S(3,3))
dB(S(2,1))
dB(S(1,1))
freq, GHz

(b)

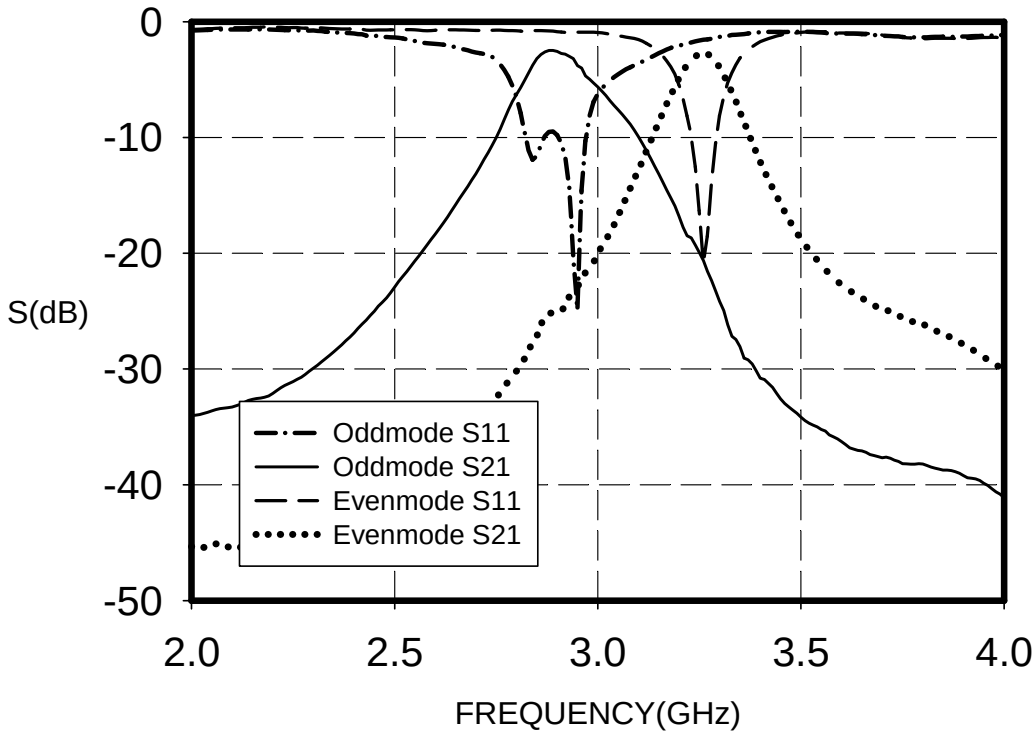
0
-10
-20
-30
-40
-50
S(dB)
2.0
2.5
3.0
3.5
4.0
FREQUENCY(GHz)
Oddmode S11
Oddmode S21
Evenmode S11
Evenmode S21

(c)

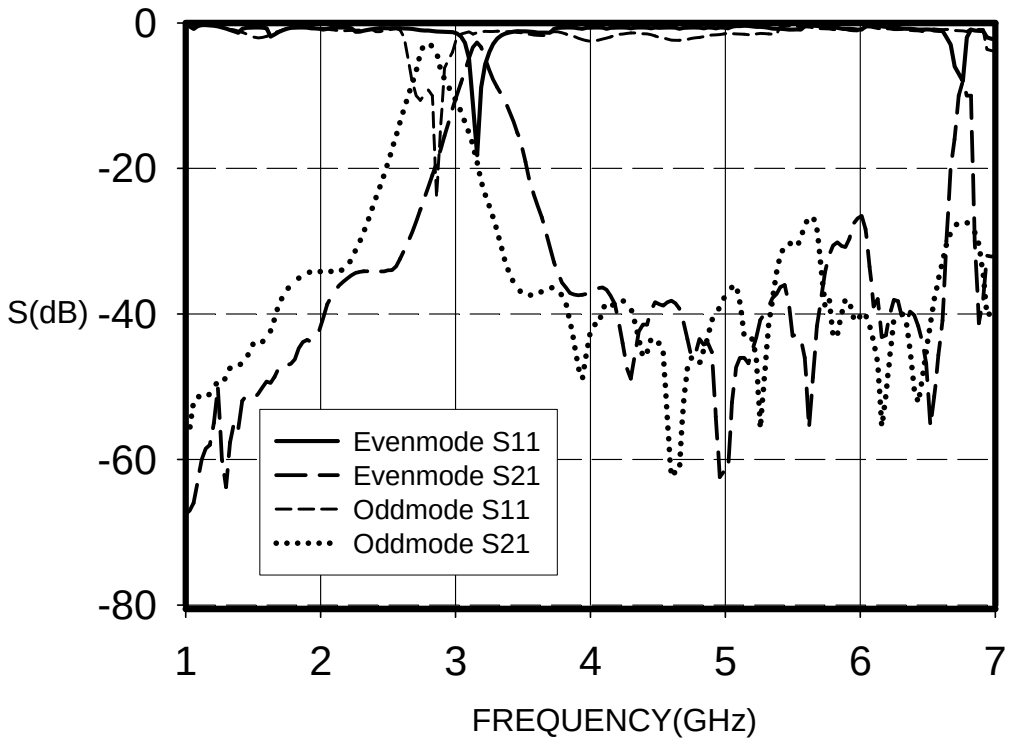
0
-20
-40
-60
-80
S(dB)
1
2
3
4
5
6
7
FREQUENCY(GHz)
Evenmode S11
Evenmode S21
Oddmode S11
Oddmode S21

(d)

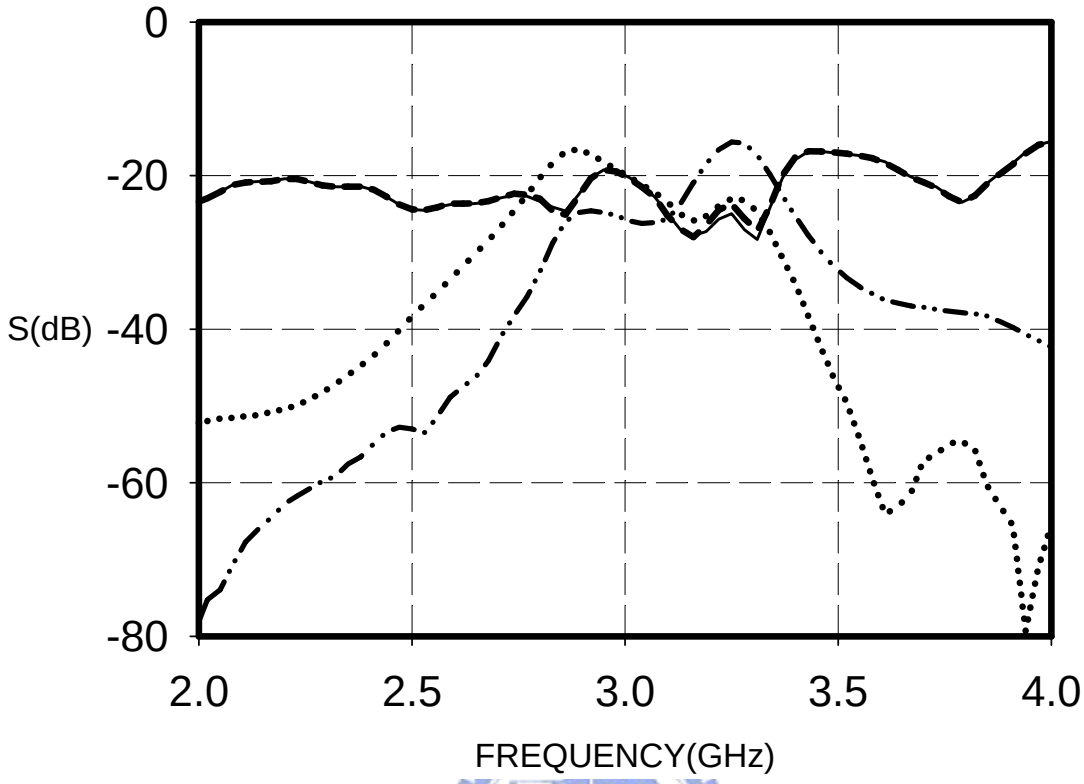

(e)

Figure 4.10 Simulated and measured results of Filter C (a) Simulated $|S_{11}|$ and $|S_{21}|$ for 2~4 GHz. (b) Simulated $|S_{11}|$ and $|S_{21}|$ for 1~7 GHz. (c) Measured $|S_{11}|$ and $|S_{21}|$ for 2~4 GHz. (d) Measured $|S_{11}|$ and $|S_{21}|$ for 1~7 GHz. (e) Measured isolation between two modes.

Figure 4.10 presents the measured return loss in the passband is better than 10 dB and the insertion loss is about 2.5~3 dB. The fractional bandwidth are 5.2% and 2 % at 2.87 GHz and 3.26 GHz respectively. The first spurious occurs at 6.8 GHz.

4.2 Design Procedure and Realization with Type II tapping

4.2.1 Third-Order Filter with Short-Ended λ/2 SIR

In this design, we continue using the design of Filter C with the same specification. The only difference is the feeding structure. In this case, we employ a coupled-line section in the matching circuit. Since the characteristic impedance of differential-mode and common-mode signal in the coupled line differs, it's convenient to use the feature to realize the transformer more easily. In addition, the length of the transformer can be effectively shortened as well as the size of the circuit. At the end, the filter is fabricated and called Filter D. The overall circuit scheme with physical dimensions are shown in Figure 4.11 and Table 4.7. The photographs and measured results are shown in Figure 4.12. and 4.13.

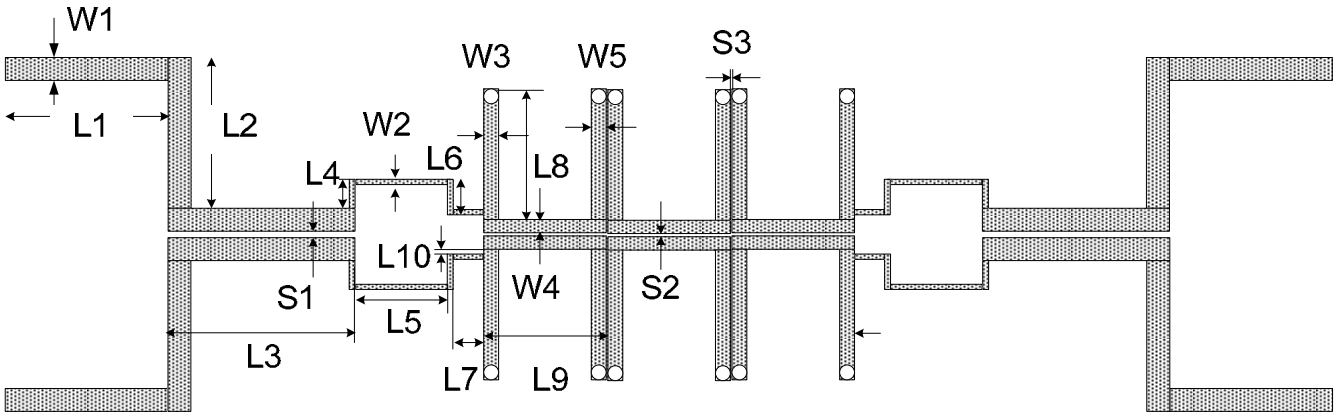

Figure 4.11 The overall circuit topology of Filter D.

W1	W2	W3	W4	W5	L1
66	24	30	44	40	508
L2	L3	L4	L5	L6	L7
500	625	93	293	114	100
L8	L9	L10	S1	S2	S3
529	420	5	6	6	12

Table 4.7 Physical dimensions of the proposed Filter D. (Unit: mil)

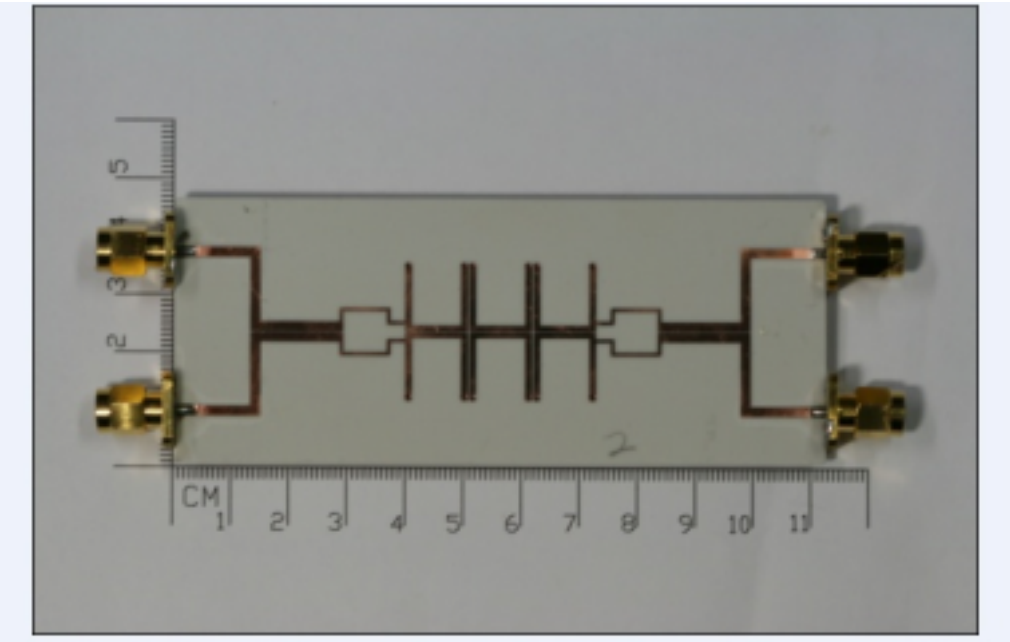

Figure 4.12 Photograph of Filter D.

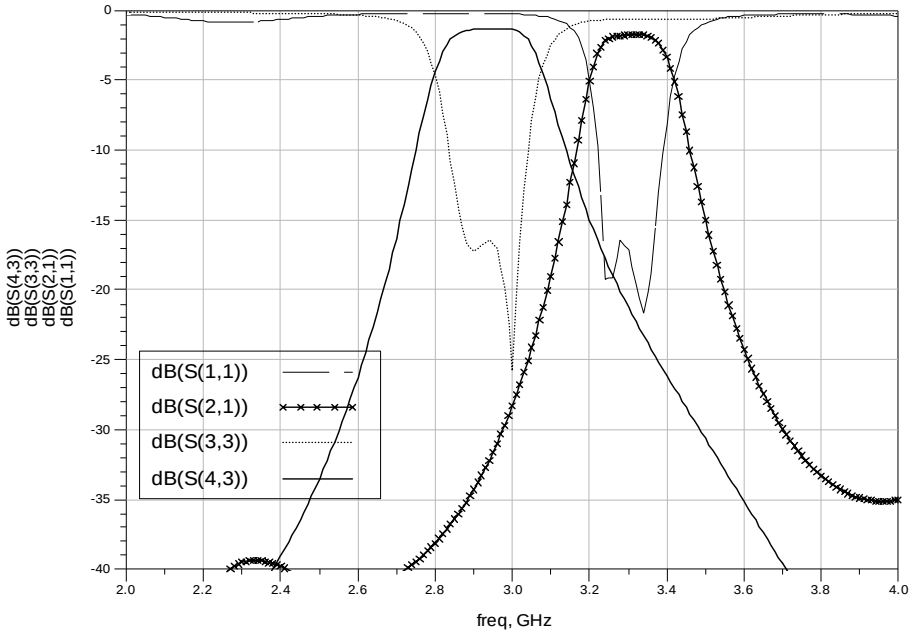
dB(S(4,3))
dB(S(3,3))
dB(S(2,1))
dB(S(1,1))
0
-5
-10
-15
-20
-25
-30
-35
-40
2.0
2.2
2.4
2.6
2.8
3.0
3.2
3.4
3.6
3.8
4.0
freq, GHz
dB(S(1,1))
dB(S(2,1))
dB(S(3,3))
dB(S(4,3))

(a)

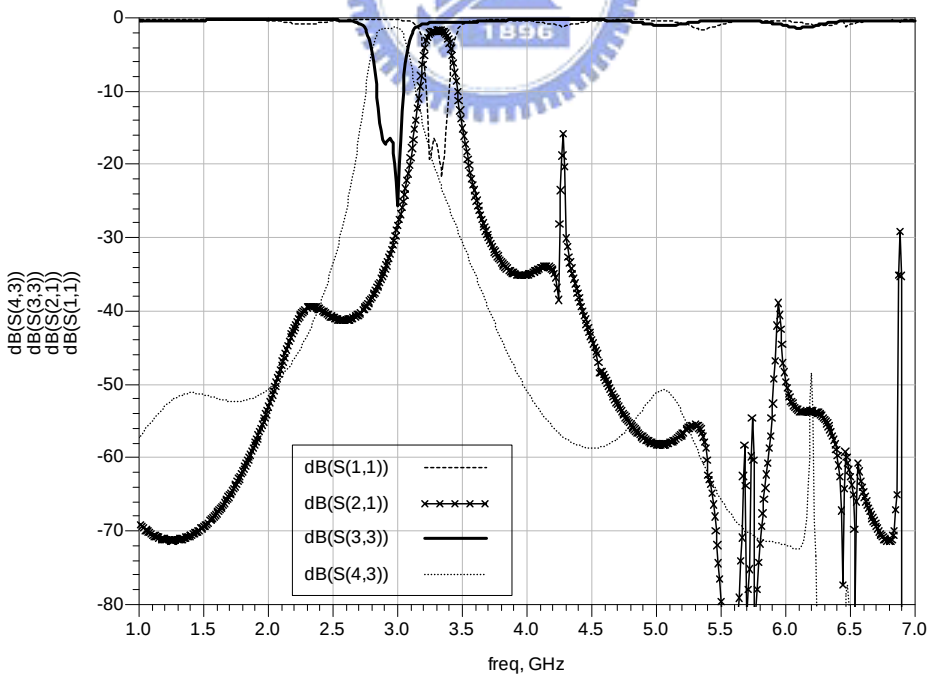
dB(S(4,3))
dB(S(3,3))
dB(S(2,1))
dB(S(1,1))
0
-10
-20
-30
-40
-50
-60
-70
-80
1.0
1.5
2.0
2.5
3.0
3.5
4.0
4.5
5.0
5.5
6.0
6.5
7.0
freq, GHz
dB(S(1,1))
dB(S(2,1))
dB(S(3,3))
dB(S(4,3))

(b)

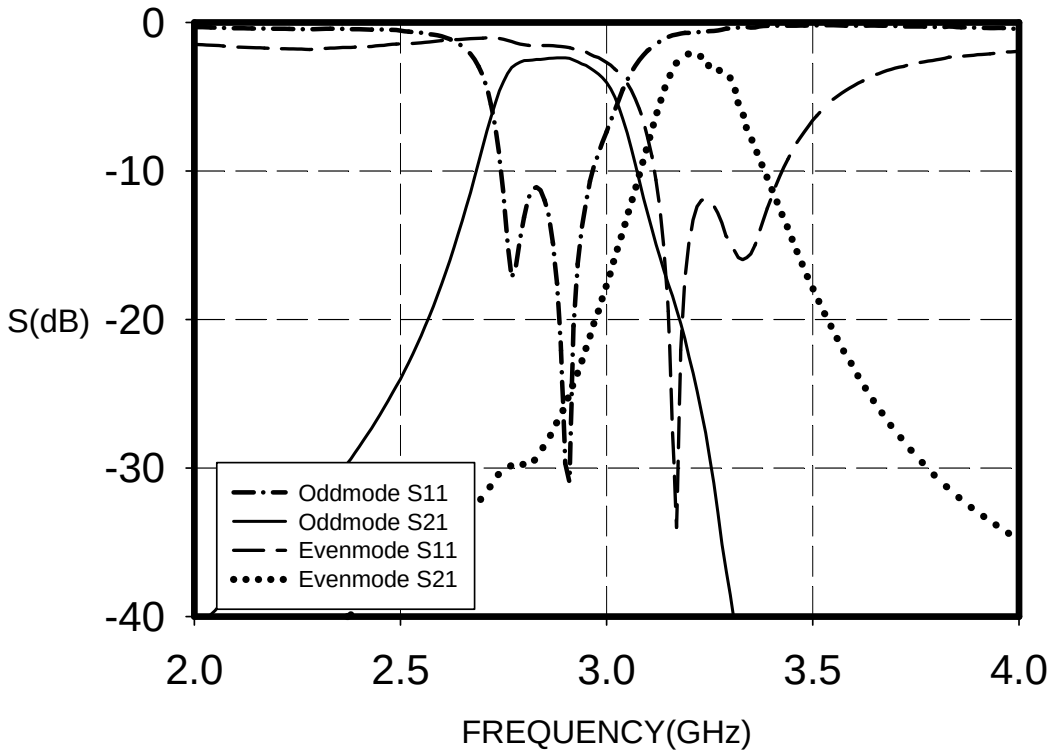
0
-10
-20
-30
-40
S(dB)
2.0
2.5
3.0
3.5
4.0
FREQUENCY(GHz)
Oddmode S11
Oddmode S21
Evenmode S11
Evenmode S21

(c)

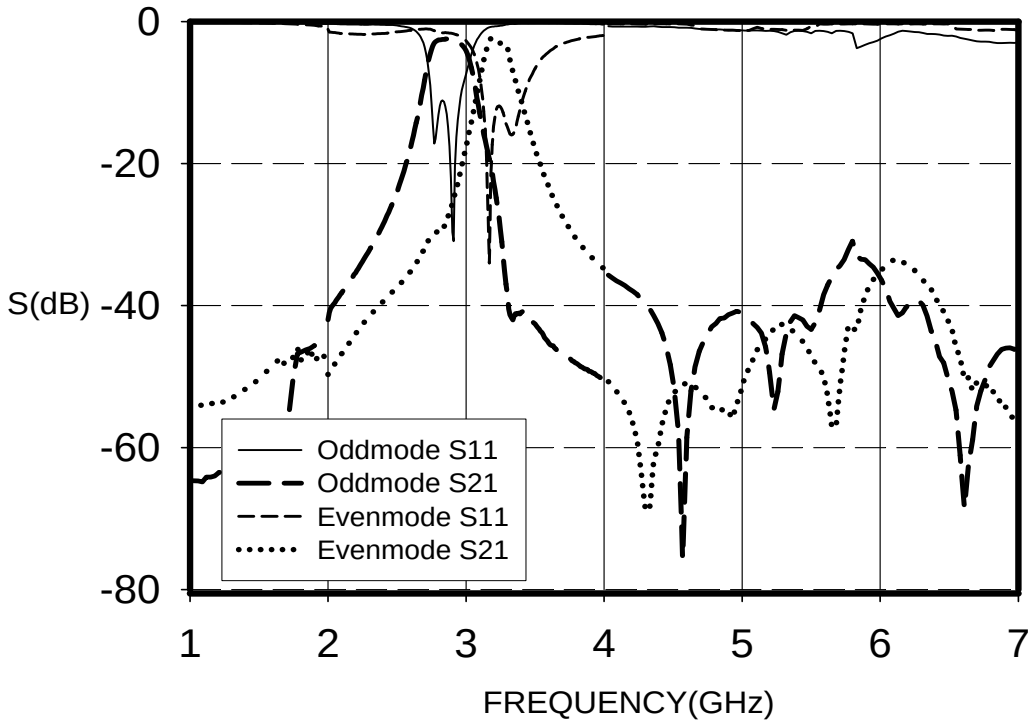
0
-20
-40
-60
-80
S(dB)
1
2
3
4
5
6
7
FREQUENCY(GHz)
Oddmode S11
Oddmode S21
Evenmode S11
Evenmode S21

(d)

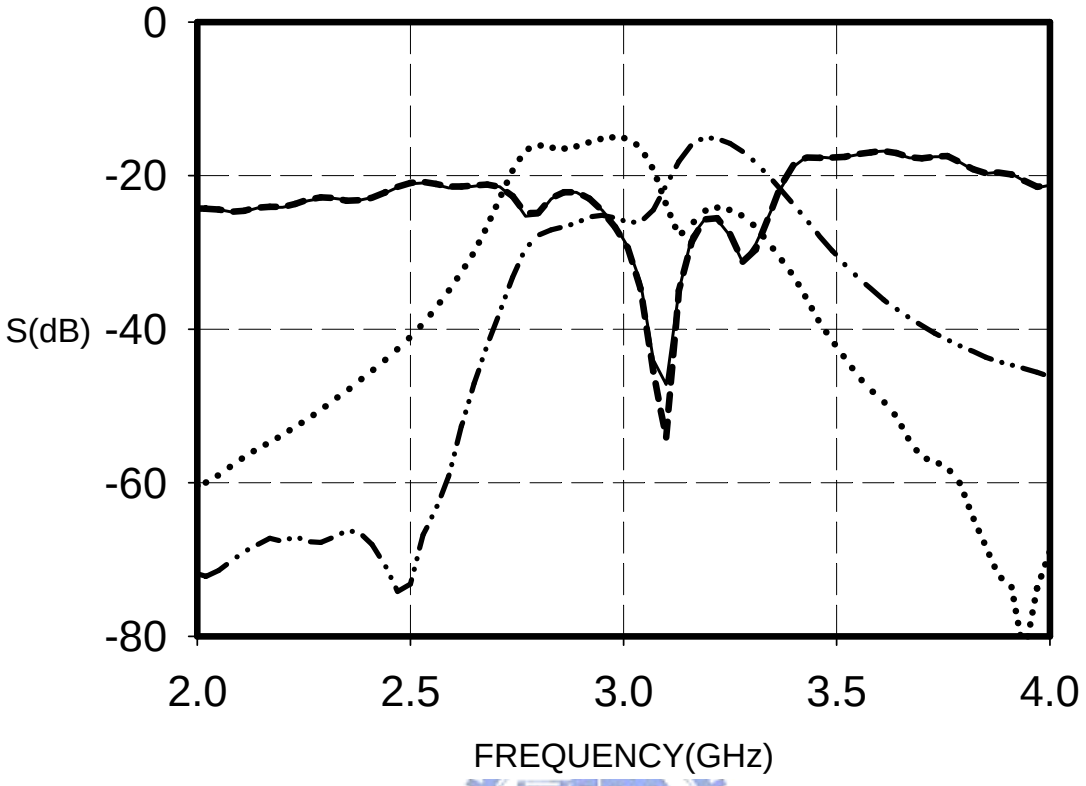

(e)

Figure 4.13 Simulated and measured results of Filter D. (a) Simulated $|S_{11}|$ and $|S_{21}|$ for 2~4 GHz. (b) Simulated $|S_{11}|$ and $|S_{21}|$ for 1~7 GHz. (c) Measured $|S_{11}|$ and $|S_{21}|$ for 2~4 GHz. (d) Measured $|S_{11}|$ and $|S_{21}|$ for 1~7 GHz. (e) Measured isolation between two modes.

Figure 4.13 presents the measured return loss in the passband is lower than 10 dB. The insertion loss is about 2.1~2.5 dB and the fractional bandwidth is 7.9% and 4.5 % at 2.79 GHz and 3.21 GHz. The first spurious occurs at the frequency higher than 7 GHz.

4.3 Design Procedure and Realization with Type III tapping

4.3.1 Third-Order Filter with Open-Ended λ/2 SIR

Similarly, a third-order Chebyshev filter can be designed with the SIRs used in Filter A. However, as mentioned in Section 2.4, two propagation modes with different effective dielectric constants and phase velocities in a coupled line will degrade the performance of the filter. For that reason, we will consider the influence during the design procedure. The passbands of the filter are designed as 2.7 GHz and 3.5 GHz with ripple level 0.1 dB as well. The fractional bandwidth is about 5~10%. Figure 4.14 shows the overall topology of the filter which we call Filter E.

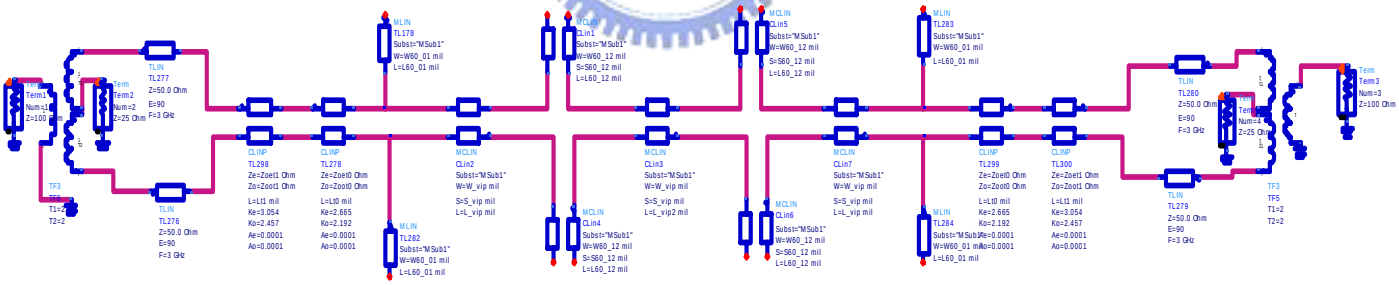

(a)

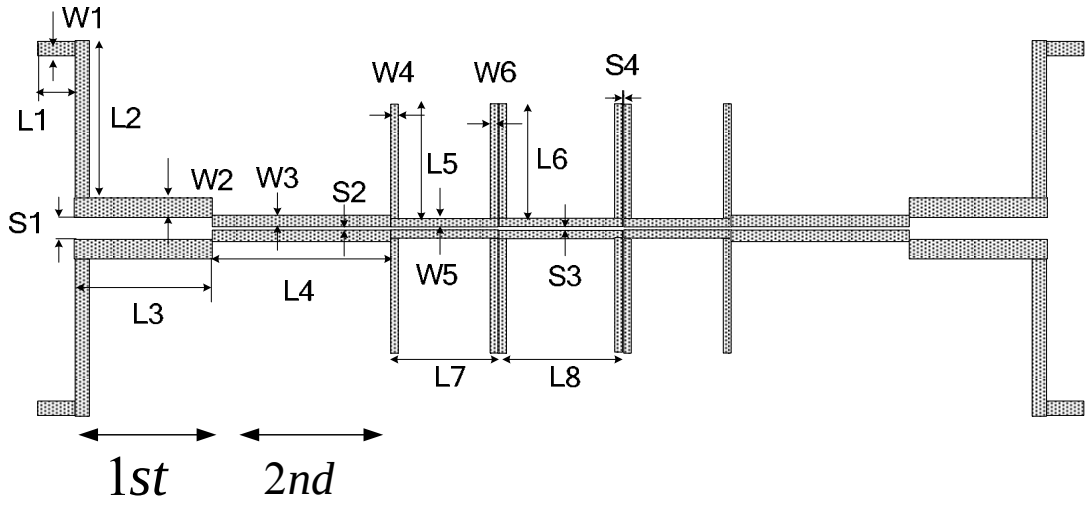

(b)

Figure 4.14 The overall circuit topology of the Filter E. (a) The circuit scheme in ADS. (b) The circuit scheme in Sonnet.

W1	W2	W3	W4	W5	L1
44	68	34	18	8	115
L2	L3	L4	L5	L6	L7
500	440	580	390	372	370
L8	S1	S2	S3	S4	
430	64	6	6	7	

Table 4.8 Physical dimensions of the proposed Filter E. (Unit: mil)

It is noted that we increase the characteristic impedance to 80 ohm to calculate the initial parameters so that the physical limit can be avoided and the required coupling in the second stage can be satisfied as well. The same consideration occurs in Filter A. On the other hand, in order to shift the spurious resonance to a higher frequency more than $2f_0$, the UIR structure is chosen for the filter with higher passband while another filter is designed using SIRs with $R<1$. Moreover, we pay more attention on the separation of the two passbands. That is, the higher the impedance ratio $R_a(=\frac{Z_{a\_high}}{Z_{a\_low}})$ is, the larger the separation becomes. Nevertheless, because of the physical limit for microstrip coupled

lines, we finally choose Z_{a_high} as 150 ohm. Table 4.9 lists the initial parameters for the filter at 3.5GHz.

f_0 (GHz)	Z_a (ohm)	Z_b (ohm)	θ_b	θ_a	Z_{oe12} (ohm)	Z_{oo12} (ohm)
3.5	80	80	60^o	30^o	110.89	62.57

Table 4.9 Initial parameters of the odd-mode filter in Filter E.

Moreover, from the coupled line theory, the effective dielectric constants of two propagation modes are different. In other words, the electrical length for even mode will be longer but shorter for odd mode relatively. This situation causes the shift of resonant frequencies for both modes which makes the separation of two passbands become smaller for the filter designed with open-end type SIRs. However, the same property in the filter with short-end type SIRs performs oppositely. Therefore, to reach the specification exaxtly, in this case, the fundamental frequency at higher passband can be chosen to be lower than expected and so does the impedance Z_{a_high} with considering the frequency shift.

In the second stage, due to the difference of two propagation modes, the coupling strength will be degraded as well as the bandwidth. To maintain the coupling, it's necessary to adjust the coupled line.

After the resonators are designed, the problem left is to find a feeding structure. In our case, using the theory in Section 3.1, we first fix the tap point at the stepped junction and obtain the load impedance form (3.5) and (3.12). For the load impedance R_{L_odd} and R_{L_even} relating to two resonant frequencies, it's necessary to find a matching circuit that can transform source impedance to R_{L_odd}, R_{L_even} at 3.5 GHz and 2.7 GHz respectively.

Thus, due to Type II tapping as discussed in previous case, it is apparent that the coupled lines can be a good configuration for our requirement. In this case, we utilize two sections of the quarter-wavelength coupled lines to realize the matching network which is feasible under the condition that R_{L_even} is higher than R_{L_odd}. Table 4.10 shows the characteristic impedances of the two-section quarter-wavelength coupled lines.

Section	Z_{oe}	Z_{oo}
1st	**58.14**	**36.46**
2nd	**105.21**	**54.84**

Table 4.10 Initial parameters of the two-section transformer in Filter E.

It the end, Filter E is fabricated and the photograph as well as the measured results are shown in Figure 4.15. and 4.17. Furthermore, we modify the layout at the junction between two coupled-line sections in the transformer to be smoother for the concern about implementation. Figure 4.16 and 4.18 shows the modified layout which we call Filter F and the measurement results.

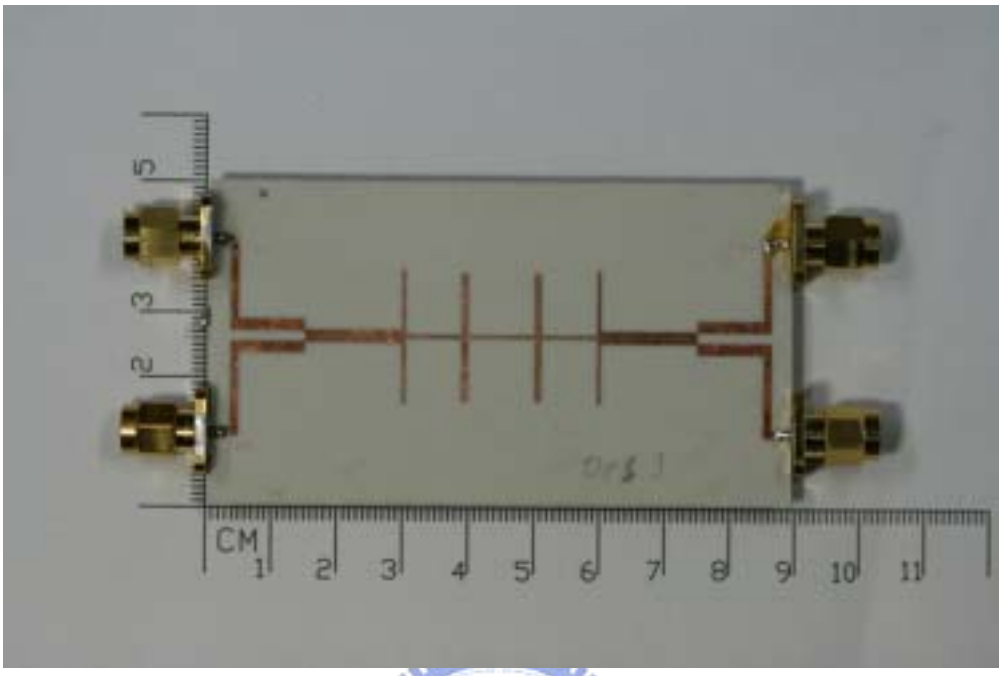

Figure 4.15 Photograph of proposed Filter E.

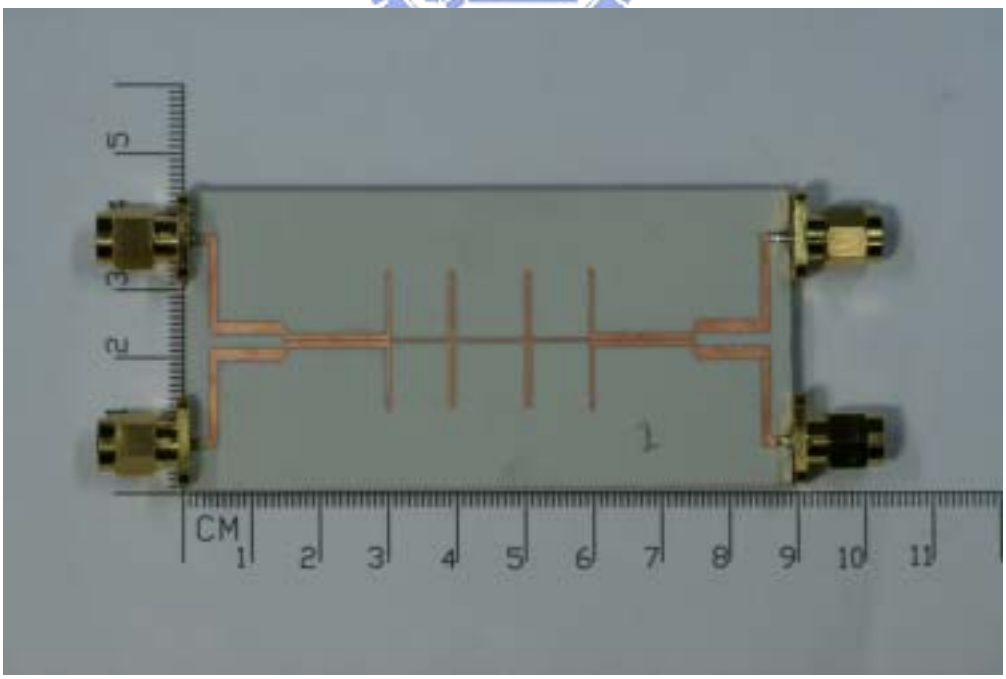

Figure 4.16 Photograph of proposed Filter F.

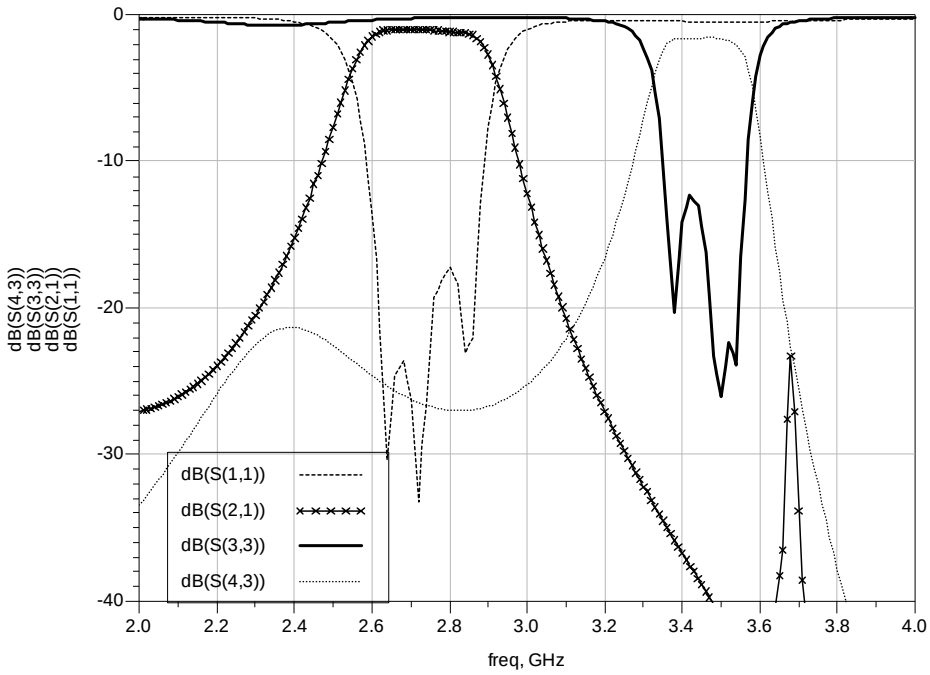
dB(S(4,3))
dB(S(3,3))
dB(S(2,1))
dB(S(1,1))
0
-10
-20
-30
-40
2.0
2.2
2.4
2.6
2.8
3.0
3.2
3.4
3.6
3.8
4.0
freq, GHz
dB(S(1,1))
dB(S(2,1))
dB(S(3,3))
dB(S(4,3))

(a)

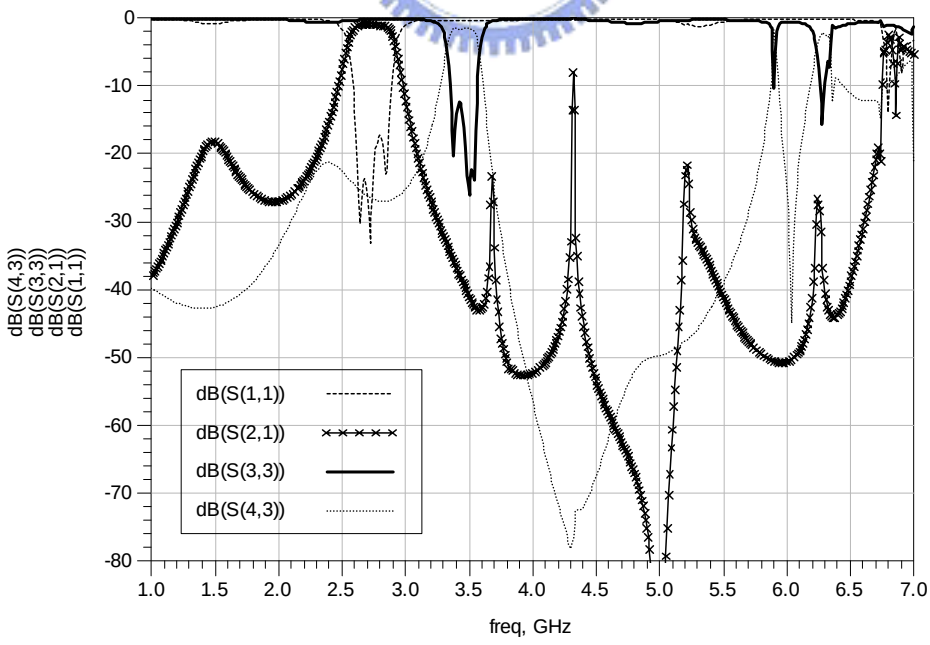
dB(S(4,3))
dB(S(3,3))
dB(S(2,1))
dB(S(1,1))
0
-10
-20
-30
-40
-50
-60
-70
-80
1.0
1.5
2.0
2.5
3.0
3.5
4.0
4.5
5.0
5.5
6.0
6.5
7.0
freq, GHz
dB(S(1,1))
dB(S(2,1))
dB(S(3,3))
dB(S(4,3))

(b)

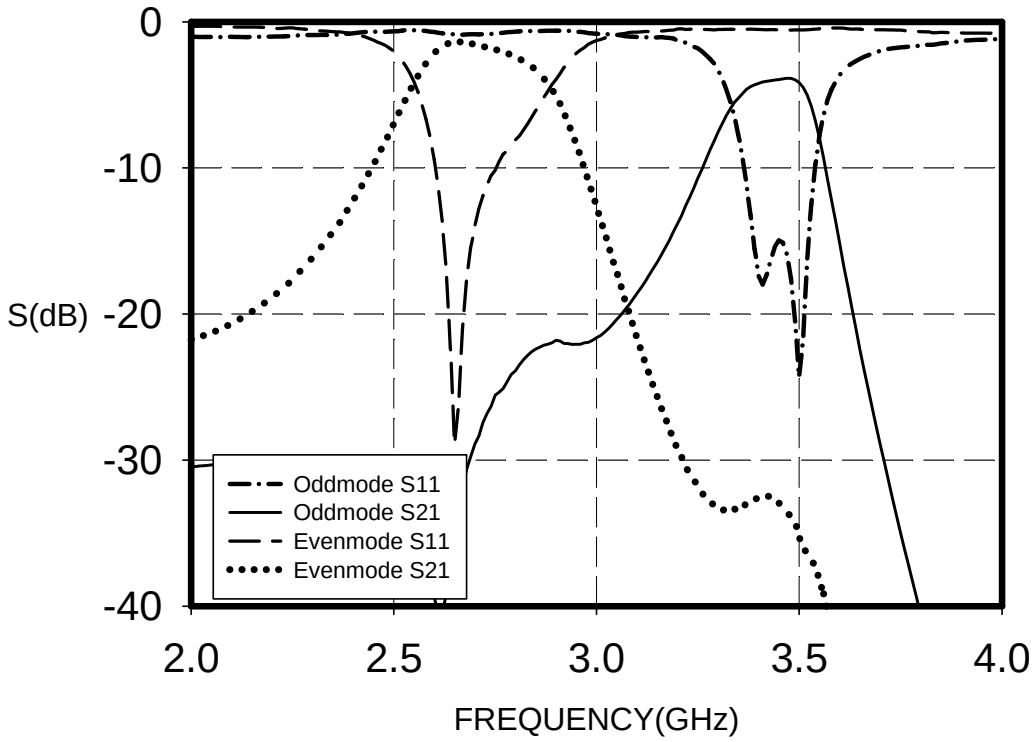
0
-10
-20
-30
-40
S(dB)
2.0
2.5
3.0
3.5
4.0
FREQUENCY(GHz)
Oddmode S11
Oddmode S21
Evenmode S11
Evenmode S21

(c)

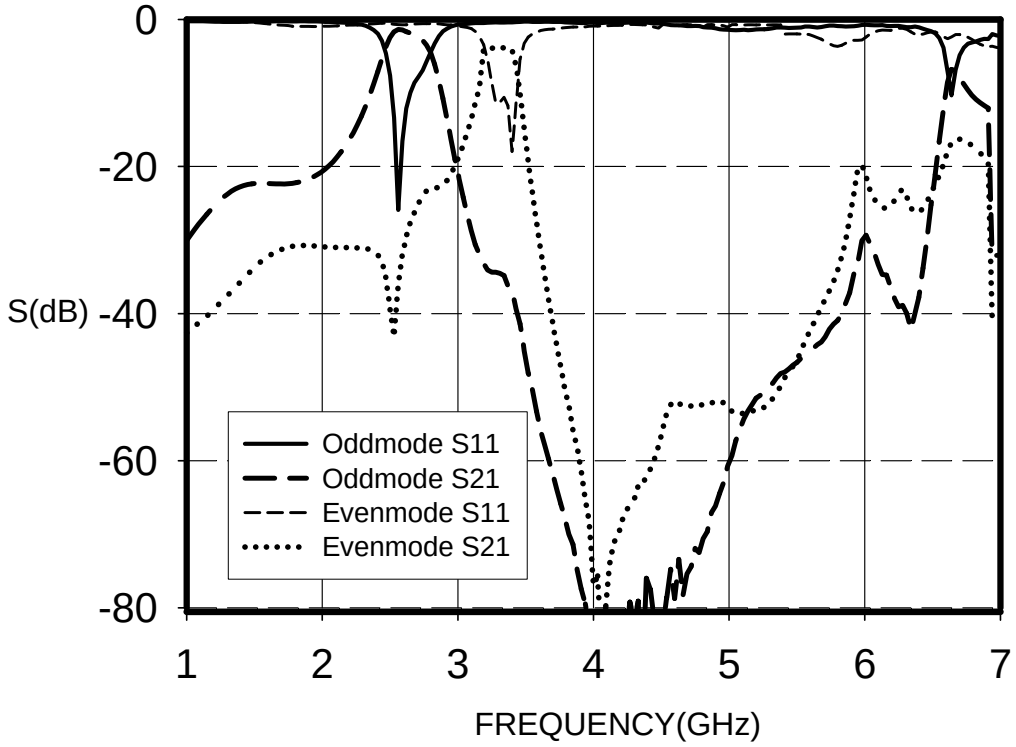
0
-20
-40
-60
-80
S(dB)
1
2
3
4
5
6
7
FREQUENCY(GHz)
Oddmode S11
Oddmode S21
Evenmode S11
Evenmode S21

(d)

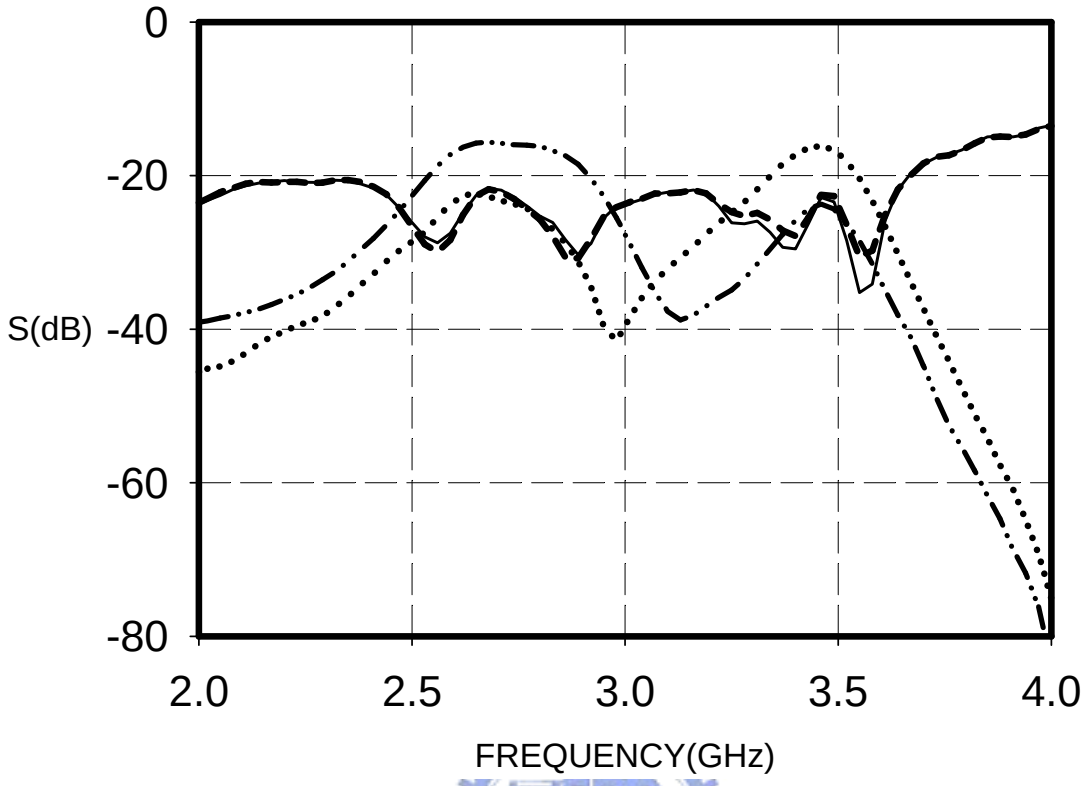

(e)

Figure 4.17 Simulated and measured results of Filter E. (a) Simulated $|S_{11}|$ and $|S_{21}|$ for 2~4 GHz. (b) Simulated $|S_{11}|$ and $|S_{21}|$ for 1~7 GHz. (c) Measured $|S_{11}|$ and $|S_{21}|$ for 2~4 GHz. (d) Measured $|S_{11}|$ and $|S_{21}|$ for 1~7 GHz. (e) Measured isolation between two modes.

Figure 4.17 presents the measured return loss in the passband is lower than 10 dB and the insertion loss is about 1.5~3.8 dB. The fractional bandwidths are 5.6 % and 4.9 % at 2.67 GHz and 3.45 GHz. The first spurious occurs near 6 GHz. These results consist with the simulated results approximately.

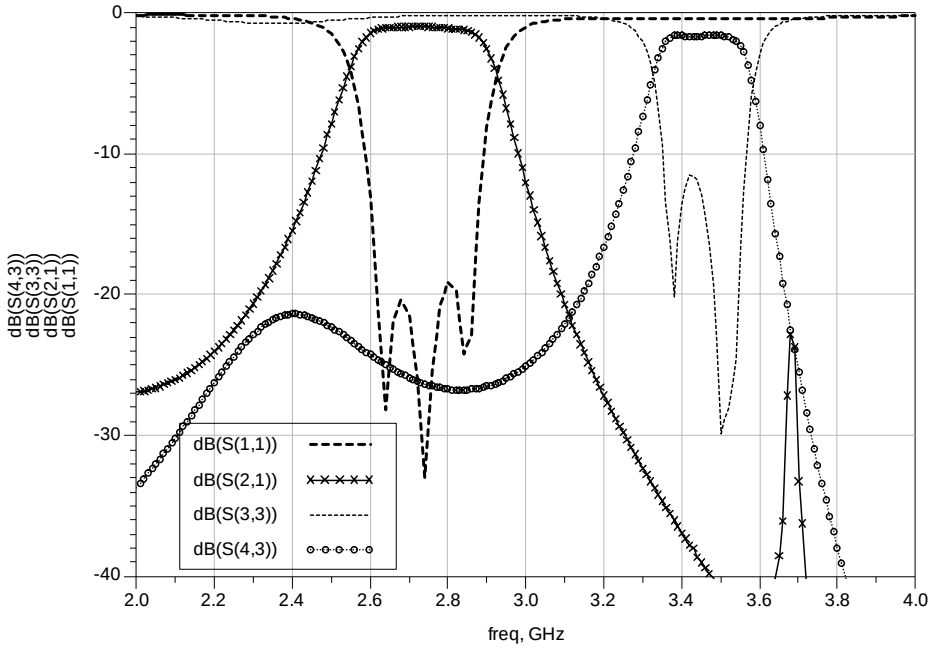
dB(S(4,3))
dB(S(3,3))
dB(S(2,1))
dB(S(1,1))
0
-10
-20
-30
-40
2.0
2.2
2.4
2.6
2.8
3.0
3.2
3.4
3.6
3.8
4.0
freq, GHz
dB(S(1,1))
dB(S(2,1))
dB(S(3,3))
dB(S(4,3))

(a)

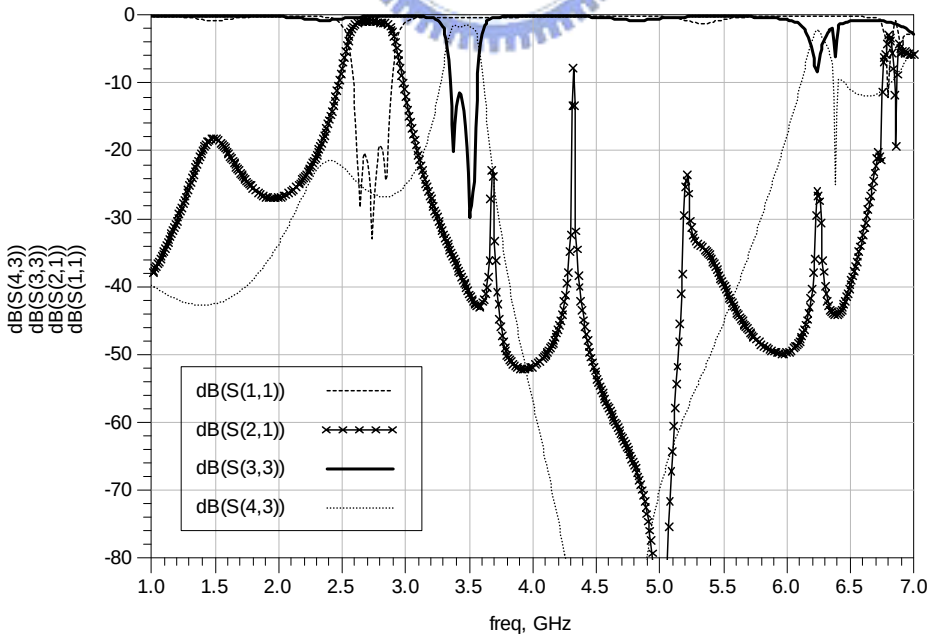
dB(S(4,3))
dB(S(3,3))
dB(S(2,1))
dB(S(1,1))
0
-10
-20
-30
-40
-50
-60
-70
-80
1.0
1.5
2.0
2.5
3.0
3.5
4.0
4.5
5.0
5.5
6.0
6.5
7.0
freq, GHz
dB(S(1,1))
dB(S(2,1))
dB(S(3,3))
dB(S(4,3))

(b)

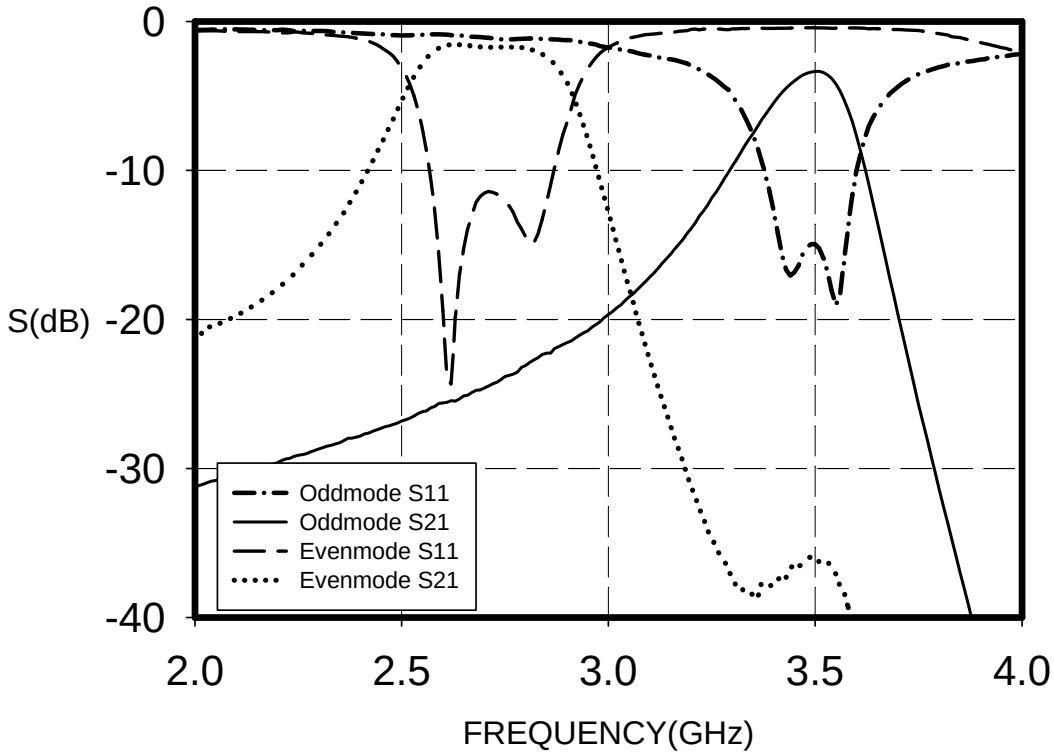
0
-10
-20
-30
-40
S(dB)
2.0
2.5
3.0
3.5
4.0
FREQUENCY(GHz)
Oddmode S11
Oddmode S21
Evenmode S11
Evenmode S21

(c)

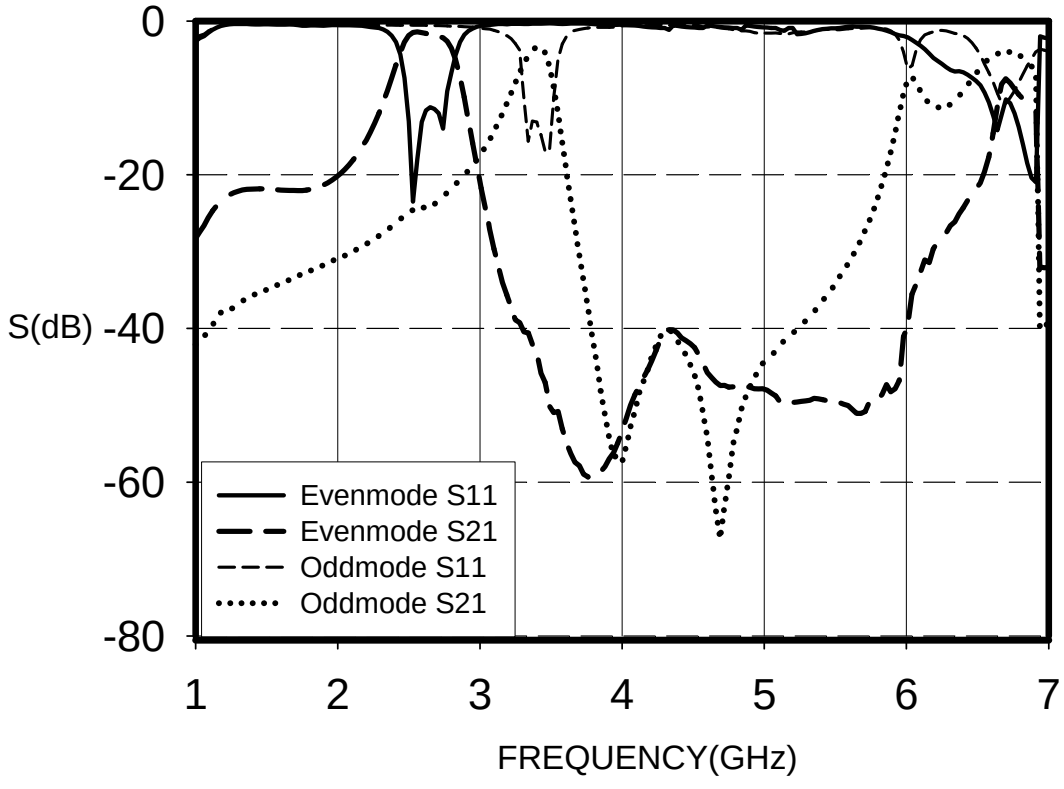
0
-20
-40
-60
-80
S(dB)
1
2
3
4
5
6
7
FREQUENCY(GHz)
Evenmode S11
Evenmode S21
Oddmode S11
Oddmode S21

(d)

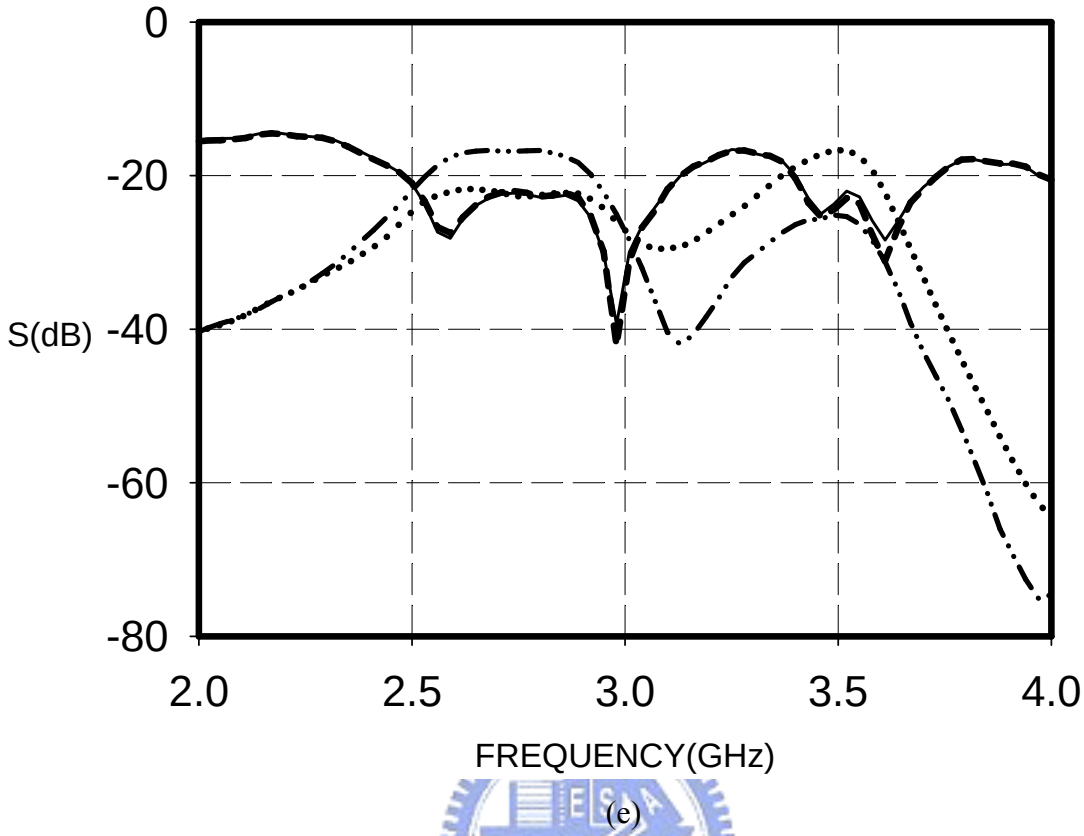

(e)

Figure 4.18 Simulated and measured results of Filter F. a) Simulated $|S_{11}|$ and $|S_{21}|$ for 2~4 GHz. (b) Simulated $|S_{11}|$ and $|S_{21}|$ for 1~7 GHz. (c) Measured $|S_{11}|$ and $|S_{21}|$ for 2~4 GHz. (d) Measured $|S_{11}|$ and $|S_{21}|$ for 1~7 GHz. (e) Measured isolation between two modes.

Figure 4.18 shows the measured in-band return loss is lower than 10 dB and the insertion loss is about 1.8~3.7 dB. The fractional bandwidth is 10 % and 5.7 % at 2.71 GHz and 3.49 GHz. The first spurious occurs near 6 GHz. These results have good agreement with the simulation..

4.3.2 Second-Order Filter with Open-Ended λ/2 SIR

Figure 4.19 presents the overall topology of the filter that we call Filter G. In this new design, we now want to set the goal to enlarge the separation of the two passbands. The

filter is designed at 2.5/3.5 GHz with ripple level 0.1 dB, and the fractional bandwidth is 4~7%. Apparently, the critical point is the coupling strength of the coupled-line section in the center of each SIR. The stronger the coupling strength is, the more the difference between Z_{oe} and Z_{oo} is, corresponding to the impedances Z_{a_high} and Z_{a_low} for two passbands respectively. Meanwhile, considering the physical limit of the coupled line in the second stage, we choose $Z_{a\_high} = 155ohm$ and $Z_{a\_low} = 70ohm$. Similary, the UIR and SIR structures are employed and operate respectively while exciting differential-mode or common-mode signal. The initial parameters are shown in Table 4.12. The overall circuit configuration with physical dimensions are shown in Figure 4.19 and Table 4.11.

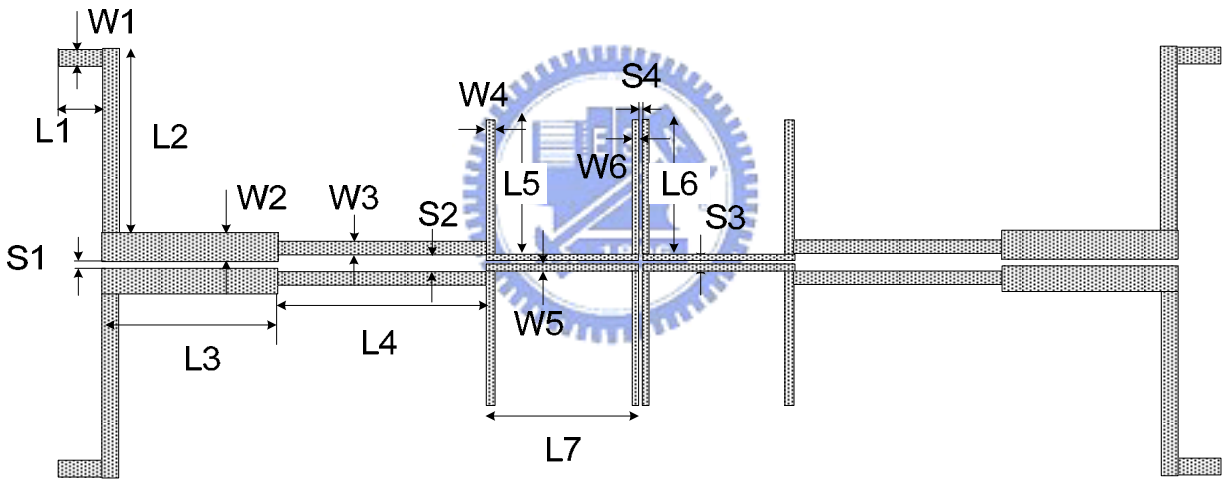

Figure 4.19 The circuit configuration of Filter G.

W1	W2	W3	W4	W5	W6
44	45	24	22	4	15
L1	L2	L3	L4	L5	L6
180	500	588	500	360	360
L7	S1	S2	S3	S4	
380	10	15	7	6	

Table 4.11 Physical dimensions of the proposed Filter G. (Unit: mil)

f_0 (GHz)	Z_a (ohm)	Z_b (ohm)	θ_b	θ_a	Z_{oe12} (ohm)	Z_{oo12} (ohm)
3.5	70	70	60^o	30^o	93.392	55.9789

Table 4.12 Initial parameters of the odd-mode filter in Filter G.

As mentioned, considering the effect of the difference for two propagation modes, the coupled lines in second stage must be adjusted to obtain enough coupling. And we design the first filter with a lower center frequency while the choice of impedance Z_{a_high} for the other filter with a lower passband can be lower. In that way, we can approach the specification as expected.

The design procedure of feeding structure is similar with Filter E. With two sections of quarter-wavelength coupled lines, we can easily transform the source impedance into different load impedance required at different passbands. The characteristic impedances of the two-section quarter-wavelength coupled lines are listed in Table 4.13.

Section	Z_{oe}	Z_{oo}
1st	**67.32**	**36.05**
2nd	**137.97**	**64.12**

Table 4.13 Initial parameters of the two-section transformer in Filter G.

Finally, the filter is designed and fabricated as Figure 4.20. The simulated and measurement results are shown in Figure 4.18.

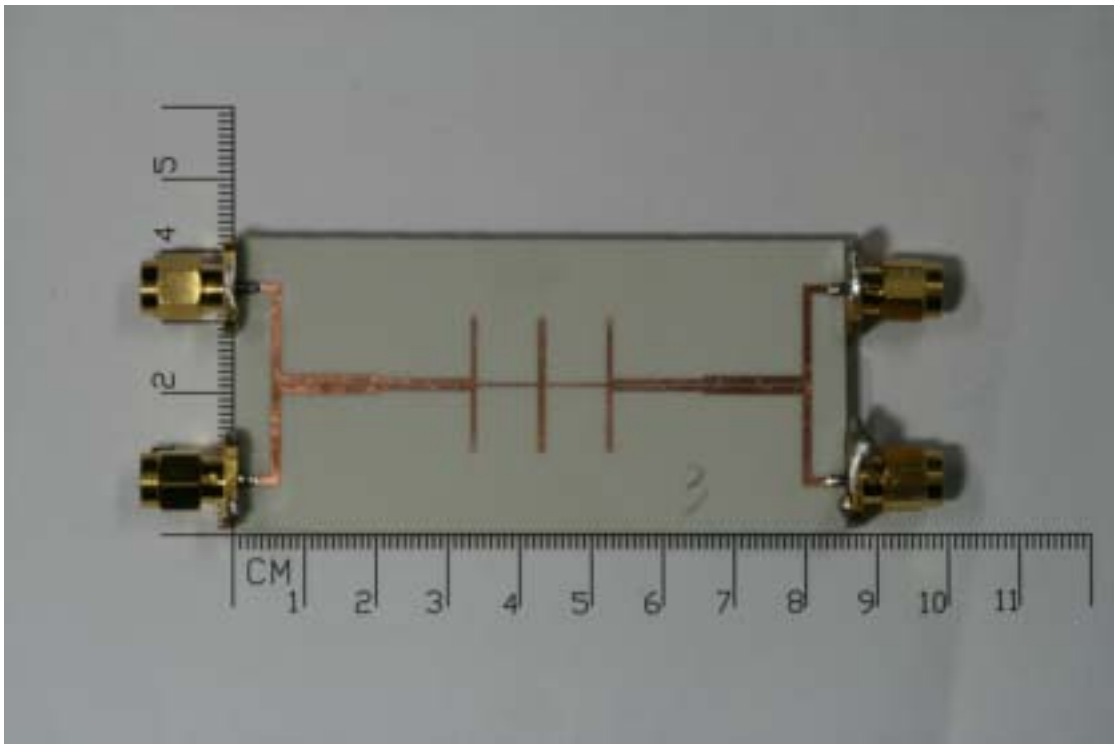

Figure 4.20 Photograph of proposed Filter G.

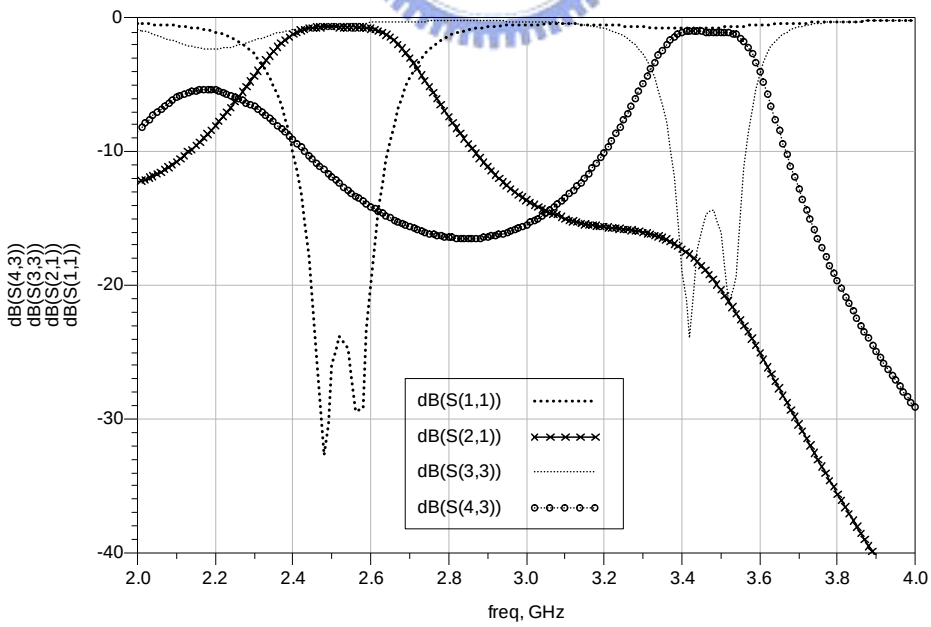

(a)

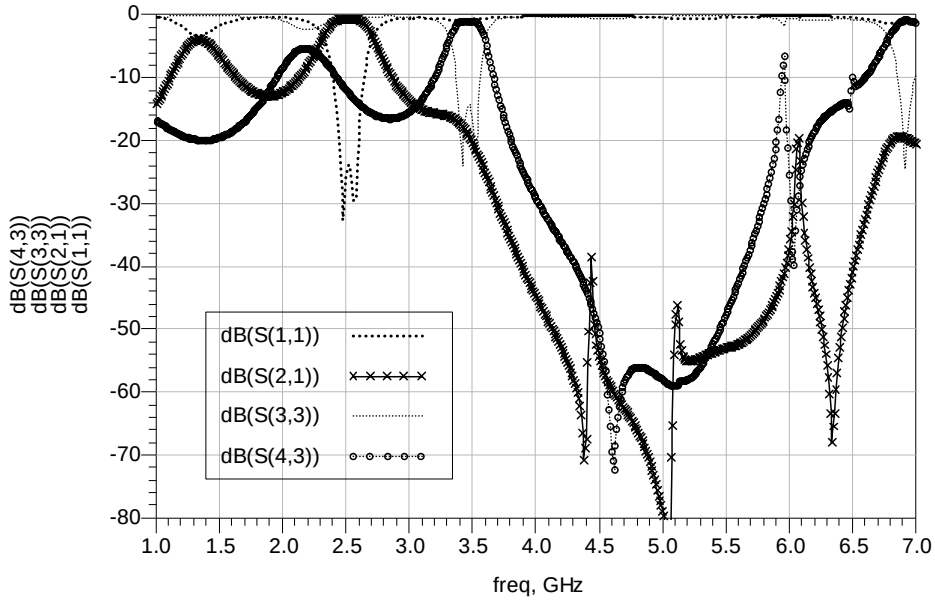
dB(S(4,3))
dB(S(3,3))
dB(S(2,1))
dB(S(1,1))
0
-10
-20
-30
-40
-50
-60
-70
-80
1.0
1.5
2.0
2.5
3.0
3.5
4.0
4.5
5.0
5.5
6.0
6.5
7.0
freq, GHz
dB(S(1,1))
dB(S(2,1))
dB(S(3,3))
dB(S(4,3))

(b)

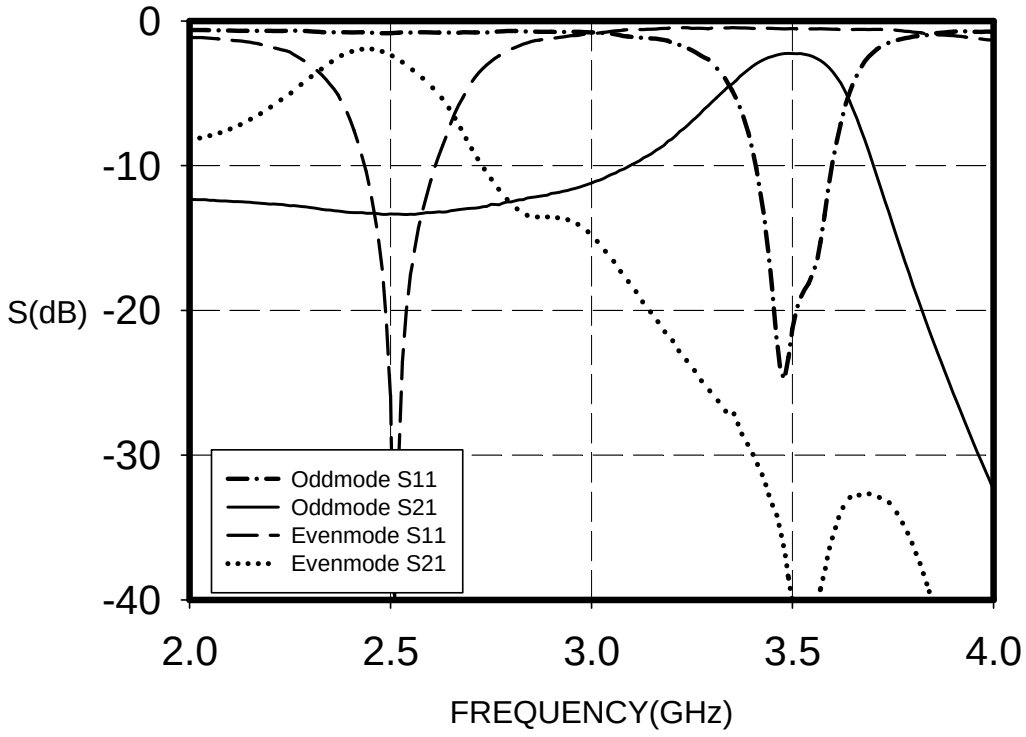
S(dB)
0
-10
-20
-30
-40
2.0
2.5
3.0
3.5
4.0
FREQUENCY(GHz)
Oddmode S11
Oddmode S21
Evenmode S11
Evenmode S21

(c)

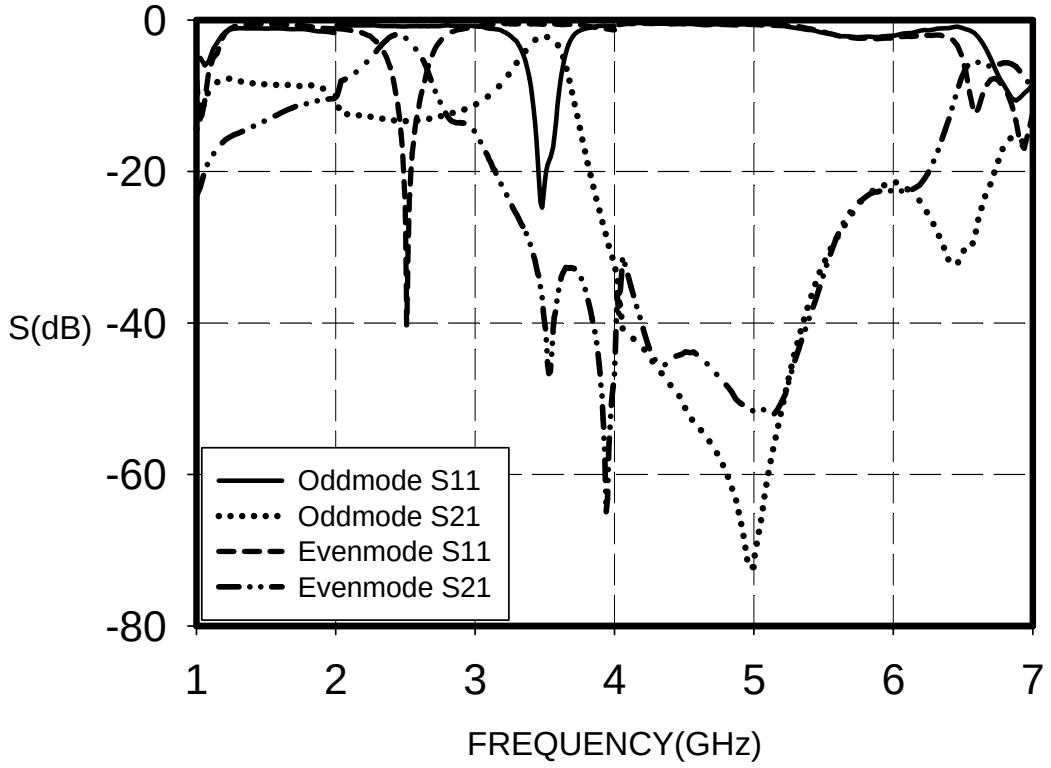
0
-20
-40
-60
-80
S(dB)
1
2
3
4
5
6
7
FREQUENCY(GHz)
Oddmode S11
Oddmode S21
Evenmode S11
Evenmode S21

(d)

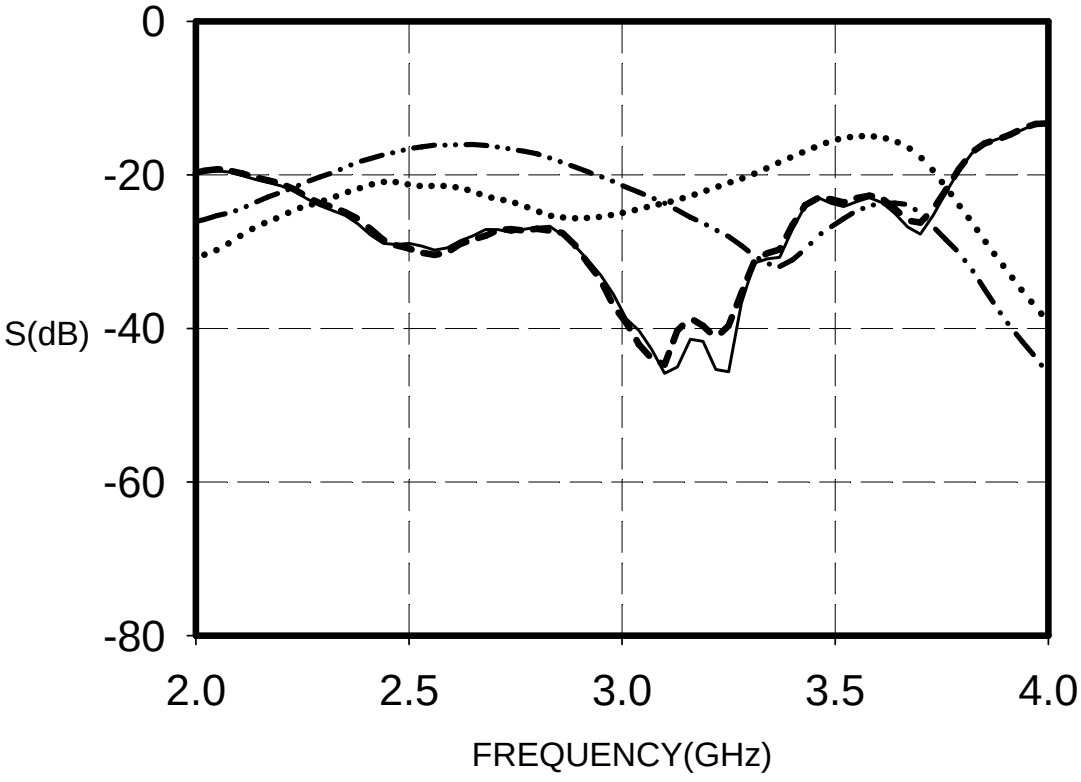
0
-20
-40
-60
-80
S(dB)
2.0
2.5
3.0
3.5
4.0
FREQUENCY(GHz)

(e)

Figure 4.21 Simulated and measured results of Filter F. (a) Simulated $|S_{11}|$ and $|S_{21}|$ for 2~4 GHz. (b) Simulated $|S_{11}|$ and $|S_{21}|$ for 1~7 GHz. (c) Measured $|S_{11}|$ and $|S_{21}|$ for 2~4 GHz. (d) Measured $|S_{11}|$ and $|S_{21}|$ for 1~7 GHz. (e) Measured isolation between two modes.

Figure 4.21 shows the measured in-band return loss is lower than 10 dB and the insertion loss is about 2.5~3 dB. The fractional bandwidth are 6.7 % and 5.4 % at 2.51 GHz and 3.49 GHz. The first spurious occurs at about 6.5 GHz. These results are nearly the same as simulation.

Chapter 5

Conclusion

In this thesis, the four-port even- and odd-mode dual band filters are proposed. Three second-order and four third-order filters are designed to approach the specifications. They can perform two different passbands while exciting differential- or common- mode signals respectively. Two types of SIRs as well as UIRs are used as the basic elements in these filters. The resonant frequency as well as the spurious resonance can be fully controlled by choosing proper impedance ratio of SIR. The coupling effect of coupled lines plays an important role in these filters. Based on the difference in phase velocities for two propagation modes, the characteristic impedances Z_{oe} and Z_{oo} can be used to combine two filters with different operating frequencies. With this property, Filter G is designed to possess wider separation between two passbands. However, applying to the internal stages between resonators, the characteristic will degrade the performance on bandwidth so that the coupled lines need to be adjusted. Moreover, focus on the feeding structure, Filter A,B, and C utilize Type I tapping to transform the same load impedance to source. In these cases, the matching circuit needs to avoid unwanted coupling between feed lines. On the contrary, the property of coupling is employed in Filter D, E, and F to accomplish the impedance matching.

The simulation and measurement results show that out-band $|S_{21}|$ for the filters, e.g. Filter A, E, F and G, which designed with open-end type SIRs can not be suppressed as lower as possible especially at low frequency. This situation might be the contribution of the antiparallel coupled-line section in the internal stages. Figure 5.1 presents the comparison of coupling at internal or external stages realized with parallel, antiparallel

coupled lines as well as the tapped lines.

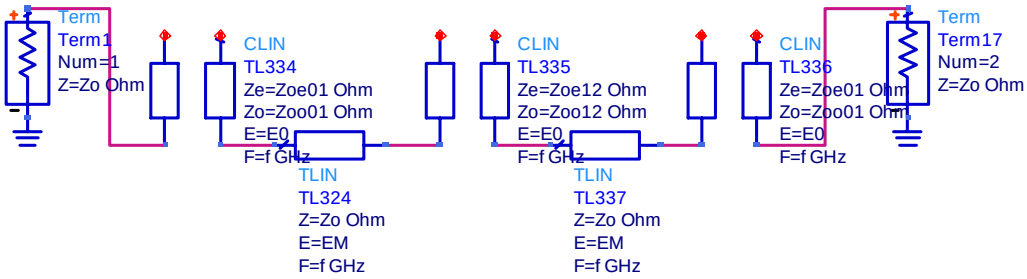

(a) Antiparallel-coupled lines are used for all coupling stages.(Hairpin-comb)[4]

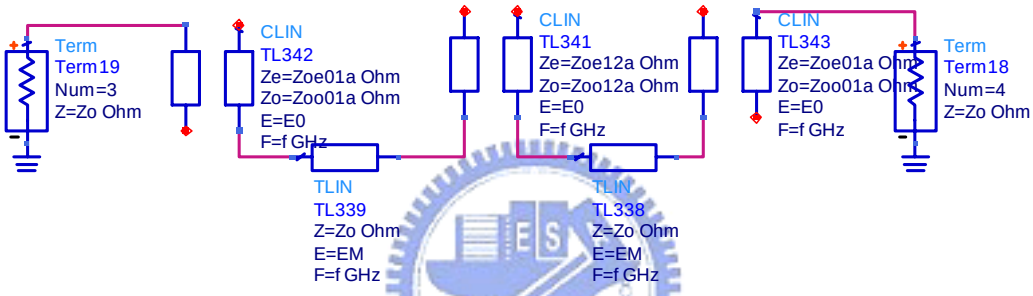

(b) Parallel-coupled lines are used for external stages while the antiparallel-coupled line is utilized in the internal stage.

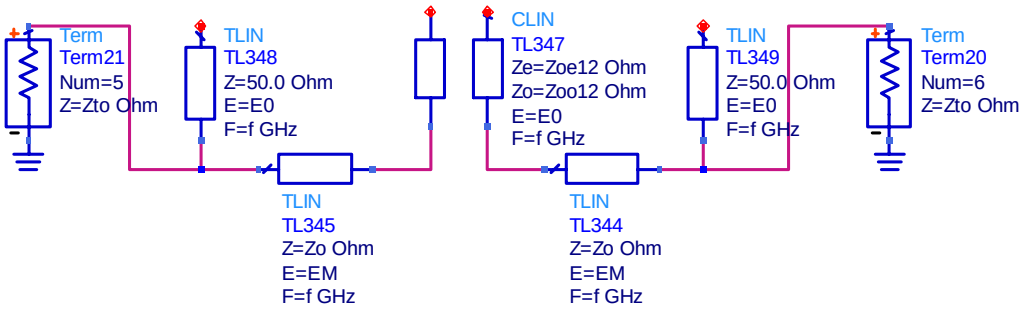

(c) Tapped lines are employed in external stages while the internal stage uses the antiparallel-coupled line.

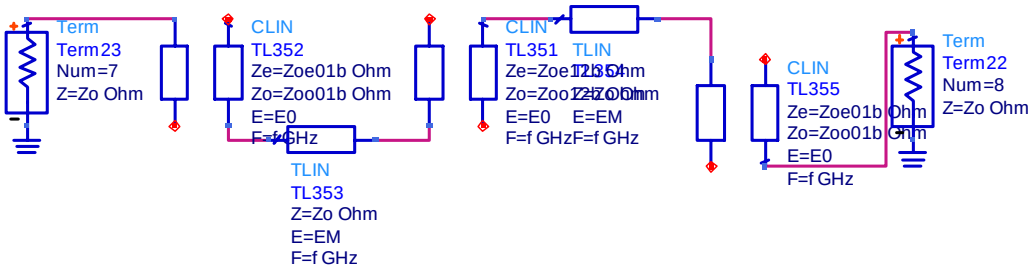

(d) Parallel-coupled lines are employed for all coupling stages.[3]

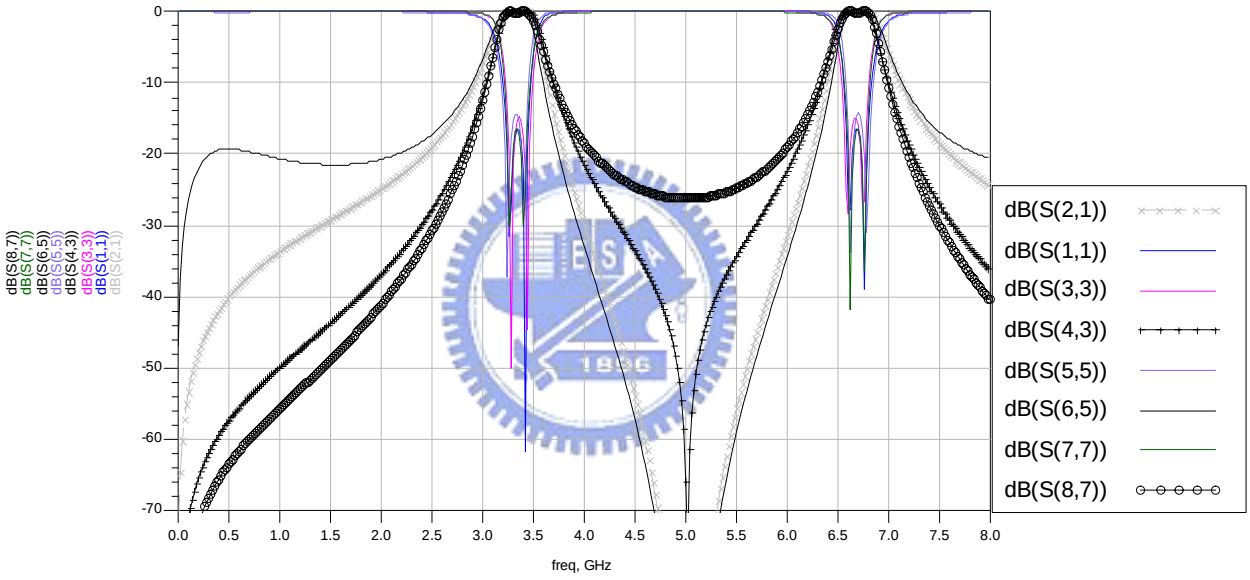

(e)

Figure 5.1 The comparison of four circuits. (a) Hairpin-resonator filter. (b) Type I filter in Seciton 2.6. (c) Type III filter in Section 3.2. (d) Parallel-coupled line resonator filter. (e) Simulated results for S11 and S21.

In Figure 5.1(e), it's observed that for circuits with antiparallel coupled-line sections possess the property that the out-band $|S_{21}|$ can't be restrained at lower frequency. For

Type III filter, the condition performs severely. It's supposed that the filter with tapped coupling instead of gap coupling is lack of effect of capacitances that can block the low-frequency signal. On the other hand, the filter with parallel-coupled line shows the out-band $|S_{21}|$ will rise at the higher frequency.

The measured results for Filter A and B show the two passbands become farer than simulated results. It's because the inaccuracy on fabrication that the gap for the coupled line in the center of a SIR is smaller than the designed one. Similar situation happened in Filter C, D, and F. In addition, the error of bandwidth might result from the gap inaccuracy of the coupled-line section in the second stage.

In the future, the defected ground structure can be employed in order to achieve required bandwidth and to widen the separation of two passbands more flexibly. It's for the reason that the even-mode impedance can be much more increased . Furthermore, the vertically installed planar (VIP) structure can be another configuration to replace the coupled line in the center segment of each SIR. Since the phase velocities for two modes vary much more , it's more flexible to design the filter with wider separation between two passbands. The characteristics of parallel and antiparallel coupled lines in stopband can be utilized to design other filter structures with more flexibility.

References

[1] D. M. Pozar, *Microwave Engineering*, 2nd ed. New York: Wiley, 1998, ch. 8.

[2] J. S. Hong and M. J. Lancaster, *Microstrip Filter for RF/Microwave Applications*. New York: Wiley, 2001, ch. 8.

[3] S. B. Cohn, "Parallel coupled transmission-line resonator filters," *IRE Trans. Microw. Theory Tech.*, vol. MTT-6, no. 4, pp. 223-231, Apr. 1958.

[4] G. L. Matthaei, N. O. Fenzi, R. J. Forse, and S. M. Rohfing, "Hairpin-comb filters for HTS and other narrowband applications," *IEEE Tran. Microw. Theory Tech.*, vol. 45, no. 8, pp. 1226-1231, Aug. 1997.

[5] J. S. Hong and M. J. Lancaster, " Couplings of microstrip square open-loop resonators for cross-coupled planar microwave filters," *IEEE Tran. Microw. Theory Tech.*, vol. 44, no. 11, pp. 2099-2109, Nov. 1996.

[6] J. T. Kuo, M. J. Maa, and P. H. Lu, "A microstrip elliptic function filter with compact miniaturized hairpin resonators," *IEEE Tran. Microw. Guided Wave Lett,* vol. 10, no. 3, pp. 94-95, Mar.2000.

[7] M. Sagawa, K. Takahashi, and M. Makimoto, "Miniaturized hairpin resonator filters and their application to receiver front-end MIC's," *IEEE Tran. Microw. Theory Tech.*, vol. 37, no. 12, pp. 1991-1997. Dec. 1989.

[8] Makimoto and S. Yamashita, "Bandpass filters using parallel coupled stripline stepped-impedance resonators," *IEEE Tran. Microw. Theory Tech.*, vol. MTT-28, no. 12, pp. 1413-1417, Dec. 1980.

[9] M. Sagawa, M. Makimoto, and S. Yamashita, "Geometrical structures and fundamental characteristics of microwave stepped-impedance resonators," *IEEE Tran. Microw. Theory Tech.*, vol. 45, no. 7, pp. 1078-1085. Jul. 1997.

[10] C.-H. Wu, C.-H. Wang, C. H. Chen, “Balanced coupled-resonators bandpass filters using multisection resonators for common-mode suppression and stopband extraction,” *IEEE Tran. Microw. Theory Tech.*, vol. 55, no. 8, pp. 1756-1763. Aug. 2007.

[11] M. Makimoto and S. Yamashita, *Microwave Resonators and Filters for Wireless Communication-Theory and Design.* Berlin, Germany: Springer, 2001, pp.79-83.

[12] G. L. Matthaei, L. Young, and E. M. T. Jones, *Microwave Filters, Impedance Matching Network, and Coupling Structures.* Norwood, MA: Artech House, 1980.

[13] D. G. Swanson, “Narrow-band microwave filter design,” IEEE Microwave Mag., vol. 8, no. 5, pp. 105-114, Oct. 2007.

[14] E. M. T. Jones and J. T. Bolljahn, “Coupled-strip-transmission-line filters and directional couplers,” *IRE Trans.*, PGMTT-4, No2, pp. 78-81, Apr. 1956.

[15] H. Ozaki and J. Ishii, “Synthesis of a class of strip-line filters,” *IRE Trans.*, PGCT-5, pp. 104-109, Jun. 1958.

[16] J. S. Wong, “Micorstrip tapped-line filter design,” *IEEE Tran. Microw. Theory Tech.*, vol. MTT-27, no. 1, pp. 44-50, Jan. 1979.

[17] K. C. Gupta, R. Garg, I. Bahl, and P. Bharita, Microstrip Lines and Slotlines. Dedham, MA: Artech House, 1980.

[18] J. T. Kuo and E. Shih, “Microstrip stepped impedance resonator bandpass filter with an extended optimal rejection bandwidth,” *IEEE Tran. Microw. Theory Tech.*, vol. 51, no. 5, pp. 1554-1559. May. 2003.

[19] C. Monaon, “A small dual-frequency transformer in two sections,” *IEEE Tran. Microw. Theory Tech.*, vol. 51, no. 4, pp. 1157-1161. Apr. 2003.